On the design and monitoring of photovoltaic systems for rural homes

Nathaniel John Williams

Submitted in partial fulfilment of the requirements for the degree of

MAGISTER SCIENTIAE

in the Faculty of Science at the
Nelson Mandela Metropolitan University

January 2011

Supervisor: Prof. E. Ernest van Dyk
Co-Supervisor: Dr. Frederik J. Vorster

Declaration by Student

Name: Nathaniel John Williams

Student Number: 209911328

Qualification: Magister Scientiae

In accordance with Rule G4.6.3, I hereby declare that the above-mentioned thesis is my own work and that it has previously not been submitted for assessment to another University or for another qualification.

Signature:

Date:

Dedication

This work is dedicated to my grandparents, Jean and Ebbie Williams, and my parents, Kurt and Brenda Williams, whose unyielding support of all my life's adventures made this work possible.

Acknowledgements

My sincere thanks to:

- Prof. E.E. van Dyk for his superb guidance, support and encouragement throughout this project.
- Dr. F.J. Vorster for his enthusiasm, guidance and valued conversations throughout this project.
- Dr. E. Ferg from the Chemistry Department and his students at the battery testing laboratory for their advice and assistance regarding the battery testing component of the work.
- Jualine Ferreira for all of her invaluable assistance.
- D. O'Conner and J.B. Wessels for their technical assistance.
- David Gola and family for their hospitality and cooperation in Tyefu.
- André and Eon Friend at Telecom Techniques for their assistance in supplying system components.
- Anthony Sullivan and the Rhodes University Department of Physics and Electronics for their assistance, on short notice, with technical issues in the field.
- My colleagues at the Centre for Energy Research past and present for their assistance and various contributions toward making the CER an enjoyable place to work including B. Bulter, J. Crozier, T. Hückel, F. Montealegre, M. Munji, Dr. W. Okullo, Dr. C. Radue, R. Schultz and Dr. N. Thantsha.

Contents

Summary

It is estimated that 1.6 billion people today live without access to electricity. Most of these people live in remote rural areas in developing countries. One economic solution to this problem is the deployment of small domestic photovoltaic (PV) systems called solar home systems (SHS).

In order to improve the performance and reduce the life cycle cost of these systems, accurate monitoring data of real SHSs is required. To this end, two SHSs typical of those found in the field were designed and installed, one in a rural area of the Eastern Cape of South Africa and the other in the laboratory.

Monitoring systems were designed to record energy flows in the system and important environmental parameters. A novel technique was developed to correct for measurement errors occurring during the utilization of pulse width modulation charge control techniques. These errors were found to be as large as 47.6%. Simulations show that correction techniques produce measurement errors that are up to 20 times smaller than uncorrected values, depending upon the operating conditions.

As a tool to aid in the analysis of monitoring data, a PV performance model was developed. The model, used to predict the maximum power point (MPP) power of a PV array, was able to predict MPP energy production to within 0.2% over the course of three days. Monitoring data from the laboratory system shows that the largest sources of energy loss are charge control, module under performance relative to manufacturer specifications and operation of the PV array away from MPP. These accounted for losses of approximately 18-27%, 15% and 8-11% of rated PV energy under standard test conditions, respectively. Energy consumed by loads on the systems was less than 50% of rated PV energy for both the remote and laboratory systems.

Performance ratios (PR) for the laboratory system ranged from 0.38 to 0.49 for the three monitoring periods. The remote system produced a PR of 0.46. In both systems the PV arrays appear to have been oversized. This was due to overestimation of the energy requirements of the loads on the systems. In the laboratory system, the loads consisting of three compact fluorescent lamps and one incandescent lamp, were used to simulate a typical SHS load profile and collectively consumed only 85% of their rated power. The

predicted load profile for the remote system proved to be significantly overestimated.

The results of the monitoring project demonstrate the importance of acquiring an accurate estimation of the energy demand from loads on the system. Overestimations result in over-sized arrays and energy lost to charge control while under-sized systems risk damaging system batteries and load shedding. Significant under-performance of the PV module used in the laboratory system, underlines the importance of measuring module IV curves and verifying manufacturer specifications before system deployment. It was also found that significant PV array performance gains could be obtained by the use of maximum power point tracking charge controllers. Increased PV array performance leads to smaller arrays and reduced system cost.

Keywords: Photovoltaic Systems, Solar Home Systems, Monitoring, System Design, Performance Analysis, Rural Electrification.

Nomenclature

α PV short-current irradiance dependence coefficient

β PV open circuit-voltage irradiance dependence coefficient

$\eta_{A,mean}$ Mean Array Efficiency

$\eta_{S,mean}$ Mean System Efficiency

η_{tot} Overall Efficiency

γ PV open circuit-voltage temperature dependence coefficient

C_{20} 20 hour Battery Capacity Rating

d_{auto} Day of autonomy

E_{load} Load Energy

E_{PV} PV energy

f_{PWM} PWM frequency

FF_0 Ideal fill factor

FF_s Fill factor with infinite shunt resistance

G Irradiance

G_0 Irradiance at STC

h_{sun} Sun hours

I_{AVG} Average current during PWM

I_{BT} Battery current

I_{LD} Load Current

I_{MAX} Off pulse PV current during PWM

I_{max} Maximum Current

I_{MIN} On pulse PV current during PWM

I_{MPP} Maximum Power Point Current

I_{PV} PV current

I_{sc} Short-Circuit Current

L_C Array Capture Losses

L_S System Losses

n_{MPP} PV module ideality factor at MPP

P_{dis} Dissipated Power

P_{EST1} PWM PV power estimation method one

P_{EST2} PWM PV power estimation method two

P_{load} Load Power

P_{MPP} Maximum Power Point Power

P_{peak} Rated PV peak power

R_{dl} Input resistance of data logger

R_{equiv} Equivalent resistance

R_{sh} Shunt resistance

R_s Series resistance

T PV module temperature

T_0 PV module temperature at STC

$t_{integration}$ Data logger integration time

t_{settle} Data logger settling time

V_{AVG} Average voltage during PWM

$V_{drop_{max}}$ Maximum shunt voltage drop

V_{MAX} On pulse PV voltage during PWM

V_{MIN} Off pulse PV voltage during PWM

V_{MPP} Maximum Power Point Voltage

$V_{oc,bat,SOC(X\%)}$ Open-circuit battery voltage at X% SOC

V_{oc0} PV open circuit-voltage at STC

V_{oc} Open-Circuit Voltage

v_{oc} PV module thermal voltage normalized to open-circuit voltage

Y_A Array Yield

Y_f Final Yield

Y_r Reference Yield

A:L Array to Load Ratio

AC Alternating Current

AM1.5 Standard Spectrum Air Mass 1.5

BOM Back of Module

CER Centre for Energy Research

CFL Compact Fluorescent Lamp

CI Clearness Index

d PWM duty cycle

DAQ Data Acquisition

DC Direct Current

DOD Depth of Discharge

EMC Electromagnetic Compatibility

FF Fill Factor

I Current

IEA International Energy Agency

IEC International Electrotechnical Commission

IV Current-Voltage

JRC Joint Research Centre

k Boltzmann's constant

LED Light Emitting Diode

LVD Low Voltage Disconnect

MOSFET MetalOxideSemiconductor Field-Effect Transistor

MPP Maximum Power Point

MPPT Maximum Power Point Tracking

n Ideality factor

NMMU Nelson Mandela Metropolitan University

P Power

POA Plane of Array

PR Performance Ratio

PSO Particle Swarm Optimization

PV Photovoltaic

PWM Pulse Width Modulation

q Elementary charge

R Resistance

SHS Solar Home System

SOC State of Charge

STC Standard Test Conditions

TV	Television
UF	Usage Factor
V	Voltage
VI	LabView Virtual Instrument

Chapter 1

Introduction

1.1 Background

There are 1.6 billion people in the world today that are living without access to electricity [1]. Many of these people live in remote rural areas in developing countries. It is well known that access to electricity and modern forms of energy are essential to all sectors of development. Bringing access to electrical services to rural people through grid-extension can be prohibitively expensive due to long distances and difficult terrain coupled with low population density and low per capita energy consumption.

Access to electricity impacts all areas of the lives of rural people. From education and healthcare to agriculture and economic development, electricity access is part of the essential infrastructure of any modern community. High quality electric lighting impacts significantly on the amount of time students spending studying [2]. Rural students often have many responsibilities after school hours leaving few daylight hours available for studies. Kerosene lamps are often used as a light sources for this purpose but produce low quality light and emit potentially hazardous particulates [3]. This old technology strains eyes and puts rural people at risk of respiratory illness. The fire risk from the use of kerosene lamps is also significant.

Electric lighting not only prevents exposure to the dangers of more traditional lighting technologies, but increases the quality of healthcare services. During interviews with rural community leaders in the Mpika district of Zambia, the need for reliable and high quality lighting for midwives to deliver their services at all hours was highlighted as a major concern [4]. Emergency medical services are difficult to administer in the dark of night in non-electrified communities. Furthermore, many medical technologies, as basic as refrigerators for vaccines, require a source of electricity. Access to clean water can be efficiently supplied via electric pumps.

Hours of economic productivity can be greatly extended with the aid of artificial light.

Larger sources of electricity can power hand tools and light industrial equipment that drastically increase productivity in village industries. Agricultural production benefits greatly from water pumping and irrigation powered by electricity. The development of all economies rely upon access to affordable electrical energy.

Extending electrical grids to these areas is often extremely expensive. The long distances and difficult terrain over which power lines must be carried increase the investments required to connect rural areas to national grids [5, 6]. The problem is compounded by low population density and low per capita energy consumption, which means unaffordable tariffs for the typically poor rural population would be required to make any return on the investment.

It is often the case that this energy can be provided much more economically by producing the energy on-site using renewable energy technologies such as wind, micro-hydro and solar power. There are several models for electricity distribution using renewable energy in rural communities. Communities with higher energy demand and higher population density can be supplied by micro-grids. These isolated grids are powered by renewable energy often in hybrid systems with diesel generators and deliver power directly to consumers.

Another option is the use of centralized battery charging facilities. Many rural people in developing countries are already accustomed to travelling long distances to charge lead-acid batteries. This service can be provided locally with a charging station powered by photovoltaic modules for example.

Perhaps the most wide spread model for rural electrification using renewable energy in the developing world is the solar home system (SHS). This distributed form of energy production generates electricity and stores energy on-site at the household of the consumer and is the subject of this study.

1.2 Solar Home Systems

Solar home systems consist of a photovoltaic (PV) array, a storage battery, a battery charge controller and electrical loads which provide services to system users. The system operates autonomously to provide a clean, quiet and convenient source of electrical power. Typical rural solar home systems utilize arrays less than 100W with 50W being typical. With this size of system, lighting devices utilizing energy efficient technologies such as light emitting diodes (LED) and compact fluorescent lamps (CFL), radios and small televisions (TV) can be powered.

Solar home systems have been recognized by international organizations such as the World Bank and national governments as cost-effective alternatives to grid extension

[7]. A pilot project started in 2000 supported by the Zambian Government introduced 100 solar home systems in the town of Nyimba. A study by Gustavsson reported that beneficiaries of this project, who participated on a fee for service basis, were satisfied with the services they received. The most popular applications of the systems were lighting and entertainment appliances such as TVs and media players. Notably, nearly half of the respondents expressed the opinion that it was children that benefited the most from the technology [2].

The impacts of solar home systems on quality of life and human development in rural areas is undisputed. The rate of solar home systems installation in developing countries will grow with reduced system cost. The prices of system components are continuing to fall. However the fastest way to reduce the cost of a system is to optimize its design. For this, it is essential to have a firm understanding of how these systems operate in the field to inform design improvements and innovations. To achieve this goal, accurate and detailed monitoring data is required.

1.3 Monitoring

The goal of solar home system monitoring is to acquire data on the energy flows within the system and relevant environmental parameters that affect system performance [8]. With this information, various system designs can be compared and sources of energy loss determined.

Various guidelines and standards exist for the performance evaluation of SHSs. For the purpose of comparing systems of different sizes, parameters normalized to the nominal array power are used [9, 10, 11, 12]. A deeper analysis accompanied by testing of individual system components can be used to estimate the magnitude of various loss mechanisms in systems such as charge controller voltage drops, battery efficiency and PV array capture losses due to various operating conditions.

1.4 Objectives

The objectives of this study are to characterize the operation of typical rural solar home systems, to quantify loss mechanisms and to formulate recommendations on the improvement of a SHS design and performance. This will be achieved through testing of individual system components by various standard methods and thorough monitoring of SHSs both in a controlled laboratory setting and in the field. Analysis of this data will be aided by the development of a model to predict optimal solar array performance.

1.5 Outline

The following chapter 2 will provide an introduction to SHS components and SHS design. Chapter 3 will address evaluation methods of SHS components. Chapter 4 discusses the monitoring system design process. A significant issue came up in the design of the monitoring system regarding a measurement error arising from the method of charge control utilized in most SHSs. This problem will be examined in detail and solutions offered in chapter 5. Chapter 6 develops a PV performance model that will be used in the subsequent chapter to analyze system energy losses. Chapters 7 and 8 contain in-depth analyses of monitoring data from laboratory and field located systems, respectively. Conclusions from these analyses regarding system performance and design will be contained in the final chapter.

Chapter 2

Solar Home Systems

2.1 Solar Home System Components

Solar home systems require three essential components: a photovoltaic generator to convert solar irradiation into electrical energy, a battery to store excess energy for times of low solar irradiation and electric appliances which constitute the load on the system. All but the smallest systems should also incorporate a charge controller to regulate the flow of current between system components and protect the battery from over-charge and deep-discharge [13]. Systems with which users desire to power AC appliances will also require a power inverter to convert from DC to AC current.

2.1.1 Photovoltaic Modules

The PV module utilizes the photovoltaic effect to convert incident solar radiation into electric current. A solar home system can be composed of one or many PV modules connected either in series or parallel depending on the desired system voltage. The interconnection of multiple modules is called a solar or PV array. Modules used in solar home systems are typically designed to charge 12V batteries. Higher system voltages can be obtained by connecting strings of parallel connected modules in series.

Module Properties

The current-voltage (IV) curve of a PV module describes many of the electrical properties of the module that determine its performance as an electric generator. Figure 2.1 shows an IV curve taken near standard test conditions (STC) in outdoor conditions of the 70W Helios module used in the laboratory based SHS. The shape of the IV curve describes the output current associated with each module voltage. At zero volts, the current is called the short circuit current (I_{sc}). When current is zero (when the circuit is open), the

module voltage is called the open-circuit voltage (V_{oc}). The product of the current and voltage at any point on the IV curve is the power generated at that voltage. The voltage and corresponding current that produce the largest power are called the maximum power point voltage (V_{MPP}) and current (I_{MPP})[14]. This point on the IV curve is called the maximum power point. The shape of the IV curve will have important effects on the module and solar home system performance.

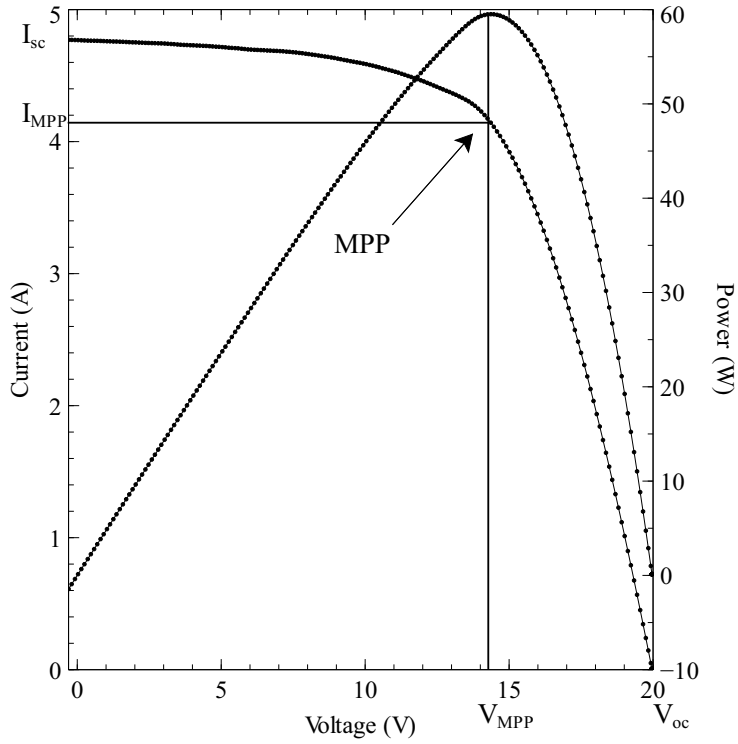

Figure 2.1: 70W Helios PV Module IV Curve

The manufacturer of the PV module provides several module characteristics that are useful in predicting the performance of the module. These nearly always include the short-circuit current, open-circuit current, and the maximum power point power, voltage and current. These values are obtained under the following standard conditions: 25 °C cell temperature, $1000W/m^2$ irradiation in the plane of array (POA) with the standard spectrum AM1.5 [15].

Environmental Impacts on PV Module Performance

Dependence on Irradiation The performance of a PV module depends upon the environment in which it is operating. The most obvious factor is the incident solar radiation. Higher levels of irradiation produce higher module output currents. The short-circuit current of the module is proportional to the incident solar radiation.

The incident irradiation is made up of two main components, diffuse and direct radiation. Sometimes the diffuse radiation is divided into diffuse and albedo radiation. Direct radiation is radiation arriving on the module directly from the sun. Diffuse radiation comes from solar radiation scattered in the atmosphere or reflected from the surrounding environment. When a distinction is made, albedo radiation is the ground reflected component of irradiance. On average, diffuse radiation represents about 30% of incident radiation in southern Africa [16]. This percentage is of course much higher on cloudy and overcast days and lower on clear days. Because direct radiation represents the majority of incident radiation on clear days, the orientation of the solar module will be important in increasing its surface area normal to incoming solar radiation.

The effect of incident solar radiation on the cell voltage is more important at low irradiance levels. The power output of a solar module can be considered approximately linearly related to incident irradiance above $800W/m^2$. Below this level the relationship is non-linear and leads to what is called low irradiance losses [17].

Dependence on Temperature The cell operating temperature also has an effect on the performance of solar cells. Solar cell voltage decreases linearly with increasing cell temperature. Temperature effects on cell current is positive but small and can typically be neglected. The power output of a solar module is therefore negatively affected by high operating temperatures [18, 19].

Shading Because PV modules are composed of strings of many series connected solar cells, it is important to avoid shading any of the modules' cells. Shading of just one cell in a string will cause a significant reduction in module output. The series connection of cells means the reduction in a single cell's current will limit the current of the entire string [20].

2.1.2 Batteries

Because of the variability of solar radiation, it is essential to have a means of energy storage for times of low irradiance, particularly during the night. Energy storage often represents the highest cost in a solar home system over its lifetime [21]. One of the only storage methods currently available that is suitable to small solar home systems is the secondary battery that converts electrical energy to chemical energy. This process can be reversed to use the stored energy when required.

While there are several secondary battery technologies available which can be used in solar home systems, the most common found in small solar home systems is the lead-acid battery [22]. Lead-acid batteries used in solar home systems are usually composed of six

series connected $2.1V$ cells giving a battery voltage of $12.6V$. Higher system voltages are sometimes desired and can be obtained by connecting two $12V$ batteries in series. Deep cycle batteries designed for deep discharge cycling should be utilized. Standard car batteries will not be able to sustain the repeated deep discharge demanded by solar home systems [23].

Battery Characteristics

The amount of charge a battery can store is measured in amp-hours (Ah). Multiplication by the battery's nominal voltage will give roughly the energy storage capacity. Manufacturers rate battery capacity for different discharge rates. Batteries used in SHS applications are typically rated at the C_{20} or 20 hour rate. Discharged at constant current over 20 hours, the battery will discharge its rated quantity of charge. Ratings are specified for batteries at 25 °C.

For example, a 100Ah C_{20} battery will discharge 5A over 20h at 25 °C before reaching zero state of charge. Batteries discharged at higher rates and at lower temperatures will produce less total charge[23]. The state of charge (SOC) of a battery refers to the percentage of charge remaining of its full capacity. Conversely, depth of discharge (DOD) refers to the percentage of charge capacity already discharged. Battery lifetime is typically specified as the number of charge/discharge cycles to a certain depth of discharge (DOD) the battery can endure before its capacity will fall below a certain percentage of its rated capacity. Higher depth of discharge reduces battery lifetime as do higher battery temperatures. As a rule of thumb, battery lifetime is cut roughly in half by an increase of operating temperature of 10 °C. Battery capacity is negatively affected by low temperatures. The optimal battery operating temperature is around 25 °C [24].

The efficiency of a battery for energy storage is slightly lower than its efficiency as a charge storage device. The battery's ability to store charge is characterized by its coulombic efficiency which is around 90%. Coulombic efficiency is very high at low SOC but decreases as the battery nears high SOC due to the electrolysis of water. The energy efficiency of the battery is around 75%. This means that a battery during a full discharge will produce 90% of the total amp-hours required to charge it but only 75% of the energy, usually measured in watt-hours (Wh) [25]. This discrepancy is due to the difference in charge and discharge voltages. The battery is charged at a higher voltage than the voltage at which it is discharged. There will then be a loss of energy, equal to the time integral of the product of current and voltage, even if the coulombic efficiency is 100%. The energy efficiency of a lead-acid battery will be the product of the energy efficiency multiplied by the ratio of discharge voltage to charge voltage [26].

Battery Maintenance and Charging

Batteries in solar home systems are typically the first components requiring replacement. While PV modules will perform satisfactorily for 25 or more years, lead-acid batteries have a much shorter service life. A study on the long term monitoring of solar home systems in Thailand found an average lifetime for initially installed batteries of 50 months [27]. Various factors affect the lifetime of the battery and proper battery maintenance and charging can extend battery life and reduce system costs.

Proper maintenance of lead-acid batteries requires regular charging while avoiding overcharge and excessive deep discharge. When left in a partially charged state, lead acid batteries undergo sulfation. Sulfation, the formation of large lead sulfate crystals on the negative electrode, can lead to permanent loss of capacity. The process of sulfation is accelerated when batteries are discharged too deeply. On the other hand, overcharging causes excessive gassing which accelerates water loss leading to increased maintenance demands and can cause the loss of active material on the electrodes resulting in permanent damage to the battery [23].

An appropriate charge algorithm along with a low voltage disconnect (LVD) mechanism can reduce the risk of battery performance losses. Most solar charge controllers utilize a three stage charge routine. In the first stage, referred to as bulk charge when the battery is in a low state of charge, the battery accepts all of the charge current produced by the solar array. When the battery voltage reaches its gassing voltage (approximately $14.4V$ at $25\,^{\circ}\mathrm{C}$ with a temperature coefficient of about $-3mV/cell/\,^{\circ}\mathrm{C}$ for series connected battery cells), the charge current is regulated in such a way as to maintain the battery voltage just below the gassing voltage [28]. This stage, called constant voltage charging, occurs when the battery has achieved about a 75% SOC. When the battery has reached it's full SOC, it is then maintained against self discharge with a small "float" charge [29].

Many charge controllers also include an equalization charge functionality. Over time, the acid in the battery becomes stratified with high concentrations of acid at the bottom of the battery which provokes sulfation. This can lead to mismatch between cell voltages. A periodic equalization charge raises the battery voltage to provoke a short period of gassing at the electrodes. This gassing serves to stir up the acid and combat stratification and also helps to equalize cell voltages [30, 31].

2.1.3 Charge Controllers

The charge controller serves to protect the system's battery from damage due to overcharge and deep discharge. There are two groups of charge controllers, those with maxi-

mum power point tracking (MPPT) and those with direct battery coupling. Most small solar home systems use direct battery coupling.

The MPPT uses an algorithm to track the maximum power point (MPP) of the PV array and maintain the array voltage at MPP. This increases the power output of the PV array but in most cases will shift the array voltage away from the optimal battery voltage. A DC to DC converter is built in to maintain the battery at the proper voltage [32].

The charge controllers (Steca Solsum 6.6 and Steca Solarix Gamma) utilized in this study couple the PV array directly to the battery. The PV array voltage is dictated by the battery voltage which varies depending upon the battery's SOC. Because of this, the PV array does not normally operate at its MPP. Figure 2.2 shows an IV curve for a battery and a PV module. Under the conditions in which the IV curves were measured, the intersection of the two curves represents the operating point of the system. The blocking diode in the Solsum controller, that will be discussed later, adds a $0.3V$ voltage drop between the PV module and the battery. This will shift the battery curve $0.3V$ to the right and in many cases push the module further from its MPP.

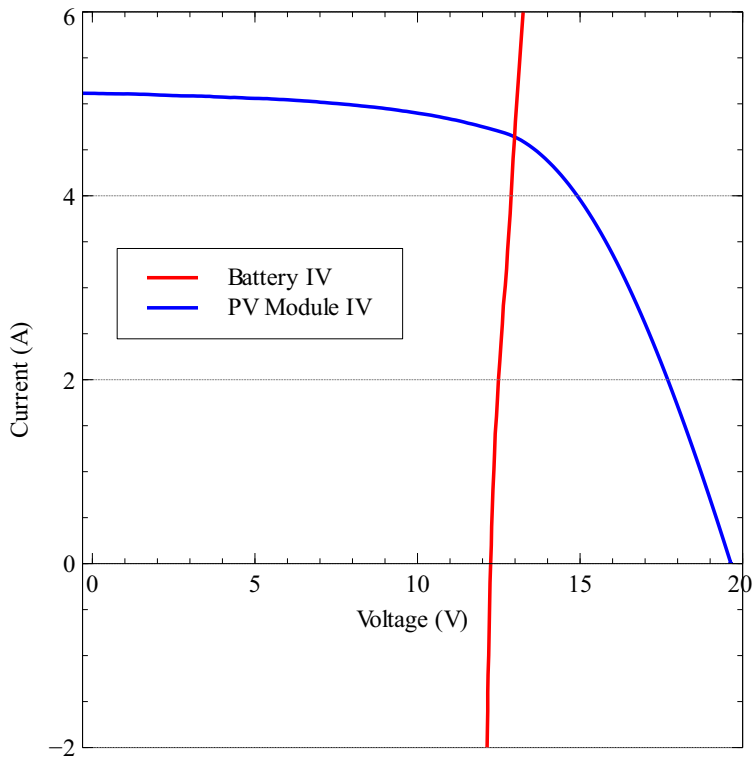

Figure 2.2: Battery and PV IV curve intersection

Over-charge protection

In order to protect against over-charging the battery, the charge current supplied by the PV array is regulated in such a way as to maintain the battery voltage just below its gassing voltage. Before the battery reaches this voltage, current is allowed to flow unregulated into the battery. Both charge controllers used in the study specify set points of 14.4V to trigger the regulation of charge current. Because the gassing voltage of the battery is sensitive to temperature, the controllers also measure the temperature of the environment in which it is installed and adjusts the set point by -3mV/cell/ °C for any deviation from 25 °C [28].

Most modern charge controllers without MPPT use a technique called pulse width modulation (PWM) to regulate the effective charge current. The charge controller chops the charge current into pulses at a fixed frequency. The duty cycle of the pulse determines the effective charge current. The controller adjusts the duty cycle to maintain the battery at the desired voltage. The duty cycle of PWM is the ratio of the time on pulse to the length of the duty cycle period. In figure 2.3 the duty cycle will be equal to t/T where t is the time on pulse and T is the period of PWM.

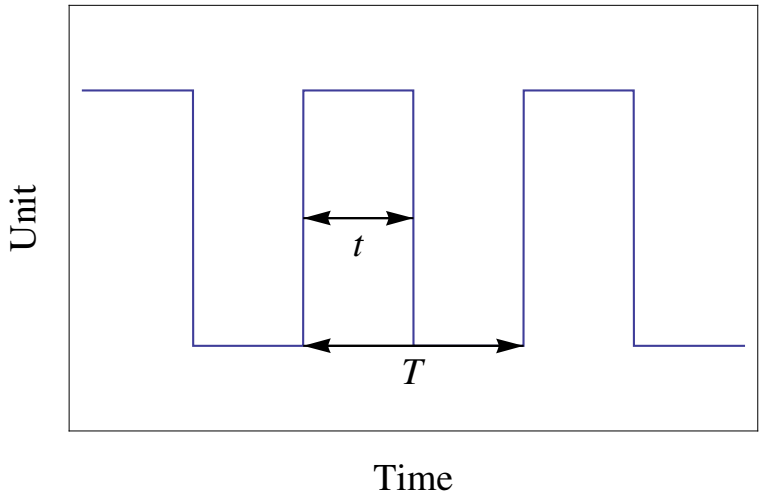

Figure 2.3: Duty Cycle Illustration

Deep-discharge protection

Charge controllers for solar home systems should also have a low-voltage disconnect feature to protect the battery from deep discharge. A low voltage disconnect function usually disconnects the loads on the system when the battery falls below a certain voltage. More advanced controllers such as the Steca Solarix series use a fuzzy logic algorithm to adapt set points to a particular battery in order to more accurately determine its state

of charge than by simple set points [33]. The Solsum 6.6 controller uses a set point of 11.1V for low voltage disconnect while the Solarix controller disconnects the load when it has determined the SOC of the battery is less than 30%.

Reconnection of the load usually occurs when the battery shows a steady voltage above a certain set point or in the case of the Solarix controller a certain SOC. This voltage is set at 12.6V for the Solsum and 50% SOC as determined by the fuzzy logic algorithm for the Solarix.

Series and shunt charge controllers

During the constant voltage charging stage when charge current undergoes PWM, the charge current from the solar array must be either diverted or stopped between pulses. Both approaches are used in modern PWM charge controllers. Controllers that divert the current through a shunt are called shunt controllers and those that open the circuit halting the current altogether are called series controllers [32, 31].

Both charge controllers used in this study are shunt type controllers. When the charge current is disconnected from the battery it is shunted through the controller bringing the solar array into a short-circuit state. The ability to be short-circuited without harm is unique to photovoltaic generators.

Each technique has advantages and disadvantages. The series controller causes much larger variation of current from the PV array. This rapid periodic change in current can cause problems with electromagnetic compatibility (EMC). Because most electric generators cannot be short-circuited without causing harm to the device, shunt controllers are only appropriate for use in PV systems. The high currents drawn from PV arrays when short-circuited can also increase the risk of development of hot spots on the solar modules [32].

Charge controller ratings and circuit protection mechanisms

Charge controllers are rated by the amount of current they can safely handle. Charge controller designs depend in part upon their current ratings. Most charge controllers incorporate components to protect the charge circuit from polarity reversal at inputs and from excessive currents. The Steca controllers used in this study include varistors across positive and negative PV array inputs to protect against high voltages caused by lightening strikes, for example.

Reverse-current protection

Reverse-current protection is also an almost universal feature of charge controllers. During the night when the irradiance is nearly zero, the battery can discharge through the solar array without proper protections. The charge controllers used in this study use two different methods which affect the overall efficiency of the charge controller. The Solsum controller uses a blocking diode on the positive terminal of the solar array input. This design is simple but the associated voltage drop of the diode decreases the energy efficiency of the controller and pushes the charging voltage of the solar array closer to open-circuit voltage. The displacement of the charging voltage can be positive or negative depending upon the position of the maximum power point on the IV curve.

The Solarix controller replaces the blocking diode with a MOSFET (metaloxidesemiconductor field-effect transistor) on the negative solar array input. This MOSFET opens the circuit when there is no incoming PV current and must operate in coordination with the shunting MOSFET during PWM to prevent a short-circuit of the battery. This design eliminates the voltage drop due to the diode and replaces it with a small ohmic voltage drop. At low current, this voltage drop will be smaller and consequently more efficient than a diode voltage drop. Below about 30A, the MOSFET design has a smaller voltage drop than the diode.

2.1.4 Inverters

The systems studied in this work do not utilize power inverters. However, if it is desired to power AC loads with a solar home system, a power inverter will be required to convert DC current to AC current. There is a large variety of power inverters on the market today, all with varying efficiency and power ratings. It is necessary to use an inverter that has a power rating higher than the maximum expected instantaneous load. One must also keep in mind however that inverters are less efficient when powering loads much smaller than their rated power.

2.1.5 Loads

Loads are the electrical appliances that consume the energy produced by the solar array and stored in the battery. The amount of power drawn by loads can be derived from its IV curve.

Typical SHS Loads

Typical SHS loads consume low power and provide services such as lighting and access to media. Various lighting technologies will be discussed in this section. Common appliances to connect rural residents to outside media like TVs and radios will also be discussed. Figure 2.4 depicts the IV characteristics of these loads.

Incandescent Lights Incandescent light bulbs are not ideal for solar home systems because of their high energy consumption. However the technology is widespread and it is not uncommon to see them used in rural SHSs. It is preferable to use other lighting technologies such as compact fluorescent lamps or light emitting diodes which have much higher luminous efficacies. The luminous efficacy of an incandescent bulb is in the range of 10-17 lm/W [34].

While LEDs and CFLs are more expensive than incandescents, a technology first demonstrated in 1879 [35], the decreased energy requirement significantly reduces the size and cost of the system and far out weighs the difference in cost of the bulbs. An incandescent bulb is an ohmic load. That is, the voltage applied to the load is proportional to the current drawn where the constant of proportionality is the load's resistance. It can be seen from figure 2.4 that this is not precisely true. This will be discussed in chapter 3 on the evaluation of SHS components.

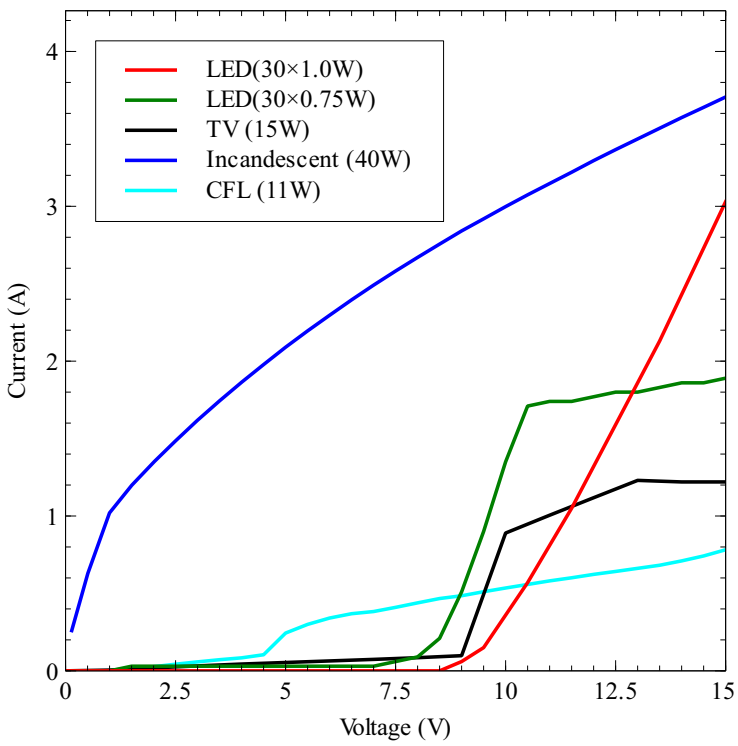

Figure 2.4: IV curves of various loads

Compact Fluorescent Lamps CFLs are a much more appropriate technology for use in solar home systems. Their energy consumption is about five times less than an equivalent incandescent bulb with luminous efficacies in the range of 50-70 lm/W [34]. Rated lifetimes are typically eight times longer than that of incandescent bulbs as well making them an overwhelmingly more economical choice in the long term [36]. CFL bulbs are not ohmic loads but can be seen as nearly so within the range of normal operating voltage. The current drawn by a CFL is regulated by an electronic ballast to prevent runaway currents resulting from the ionization of the mercury gas inside the bulb[36].

Light Emitting Diodes LED lamps offer energy savings even above those of the CFL. They have luminous efficacies in the range of 60-92 lm/W. In addition, LEDs have significantly longer lifespans, typically 3.5-5 times longer than CFLs [34]. While their cost is decreasing, it is still a more expensive technology than CFLs and in less widespread use. Table 2.1 summarizes the characteristics of the lighting technologies discussed here.

Table 2.1: Properties of various lighting technologies [34]

Technology	Luminous efficacy (lm/W)	Lifespan (hours)
Incandescent	10-17	750-2,500
CFL	50-70	10,000
LED	60-92	35,000-50,000

Small Televisions and Radios Appliances such as televisions and radios connect rural people to the outside world. They bring news, entertainment and educational programming that improves standards of living and has educational and social value as well. Radios without large speakers have low energy consumption. Small 13 inch black and white televisions are typically rated at 15W. Larger screens and color increase energy consumption.

2.1.6 Wiring

Proper wiring is also important in solar home systems. Smaller gauge wires have higher resistance and if not properly sized can result in high voltage drops and energy losses. Wire gauge depends upon anticipated currents and line lengths. Voltage drops are determined by Ohm's law with line resistance depending on the resistivity, the length and the cross section area of the conductor. This can be summarized by

$$V_{drop} = I \cdot \rho \cdot \frac{\ell}{A} \tag{2.1}$$

where I is the current flowing through the conductor, ρ is the resistivity of the conductor and ℓ and A are the length and cross sectional area of the conductor, respectively.

2.2 Solar Home System Design

2.2.1 Load Energy Requirements

Before determining the necessary components of a solar home system, it is required to determine what the system will be used for and how much energy will be required. To do so one needs the power rating of the appliances to be used and the amount of time during which the appliances will be employed. For example, a 13W CFL running for 2 hours will consume 26Wh. For small SHSs, it is usually sufficient to simply add up the energy requirements of all the anticipated loads over a typical day. Larger systems with critical loads require the construction of a load profile detailing energy consumption over a period of time and more complex design techniques.

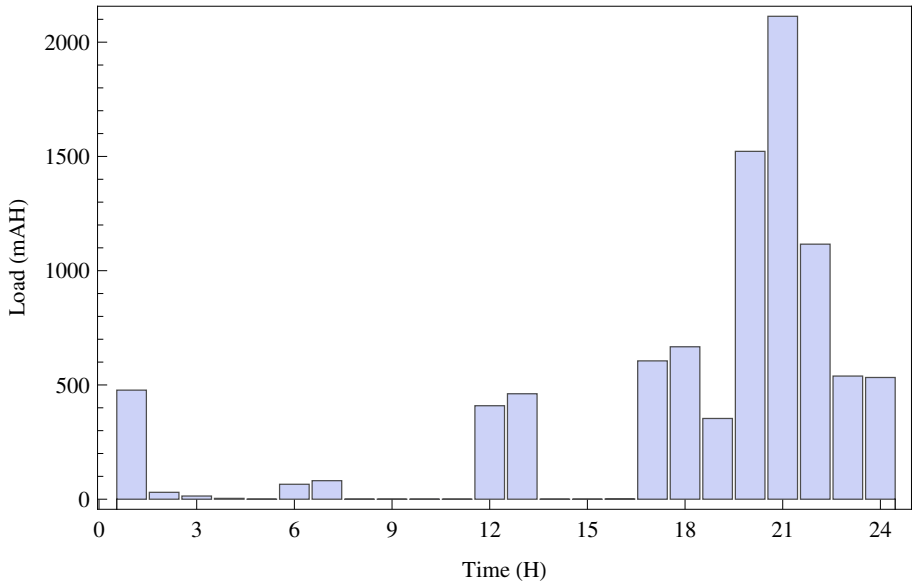

Figure 2.5: Average load profile of solar home system in New Brighton Township over 10 day period

Figure 2.5 depicts the average daily load profile of a solar home system in New Brighton township near Port Elizabeth. The load current was logged over a period of ten days and hourly charge totals in amp-hours were calculated and averaged over corresponding hours of the day. The energy profile can be approximated by multiplying the current values by the nominal system voltage of 12V. The resulting load profile describes how the user typically uses their SHS. If it is possible to directly measure the load profile through the monitoring of current energy consumption, a more accurate load estimation

can be obtained. This is often not possible, particularly when the potential user has no access to electricity. In this case it is necessary to estimate the energy requirements of the SHS user. In designing the system installed for this project in Tyefu, Eastern Cape, it was required to make a rough estimate of energy requirements. The system was to be used only for lighting. The rural home consists of four rooms: two bedrooms, a kitchen and a lounge. The resident also requested an outdoor light to illuminate her front porch at night and a lamp for her nearby rondavel (a circular hut).

Because the rondavel was to be used typically for guests which are not always present, two load profiles were created, one for weekdays and a second for weekends when the rondavel is occupied by a guest. The estimated load profiles used in the design of the system can be found in tables 2.2 and 2.3.

Table 2.2: Estimated Weekday Load Profile - Tyefu

Load	Bedroom 1	Bedroom 2	Lounge	Kitchen	Rondavel	Outdoor	Total
Hour	Watt-hours						
0	0	0	0	0	0	15	15
1	0	0	0	0	0	15	15
2	0	0	0	0	0	15	15
3	0	0	0	0	0	15	15
4	0	0	0	0	0	15	15
5	0	0	0	0	0	15	15
6	13	0	0	13	0	0	26
7	0	0	0	0	0	0	0
8	0	0	0	0	0	0	0
9	0	0	0	0	0	0	0
10	0	0	0	0	0	0	0
11	0	0	0	0	0	0	0
12	0	0	0	0	0	0	0
13	0	0	0	0	0	0	0
14	0	0	0	0	0	0	0
15	0	0	0	0	0	0	0
16	0	0	0	0	0	0	0
17	0	0	0	0	0	0	0
18	0	0	0	0	0	15	15
19	0	0	13	13	0	15	41
20	0	0	13	13	0	15	41
21	0	6.5	13	0	0	15	34.5
22	13	0	0	0	0	15	28
23	0	0	0	0	0	15	15
Daily Total	290.5Wh						

The system should be designed to sustain the average daily load on the system. The battery bank provides a buffer for days with high load or low insolation. On a day during

Table 2.3: Estimated Weekend Load Profile - Tyefu

Load	Bedroom 1	Bedroom 2	Lounge	Kitchen	Rondavel	Outdoor	Total
Hour	Watt-hours						
0	0	0	0	0	0	15	15
1	0	0	0	0	0	15	15
2	0	0	0	0	0	15	15
3	0	0	0	0	0	15	15
4	0	0	0	0	0	15	15
5	0	0	0	0	0	15	15
6	13	13	0	13	0	0	39
7	0	0	0	0	0	0	0
8	0	0	0	0	0	0	0
9	0	0	0	0	0	0	0
10	0	0	0	0	0	0	0
11	0	0	0	0	0	0	0
12	0	0	0	0	0	0	0
13	0	0	0	0	0	0	0
14	0	0	0	0	0	0	0
15	0	0	0	0	0	0	0
16	0	0	0	0	0	0	0
17	0	0	0	0	0	0	0
18	0	0	0	0	0	15	15
19	0	0	13	13	0	15	41
20	0	0	13	13	0	15	41
21	0	6.5	13	13	0	15	47.5
22	13	0	0	0	13	15	41
23	0	0	0	0	13	15	28
Daily Total	342.5Wh						

which the rondavel is in use, it was estimated that $343Wh$ would be consumed by the loads. On other days the load was predicted to be around $291Wh$. The load profile is based on two days heavy load on the weekend and five days lighter load during the week without visitors. The average load during the week is $306Wh$.

2.2.2 Solar Resource Assessment

The next step in designing a solar home system is to determine the local solar resource. Solar resource data is usually collected as the global irradiance (W/m^2) on a horizontal surface and is presented as the average daily insolation (kWh/m^2) for each month. This value is often called the number of sun hours in a day since PV modules are rated under irradiation of $1kW/m^2$.

It is seldom the case however for a SHS PV module to be mounted horizontally to the

earth. Much more useful information would be provided by values over a range of north facing (in the southern hemisphere) array tilts. Table 2.4 gives average monthly global irradiation values over a range of array tilts in Tyefu, Eastern Cape, South Africa.

Global horizontal and diffuse insolation data for the site were obtained from the meteorological reference software Meteonorm. This data was then used to calculate the POA insolation for various array tilts. For these calculations, the ground albedo (the ratio of reflected radiation to incident radiation in the environment surrounding the PV array) was estimated to be 0.26 [16]. From table 2.4 it can be observed that with a tilt of 45 or 50 degrees from horizontal, the minimum monthly insolation value during the year is lowest. This is the optimal tilt for a stand-alone SHS because it has the "best" worst month. The system will need to be designed to support the load during the month with the lowest insolation if year round use is desired. In this case the worst month is June for a 45 degree tilt and October for a 50 degree tilt with an average daily insolation of $5130Wh/m^2$. Shorter day light hours and colder weather in winter months such as June typically mean longer use of system loads such as lighting and entertainment appliances. Because of this, a 50 degree array tilt is preferred to a 45 degree tilt because of higher insolation in the winter months.

2.2.3 PV Array Sizing

With knowledge of the daily load and insolation, the required size of the PV array can be deduced. Ideally, the energy produced by a PV module with a rated power of P_{peak} will be

$$E_{PV} = h_{sun} \cdot P_{peak} \tag{2.2}$$

where h_{sun} is the average number of sun hours per day during the critical design month when insolation is the lowest. This however is not the case and various system losses will occur from low irradiance effects, temperature effects, DC system losses, non maximum power point tracking and battery storage losses.

DC System Losses Some electrical energy is always lost in transmission without super-conduction. There will therefore be losses in the DC circuit due to conductor resistances and, with some charge controllers, diode voltage drops. The magnitude of these losses will vary depending on the wire gauge and lengths used in the system as well as the charge controller design.

Systems are usually designed so that voltage drops are limited to at most 2%. Charge controller losses are linearly dependent on the resistance of circuit conductors and may include a diode voltage drop. A controller with a 0.3V voltage drop is roughly equal to

Table 2.4: Average sun hours per day on a north facing tilted surface in Tyefu, South Africa

Deg.	JAN	FEB	MAR	APR	MAY	JUN
0	6550	6100	5220	4240	3400	2860
5	6570	6170	5370	4480	3740	3200
10	6560	6220	5480	4700	4060	3530
15	6510	6220	5570	4890	4360	3840
20	6430	6200	5630	5050	4620	4130
25	6320	6150	5660	5180	4860	4390
30	6170	6060	5650	5290	5070	4620
35	6000	5950	5620	5360	5250	4820
40	5790	5800	5560	5400	5400	4990
45	5560	5630	5470	5410	5510	5130
50	5300	5430	5360	5390	5580	5240
55	5020	5200	5210	5340	5620	5310
60	4720	4950	5040	5260	5620	5350
65	4390	4680	4840	5140	5590	5350
70	4050	4370	4590	4940	5440	5230
75	3700	4040	4290	4670	5180	5010
80	3350	3700	3960	4340	4840	4700
85	3010	3340	3590	3940	4410	4290
90	2670	2970	3180	3450	3830	3730
Deg.	JUL	AUG	SEP	OCT	NOV	DEC
0	3240	3930	4790	5520	6500	6900
5	3610	4220	4960	5610	6530	6900
10	3970	4480	5110	5670	6530	6870
15	4300	4710	5240	5710	6500	6800
20	4600	4920	5330	5710	6430	6700
25	4880	5100	5400	5680	6330	6570
30	5120	5250	5440	5630	6200	6400
35	5340	5370	5440	5550	6040	6210
40	5510	5450	5420	5430	5850	5980
45	5650	5500	5370	5300	5630	5730
50	5760	5520	5290	5130	5380	5450
55	5820	5510	5180	4940	5120	5150
60	5850	5460	5040	4730	4820	4830
65	5840	5370	4870	4490	4510	4490
70	5700	5190	4640	4210	4180	4130
75	5440	4920	4350	3910	3830	3780
80	5100	4580	4030	3590	3480	3420
85	4640	4160	3650	3240	3130	3080
90	4030	3620	3210	2870	2790	2760

a 2% loss of energy in a 12V system. A typical estimation for DC losses is 5%.

Battery Losses As previously discussed, lead acid batteries have energy efficiencies of around 75%. Any power being drawn from the battery will incur this loss. Because the Tyefu system is designed uniquely for lighting, it will normally operate after dark when there is no incoming PV power. All of the power drawn by loads will thus incur battery losses.

Temperature Losses Crystalline silicon PV module output degrades by about 0.4%/ °C for cell temperatures in excess of 25 °C [37]. This loss is more difficult to predict accurately. The California Energy Commission recommends a de-rating factor of 0.89 when evaluating temperature effects [38]. This depends highly upon the operating environment of the module of course and can be more accurately accounted for with PV design software which uses more complex cell temperature models.

Low Irradiance Losses At low irradiance levels, the module power output can no longer be considered proportional to irradiance because irradiance effects on PV module voltage become important. These losses usually occur in the morning and evening for non-tracked systems and on overcast days. For non-tracking systems, the high angle of incidence for incident irradiance reduces the area for the array normal to incoming radiation and increases the reflection of radiation off of the array. These losses are more difficult to account for without modelling software and are often neglected as insignificant [39].

Non MPP Tracking Losses Losses due to array operation away from its MPP also introduce losses. These losses are also difficult to account for without more complex methods as they depend highly upon the PV array and system characteristics. The variation depends both on the module IV characteristics and environmental conditions. Systems with batteries in low states of charge typically experience larger losses of PV power.

Chen et al. [40] found that power gained by using an MPPT charge controller rather than a directly coupled controller during the winter were 14.1% in Beijing but only 3.8% in Guangzhou. Gains in the summer were actually found to be negative in both instances, most probably due to the lower efficiency of MPPT controllers and lower MPP voltages in the hotter climate [40]. The climate in the Eastern Cape is relatively temperate throughout the year. It would probably be most similar to the winter climate in Guangzhou. A rough estimate of non-MPPT tracking losses might be 5%.

It is also possible and often preferred to size the PV array based on calculations of current and charge. Because, in most cases, the operating current of the PV module lies between I_{sc} and I_{MPP}. By utilizing I_{MPP} rather than P_{MPP} in array sizing, MPPT losses no longer need to be considered. Because the PV current is likely to be slightly higher than I_{MPP}, the system will automatically be slightly oversized. This also eliminates the need for temperature considerations due to the negligible effect of temperature of PV current. This technique however is only valid for directly coupled systems without a DC to DC converter like those found in MPPT controllers.

Taking into account temperature, battery, DC and non-MPPT losses, we can determine the required array size by

$$P_{peak} = \frac{P_{load}}{\eta_{bat} \cdot \eta_{DC} \cdot \eta_{temp} \cdot \eta_{MPPT} \cdot h_{sun}}. \tag{2.3}$$

For the Tyefu system we estimate a required array of

$$94.1W = \frac{306Wh}{0.75 \cdot 0.95 \cdot 0.89 \cdot 0.95 \cdot 5.13h}. \tag{2.4}$$

From this simple calculation, it was determined two 55W mono-crystalline Siemens modules would be sufficient to power the predicted load.

One last important parameter to consider in system design is the array to load ratio (A:L). The A:L ratio is the average daily PV array energy divided by the average daily load during the worst case month. An appropriate A:L ratio ensures good battery health and lifespan. Low A:L ratios indicate battery operation at low SOC and long recovery periods from deep discharge which degrades battery service life. A:L ratios of 1.1 are commonly viewed as acceptable, however, Dunlop and Farhi recommend A:L ratios of 1.3 or more [24]. Taking into account PV losses, the predicted A:L ratios of this system is 1.5. By this measure, the size of the PV array should ensure acceptable battery life.

2.2.4 Battery Storage Sizing

In sizing the battery storage of the system, the number of days of system autonomy must be considered in conjunction with the predicted load on the system. In other words, the battery storage must be able to power the load for a desired number of days with no PV power. The number of days of autonomy will depend largely on the local climate. For Tyefu, three days of battery storage were viewed as sufficient. A balance must be struck between the loss of load probability and the cost of the system. Designing a system for a very low loss of load probability will result in a system with a very large and expensive battery bank.

Three days of energy to power the predicted load of $306Wh$ gives a requirement of $918Wh$. Batteries are typically rated in amp-hours so we will need to divide this value by the nominal battery voltage of $12V$ giving 76.5Ah. Our charge controller disconnects the load at 30% SOC to protect against deep discharge so our 76.5Ah must be equivalent to 70% DOD. By dividing our 76.5Ah by 0.70 we find a minimum battery capacity of $109.3Ah$ is required. It was decided to use two 65Ah batteries connected in parallel for a total battery capacity of $130Ah$. The following formula summarizes the battery sizing procedure:

$$C_{battery} = \frac{(E_{load}/12V) \cdot d_{auto}}{DOD} \tag{2.5}$$

where d_{auto} is the number of days of autonomy and E_{load} is the daily average load in Wh.

2.2.5 Charge Controller Selection

The selection of the charge controller will depend largely on the maximum anticipated PV and load currents. The controller should be rated at least 125% of the array's rated short-circuit current and should also exceed the maximum expected load current [41]. The Tyefu modules are rated at 3.15A short-circuit. The charge controller should then be rated above $2 \times 3.15A \times 1.25 = 7.88A$. The maximum load on the system with five 13W CFLs and one 15W CFL is 80W/12V = 6.7A. A minimum 8A charge controller is required for this system.

Different charge controller designs implement various different features that may be considered in the selection process. Some such features are maximum power point tracking and daylight timers. In the case of the Tyefu system, it was desired, for scientific purposes, to use a shunt type directly coupled charge controller. An 8A controller of this type was not locally available so a 12A controller was selected.

2.2.6 Wiring, System Placement and other Considerations

Wiring

System wiring must be selected to prevent large voltage drops and energy losses along lines. Wires carrying larger currents should be of higher gauge than lines carry low current because the higher currents result in larger voltage drops. Large voltage drops on load lines can cause loads to function improperly or, on PV lines, force the solar array to operate too close to V_{oc} resulting in large energy losses. The rondavel in the Tyefu system is located approximately 15m from the main house and because of this it was decided to use a larger gauge wire to connect the rondavel load with the distributor board.

Shading

Care should also be taken to ensure that the solar array will not be shaded at any time during the year. A module that is unshaded in the summer months when the sun passes high in the sky will not necessarily be unshaded in the winter when the sun passes at lower altitudes. In the case of Tyefu, the local environment is not heavily vegetated so shading is not a large concern. Care was however taken to ensure that the array was mounted high enough that passers by would not cause shading.

Mounting

The array for the Tyefu system is mounted on a free standing pole which provides for the easy passage of wind over the modules providing a cooling effect. Some solar home systems are roof mounted and because of the temperature sensitivity of solar cells, efforts must be made to provide for proper ventilation and temperature control.

Battery Placement

Battery performance and lifetime is highly temperature dependent. It is important to keep batteries in a cool and safe location. Battery lifetime decreases drastically with increased temperature and also decreases the cell gassing voltage. Temperature compensated charge controllers can prevent excessive gassing but the lower charge voltage can result in incomplete charges and battery capacity loss. If the gassing voltage is not compensated for temperature and excess gassing does occur, the release of hydrogen gas can result in dangerous conditions for the system's users.

2.2.7 System Modelling Software

There is a variety of commercially available software to aid in system design and modelling. These software packages include more sophisticated models to predict system performance based on device characteristics and meteorological models. One such program is PVSol. Results of system simulations for both systems studied in this work can be found in appendix A. The simulations predict a solar fraction of 83.2% and a performance ratio of 42.5% over a one year period. The solar fraction is the percentage of energy demand met by the solar generator. For a stand-alone system, this means that 83.2% of the energy demand will be met with the remaining demand not being fulfilled due to load shed. The performance ratio is a measure of system performance that will be discussed fully in chapter 7.

2.3 Summary

Solar home systems are composed of three essential components: a PV array, battery storage and system loads. Most systems will also incorporate a charge controller and, if AC power is desired, a DC to AC power inverter. The design of a system will depend on the energy requirements of the loads on the system and the environment in which the system is operating. An optimally designed system will meet the requirements of system loads while minimizing the life cycle cost of the system. This requires a balance between minimizing array size and maximizing battery life. The design process is complicated by various energy losses in the system which must be accurately assessed. These include low irradiance losses, temperature effects on both the battery and PV array, line losses and charge controller losses and losses due to non MPP tracking if a charge controller without MPPT is selected. The design process can be aided by various software tools. The components selected for the Tyefu SHS are summarized in table 2.5. Ultimately, quality of the system design will rely upon the accuracy of the information used in the design process and the skill and expertise of the system designer.

Table 2.5: Tyefu System Specifications

Component	Name	Quantity
PV Array	55W mono-crystalline Siemens PV module	2
Battery Bank	65Ah Deep Cycle Lead Acid Battery	2
Charge Controller	Steca Solarix Gamma (12A)	1

Chapter 3

Solar Home System Components Evaluation

3.1 PV Module

Many of the electrical properties of a PV module can be determined by examination of its IV curve beyond basic parameters such as I_{sc}, V_{oc}, and MPP values. The shape of the IV curve, along with the IV curves of the battery and loads determines the operating voltage of the PV array in a directly coupled system.

3.1.1 IV Curves

The IV curves in figure 3.1 for the $70W_p$ Helios H800b module used in the laboratory based system were taken at different times under different irradiance and module temperatures. Both temperature and irradiation effects can be observed. The large decrease in V_{oc} from the IV taken at $1075W/m^2$ to the one at $1000W/m^2$ is caused by the higher module temperature while the increase in I_{sc} is attributed to the rise in irradiance. There is also a smaller but observable difference in V_{oc} between the curves taken at $1075W/m^2$ and $916W/m^2$ which have a module temperature difference of only 2.6 °C. The I_{sc} and V_{oc} values obtained from the IV curves follow the order of the POA irradiance and the reverse order of module temperature respectively as expected. The module V_{oc} also has a significant irradiance dependence but only becomes important at low irradiance below $800W/m^2$.

The maximum power of the module was extracted from an IV curve measured near STC at 25.1 °C back of module temperature and $1000W/m^2$ and was found to be 59.5W. This was achieved under outdoor conditions by cooling the module with water as the irradiance approached $1000W/m^2$. This is lower than the 70W module rating supplied

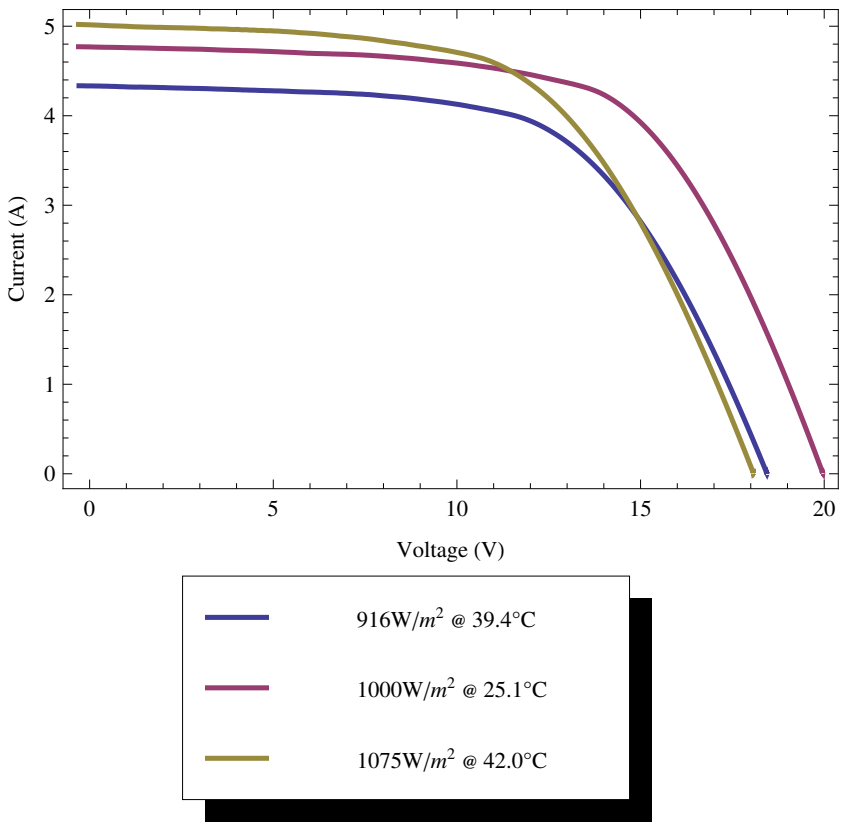

Figure 3.1: 70W Helios PV module IV curves

at STC. Modules are typically guaranteed to produced at least 80% of rated power over 20 - 25 years. At 85%, this module is still operating within this range.

The IV curve was not taken under AM1.5 but deviations from this standard cannot be corrected for without information about the spectral response of the module and the spectrum under which the measurements were taken. To correct for temperature, an adjustment of $-2.3mV/cell/\,^{\circ}\mathrm{C}$ is made to the module voltage for crystalline silicon cells [37]. This is a theoretically calculated temperature coefficient. The temperature coefficient of this particular module was determined experimentally to be $-1.8mV/cell/\,^{\circ}\mathrm{C}$ as will be discussed in more detail in chapter 6. The theoretical temperature coefficient for this module of 36 series connected cells is $-82.8mV/\,^{\circ}\mathrm{C}$. This temperature correction is only valid when irradiance effects on module voltage are considered to be small above $800W/m^2$. Module current is linearly related to irradiance. Temperature has a small positive effect on PV current but is small enough to be neglected. To correct the measured MPP power for irradiance, it must be multiplied by a factor of $1000W/m^2$ divided by the measured irradiance. Table 3.1 lists the measured maximum power point performance parameters for this module.

It can be seen from table 3.1 that the module is not performing at its rated power. The

Table 3.1: Maximum Power Point Performance Parameters

	I_{MPP}	V_{MPP}	P_{MPP}
Measured	4.143A	14.36V	59.5W

slope of the IV curve near V_{oc} indicates a high series resistance (R_s). This may in part be due to the measurement being made at the end of the wires drawing the current from the module to the charge controller. The resistance of these lines will effectively add to the internal series resistance of the module. The two lengths of approximately 15m of $4mm^2$ copper wire add a series resistance of about 0.136Ω. Using curve fitting methods on IV curves for parameter extraction developed at the Nelson Mandela Metropolitan University (NMMU) Centre for Energy Research (CER), the total series resistance reflected in the IV curve is 0.45Ω. Even when considering the contributions of line losses, the module series resistance is still high.

The problem of voltage drops across wiring could be avoided by taking the IV curve voltage measurements at the module junction box however the current and voltage at the end of the lines leading to the charge controller will be the effective PV power arriving at the charge controller. This is where the monitoring system will take measurements and effectively lumps these line losses into the PV losses. This lumping in the monitoring system could be avoided by the use of sense wires. The reasoning behind the choice of measurement location will be discussed in chapter 4 on the monitoring system design.

3.1.2 Module Parameters

Several module parameters useful in the modelling of PV module performance can be extracted from IV curves. Basic parameters such as I_{sc}, V_{oc}, I_{MPP}, V_{MPP} and P_{MPP} can be easily obtained and corrected for temperature and irradiance effects as has already been seen. Curving fitting methods developed at the CER using both one and two diode models can be used to deduce other parameters such as the series resistance, as has been previously discussed, but also shunt resistance (R_{sh}) and the module ideality factor (n) [42]. Table 3.2 summarizes the Helios module performance parameters measured and device parameters extracted from its IV curve using the one diode model.

The ideal solar cell will have no series resistance, infinite shunt resistance and an ideality factor of one. When examining an IV curve, the effects of the shunt resistance can be seen in observing the slope at I_{sc}, the series resistances affects the slope at V_{oc} and the ideality factor determines the shape of the knee of the curve. The ideal IV curve will approach a rectangular shape formed with the voltage and current axes.

Table 3.2: PV Module Parameters

Parameter	Value
I_{sc}	4.769A
V_{oc}	19.96V
I_{MPP}	4.143A
V_{MPP}	14.36V
P_{MPP}	59.5W
R_s	0.45Ω
R_{sh}	120.7Ω
n	67.7

3.2 Battery

In evaluating the battery of a SHS, it is important to know accurately the SOC of the battery and, in long term monitoring, its actual capacity. Monitoring the state of charge of lead acid batteries is not easy to do without manual measurement and was thus not employed in the study. Because of the significant cost incurred by battery replacement in SHSs, monitoring the degradation of battery capacity over time is of great interest. Periodic tests of battery capacity were made for the laboratory based system.

3.2.1 S.G. Test

One of the most accurate ways to determine the state of charge of a battery is to measure the specific gravity of the electrolyte. Because this measurement is difficult to automate and is not possible in gel type and sealed lead acid batteries, this method was not employed in this study.

3.2.2 Charge-Discharge Test

In order to monitor the capacity of the battery in the laboratory SHS, it was taken periodically to the NMMU battery testing facility hosted in the Chemistry department at the NMMU. The test involves a full battery discharge at its C_{20} rate until its voltage falls below 10.5V when it is considered to be at 0% SOC followed by a full charge. The charge algorithm begins with a constant current charge at 30A. When the gassing voltage of 14.7V is achieved, the battery is put under a constant voltage charge regime. The final two hours of the 20 hour charge is at a constant current of 4A to provide an equalization charge. This discharge-charge cycle is then repeated. The total amp-hours drawn during the second discharge represents the actual battery capacity. After discharge, the battery is recharged before being reconnected to the SHS.

The test is described in figure 3.2. It can be observed that battery voltage drops

sharply as it approaches 10.5V indicating total depletion of charge. The steady rise of voltage during constant current charge can be clearly seen up to the gassing voltage. At this point when the constant voltage charge begins, the current drops rapidly. Battery voltage during the equalization charge surpassed 16V during the second charge cycle, well beyond the gassing voltage.

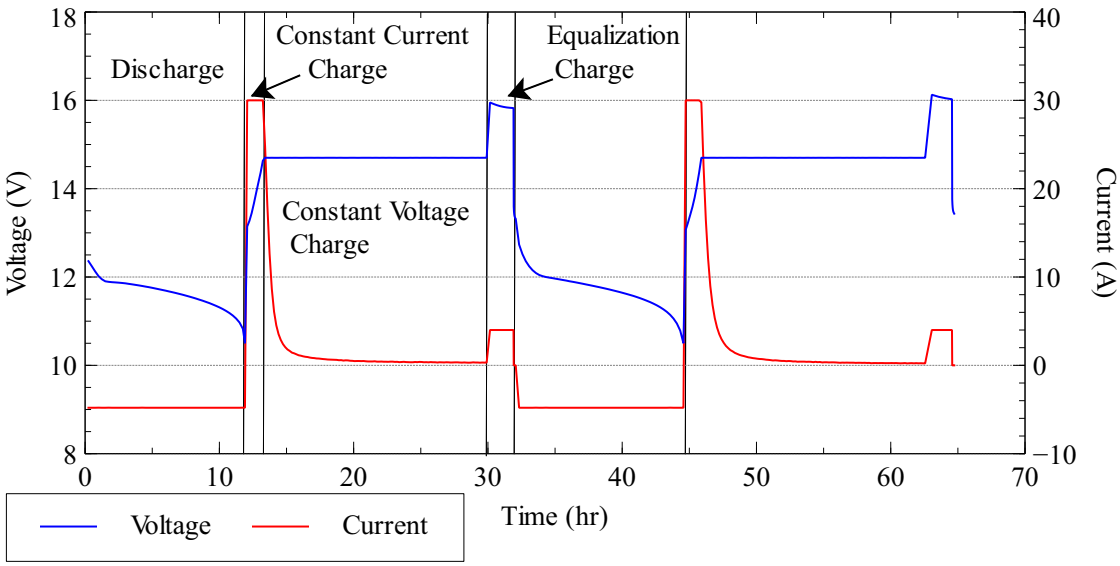

Figure 3.2: Battery Charge-Discharge Test

On May 1st, 2010, the initial test on the 96Ah deep-cycle lead acid battery showed good results with a measured capacity of 96.2Ah. Because of an equipment failure at the battery testing facility, the battery was not retested before monitoring began in June 2010. The next test showed a large decrease in capacity to 63.7Ah. Some of the lost capacity is likely due to the period of disuse. It is therefore difficult to determine what effect the initial period of cycling on the SHS had on the capacity. A month later the battery had shown a small increase in capacity. It is possible that the long period of disuse caused some sulfation that was reversed slightly during a period of cycling. PWM charge methods are known to help break up large sulfate crystals and recover battery capacity [43, 44]. The results of the battery tests will be examined in more detail in chapter 7 on the results of the laboratory SHS monitoring program.

3.3 Charge Controller

In characterizing a charge controller, it is important to know the accuracy of its set points as well as its efficiency in delivering power between system components. The set points can normally be checked with a power supply and a voltmeter.

3.3.1 Bench Test and Set Points

Accurate set points in charge controllers are important to prevent damage to system components. Some controllers have adjustable set points, particularly on low voltage disconnect. It may be desired to set the low voltage disconnect at a higher voltage in order to decrease DOD and increase battery life.

The charge controllers in this study do not allow for set point adjustment. The Solarix controller does not have fixed set points, but uses a "fuzzy logic" algorithm as previously discussed (although it is possible to set the controller to use fixed set points). The Solsum controller relies on fixed set points. The test procedure, adapted from the MSc dissertation of E.L. Meyer [45] for PWM charge controllers, can be found in appendix B and requires a power supply and voltmeter.

Table 3.3 gives the results of this test for the Solsum controller compared to the manufacturer specifications. The ambient temperature during the test was measured at 25 °C, the temperature at which the set points are quoted. The temperature sensor used for temperature compensation is located inside the charge controller and may differ from the ambient temperature. This discrepancy could account for some of the deviation from the specified gassing regulation set point. The $0.3V$ difference would imply a temperature of 41.7 °C and indicates the entire difference cannot be explained by temperature compensation. The final charge voltage is the float charge voltage at which the charge controller maintains the battery after a fixed period of charging at the gassing regulation voltage. This set point can not be determined by this method but can be observed by monitoring the data. This will be discussed in chapter 7.

Table 3.3: Charge Controller Set Points

Set Point	Tested	Spec'd
Low Voltage Disconnect	11.2V	11.1V
Load Reconnect	12.6V	12.6V
Gassing Regulation	14.1V	14.4V

3.4 Loads

3.4.1 Load IVs

Direct current loads are usually characterized by their IV curves. The following are IV curves of typical loads on rural SHSs. They were measured by connecting the loads to a variable power supply and measuring the current drawn by the load at various voltages.

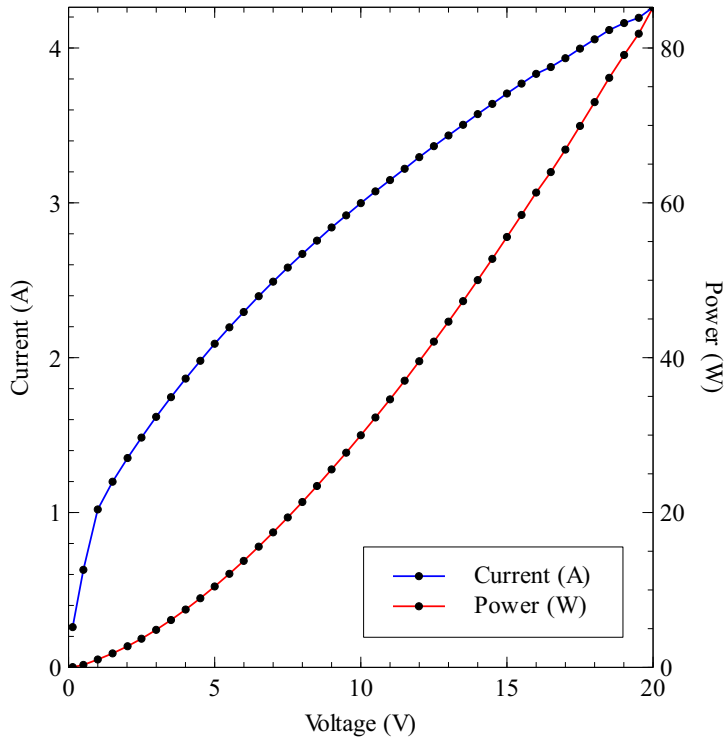

Figure 3.3: 40W Incandescent Bulb IV and Power Curves

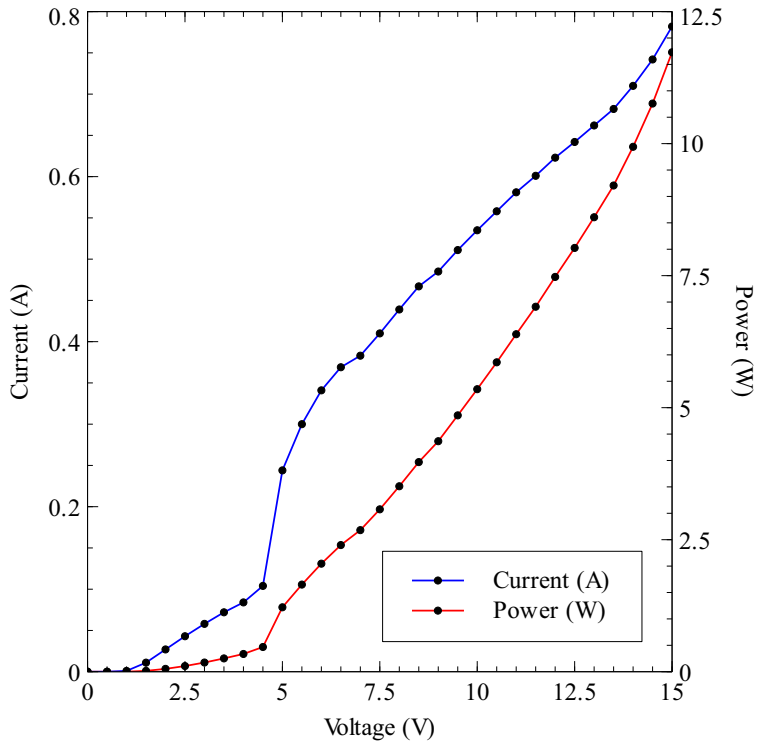

Figure 3.4: 11W CFL IV and Power Curves

Incandescent Bulb Figure 3.3 shows IV and power curves of a 40W incandescent bulb. As noted in chapter 2, the load is not exactly ohmic. This is due to the increasing temperature of the filament with rising current. As current rises, the resistance of the filament increases. The bulb drew 39.5W at 12V during the test which is in close agreement with its rated power of 40W. The roughly ohmic nature of the load means there is a quadratic relationship between power and voltage. The power drawn by the load increases quickly with increases in battery voltage.

CFLs Figure 3.4 shows the IV curve of an 11W CFL. The current drawn by a CFL is temperature dependent. For this experiment, the bulb was placed under 15V and allowed to heat up until the current drawn by the bulb stabilized. The voltage was then decreased in steps of 0.5V. The IV curve obtained shows a roughly linear relationship between voltage and current in the voltage range from 6V - 15V. The sharp increase observed between 4.5V and 5V signals the start of current conduction through the mercury gas inside the CFL tube and the production of light. The current drawn below 5V is the current drawn by the start-up mechanism in the electronic ballast attempting to raise the bulb temperature and restart conduction.

The power drawn by the CFL shows a similar quadratic relationship with voltage in the linear regions from 6V and up. The 11W CFL only drew 7.5W at the voltage as which it was rated, 12V. 11W was not drawn until the voltage surpassed 14.5V.

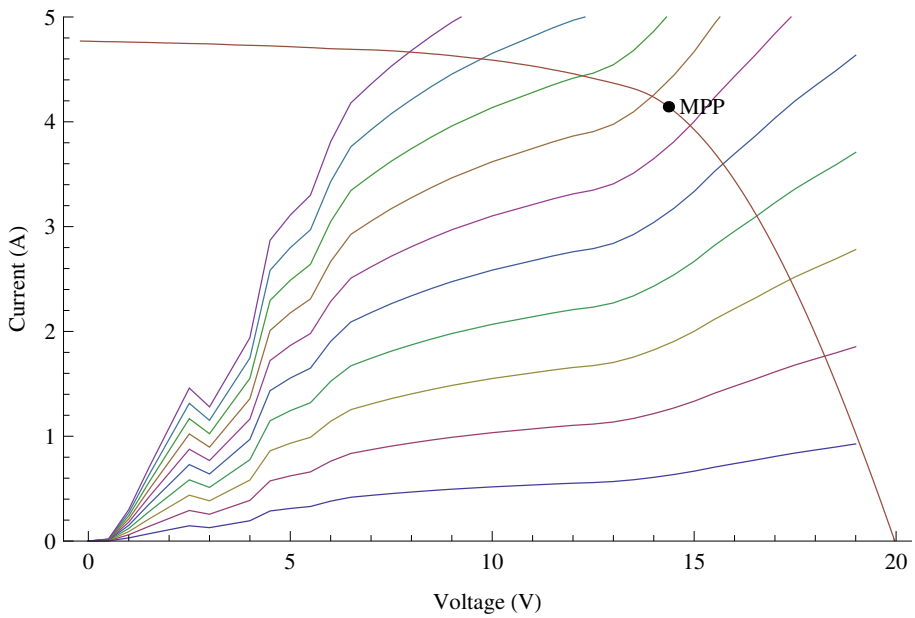

Figure 3.5: Multiple CFL IVs and PV IV intersections

Figure 3.5 demonstrates the importance of the battery in a PV system not just as a storage device but also as a voltage regulator. The figure shows the IV curves for parallel

connected 7W CFLs with the lowest curve being only one CFL and the following curves increasing the number of bulbs in steps of one. The IV curve of a PV module taken near STC is also plotted.

The intersection of the PV module and single CFL IV curves takes place around 19.0V. This is much higher than the voltage at which the CFL is rated and continued operation at this voltage could damage the bulb. It would take about eight equivalent CFLs to move up the IV curve towards a 12V operating point as seen in figure 3.5. The battery not only stores charge but regulates the system voltage as well.

LEDs Figure 3.6 shows the IV and power curves of a 1W LED lamp produced by Waco. In figure 3.7 the same curves are given from a 0.75W LED lamp from Phocos. There appears to be a ballast attached to the Phocos lamp and from comparison between the two IV curves, it seems there is a current regulation mechanism built into the Phocos LED lamp. The LED cut-off voltages can be clearly seen at 7.5V for the Phocos lamp and 9V for the Waco lamp.

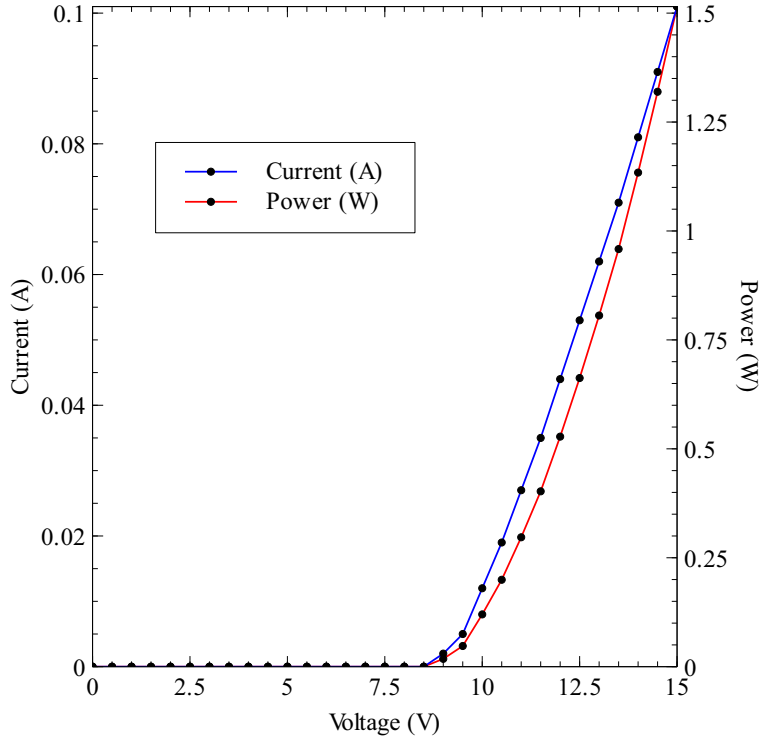

Figure 3.6: Waco 1W LED Lamp IV and Power Curves

The Phocos LED lamp quickly rises to a current level of around 60mA. There is no current control on the Waco lamp which rises sharply in current with increasing voltage. This gives the Phocos lamp a more linear power dependence on the operating voltage range as opposed to a quadratic dependence for the Waco lamp.

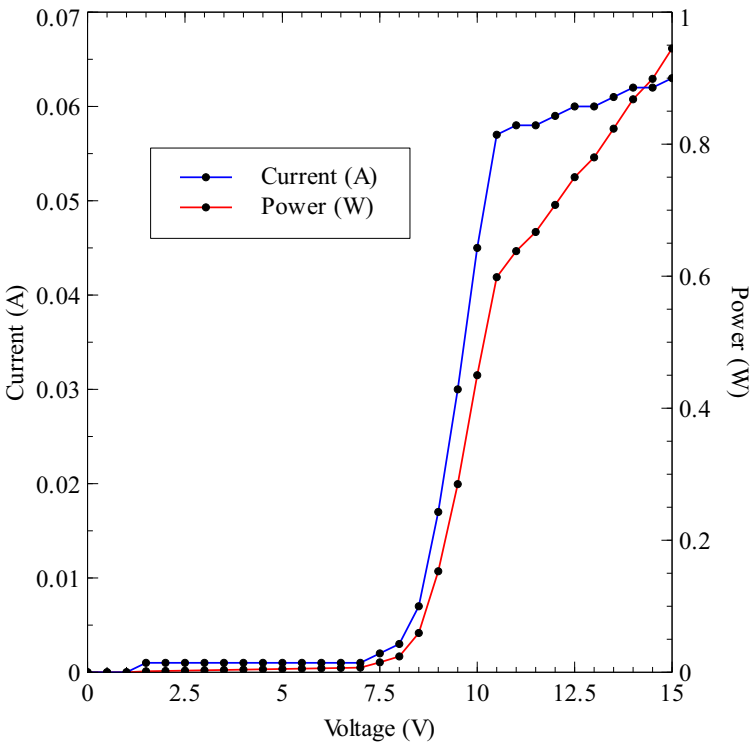

Figure 3.7: Phocos 0.75W LED Lamp IV and Power Curves

Power consumption for the lamps were lower than advertised at 12V. The 0.75W Phocos lamp drew 0.71W at 12V while the 1W Waco lamp drew only 0.53W. The lack of current regulation on the Waco LED lamp put the lamp at its rated power somewhere between 13.5V and 14V. The Phocos drew its rated power at 12.5V.

While these low power ratings are attractive, it must be noted that it would take an estimated 12 of the 0.75W Phocos lamps to equal the luminous output of an 11W CFL. The cost of a single 0.75W LED lamp is about twice that of the CFL at locally quoted prices.

Small Television The IV curve in figure 3.8 indicates that the black and white television tested is a constant current device. At operating voltages above 12V the television drew an almost constant current of 1.22A. The IV curve was measured with the TV tuned to a frequency without a signal. The noise produced a more constant current reading because fluctuations in volume and picture cause variations in the amount of current drawn. Measurements were taken at a comfortable listening volume, about halfway between the maximum and minimum levels.

The current drawn by the TV increases with increasing contrast, brightness and volume. The current drawn with all of these parameters minimized was 1.13A and with all parameters maximized 1.29A. At 12V the TV drew 13.4W. The constant current charac-

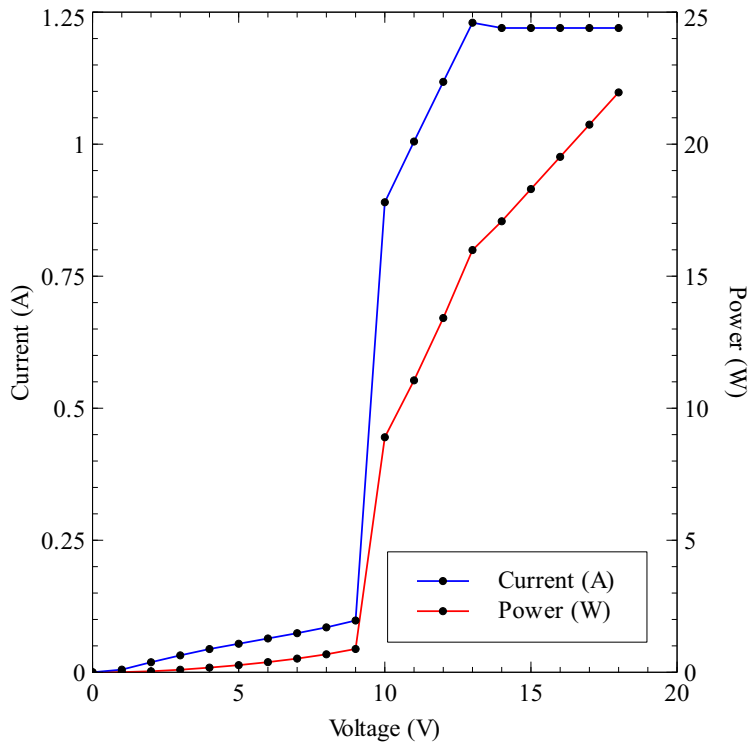

Figure 3.8: Small Black and White TV IV and Power Curves

teristic of the TV produces a linear power-voltage dependence in the range of operating voltages.

The IV characteristics of system loads will have important implications on the system operating voltage. The system operating voltage will in turn effect the energy consumption of loads. It can be concluded that constant current loads are preferable to ohmic loads because their power requirements do not depend as strongly on system voltage.

3.5 Summary

A firm understanding of the operation of individual SHS components is required to understand the operation of the system as a whole. IV characteristics of PV modules, batteries and loads combine to determine the system operating voltage. Operating voltages which are located far from the PV array's MPP will induce large losses of potential PV energy. High system voltages will increase load energy consumption, particularly for ohmic loads. The system voltage must be regulated in order to protect both the system battery and loads. IV curve measurements of PV modules before deployment ensures that modules are operating according to manufacturer specifications. The accuracy of charge controller set points must be verified to ensure efficient system operation. Effective charge control methods can extend battery life cycles and reduce overall SHS costs. With this under-

standing of SHS components, system performance as a whole can be explored through a thorough monitoring program.

Chapter 4

SHS Monitoring System Design

The designer of a SHS monitoring system must make both technical and cost considerations. The first step is to determine what parameters should be monitored. In this study it was decided to monitor the energy flows in the system which requires measurement of both current and voltage. Some monitoring programs have elected to monitor only current in order to reduce the number of required channels on the data logger [27, 46, 47]. While this does reduce cost, it comes at the expense of information on the voltages and power flows in the system.

Environmental parameters are also important in solar home systems. In the laboratory based system studied here it was decided to monitor the solar irradiance and three temperature parameters, the back of module temperature, ambient temperature and battery temperature. Limited channels on the mobile data logger necessitated the sacrifice of battery temperature measurement.

4.1 Data Acquisition

Data acquisition devices are necessary to log acquired data. In mobile and remote applications, a data logger is required. For laboratory experiments it is possible to use PC based data acquisition boards (DAQ boards).

4.1.1 Measurement Requirements

Mobile System Measurements The system to be monitored by the mobile data logging system is a rural household in a village called Tyefu in the Eastern Cape. The design of this SHS was described in chapter 2. The home is grid connected and the system is used only for lighting.

The mobile data logging system must measure both voltage and thermocouple signals.

The voltage and current from the PV array, battery and load must be measured. In order to determine total energy consumption in the household, it was decided to also determine the AC power thus requiring the measurement of AC current and voltage. Environmental conditions should also be monitored such as battery, PV array and ambient temperatures as well as irradiance.

Because of the limited number of channels on the data logger and the added expense of acquiring one with more inputs, it was decided that AC voltage and battery temperature measurement were not necessary. The AC voltage should be relatively stable around $220V$. The battery temperature is unlikely to provide data of great interest under such operating conditions. Table 4.1 summarizes the data logger channel assignments.

Table 4.1: Mobile Data Logger Channels

Differential Channel	Single Ended Channel	Assignment
1	1	Load Current
	2	
2	3	Battery Current
	4	
3	5	PV Voltage
	6	
4	7	Battery Voltage
	8	
5	9	Load Voltage
	10	
6	11	PV Current
	12	
7	13	AC Current
	14	Pyranometer
8	15	Array Temperature
	16	Ambient Temperature

Laboratory System Measurements The laboratory based system has similar requirements but because it is meant to simulate a SHS in a non-grid connected environment with no power inverter, AC measurements are not applicable. This system made use of two DAQ boards, one to make analogue voltage measurements and the other for temperature measurements. The channel assignments are summarized in table 4.2.

4.1.2 Data Loggers

The mobile logger utilized a CR1000 data logger from Campbell Scientific. The logger has 8 differential or 16 single ended channels with analogue input voltage ranges of

Table 4.2: Lab DAQ Channels

Analogue Card	
Channel	Assignment
1	Load Voltage
2	Load Current
3	PV Voltage
4	Battery Voltage
5	Battery Current
6	PV Current
7	Open
8	Pyranometer

Thermocouple Card	
Channel	Assignment
1	Ambient Temperature
2	Battery Temperature
3	Array Temperature

$\pm 5000mV$, $\pm 2500mV$, $\pm 250mV$, $\pm 25mV$, $\pm 7.5mV$ and $\pm 2.5mV$. Voltage measurements are possible with three different integration times: $250\mu s$, $16.7ms$ for $60Hz$ noise rejection and $20ms$ for $50Hz$ noise rejection. Execution rates can range for $10ms$ to $30min$. It is also capable of period averaging measurements, pulse counting and compensated thermocouple measurements via a built-in thermistor [48].

The logger requires a $12V$ power supply. Current drain for this application is typically around $1mA$. The CR1000 is highly programmable with the CR Basic programming software included in the PC400 software package [48]. This programmability turns out to be very important when monitoring SHSs with PWM as will be seen in chapter 5.

When making measurements, the data logger first allows for a programmable settling time and then integrates the signal over the specified period. Scans are made on regular programmed intervals and measurements across the channels are made sequentially. Derived variables can also be computed and treated as measured data. In the application, the measurement of power is very important and is calculated and treated as a logged parameter. Data is recorded at fixed intervals. The data collected during the scans on the record interval is processed into averages, maximum, minimums, standard deviations or other desired values and recorded in the data logger memory.

4.1.3 Data Acquisition Boards

The laboratory based SHS monitoring system utilizes a PC based DAQ system interfaced with a LabView program which controls measurement and records data. The voltage measurements were made with a PCI730 AD card and temperature measurements by a

PCI773 TC card, both from Eagle Technology.

The PCI730 card has analogue voltage input ranges of $\pm 2.5V$,$\pm 5V$ and $\pm 10V$ with 14bit resolution, a maximum sampling rate of $100kHz$ and 8 differential or 16 single ended analogue channels [49]. The PCI773C thermocouple board has 16 channels with 14bit analogue resolution and a maximum sampling rate of $10kHz$ [50].

The PC based LabView programming environment allows for more control over the measurement process than with the data logger. The number of samples collected during each measurement is programmable as well as the sampling rate. In this way, waveforms can be collected and analyzed which is important in dealing with PWM measurements. The order and frequency of channel scans is also determined by the LabView programming as well as the record interval. Data is recorded as averages on regular intervals in a file on the PC.

4.2 Current Measurement

The current flows in the SHS are likely the most important measurements to take. The currents represent the flow of charge and consequently energy between the system's components. In this study, current measurements were made in both systems on the PV array, battery bank and total load. The simplest way to make these current measurements is to measure the voltage drop across a shunt resistor of known value. The current value can be calculated by application of ohm's law

$$I = \frac{V}{R}. \tag{4.1}$$

The shunt will dissipate some energy as the current flows through it so selection of an appropriate shunt must be made carefully. This energy dissipation can be avoided if the current is measured by alternate means as will be discussed later.

Shunt Selection Two things must be considered when selecting a shunt, the voltage drop and energy loss associated with its resistance and the measurement resolution of the measurement device. Ideally, a shunt will be as small as possible to minimize the voltage drop and energy loss. However, the resolution of the measurement device will limit the accuracy of very small voltages. The maximum voltage drop a shunt will create is

$$V_{drop_{max}} = I_{max} \cdot R_{shunt}. \tag{4.2}$$

More accurate measurements will result when the input voltage range of the device

is filled out as much as possible without exceeding the upper limit. The smallest input range on the CR1000 is ± 7.5mV. In designing the Tyefu SHS it was determined that the charge controller must be rated to handle at least 7.88A. The data logging system should be able to measure this size of current as well. Solving for R_{shunt} in equation 4.2 gives

$$R_{shunt} = \frac{V_{drop_{max}}}{I_{max}}. \tag{4.3}$$

Using 8A and 7.5mV, a shunt resistance of $0.1m\Omega$ was obtained. The smallest suitable shunt available in this case was $10m\Omega$. From equation 4.2 we find a maximum voltage drop of 80mV. Using

$$P_{dis} = I_{max}^2 \cdot R_{shunt} \tag{4.4}$$

we find the maximum power that will be dissipated by each shunt is 0.64W. This is less than 1% of the PV array rated power and was deemed acceptable. The 80mV drop spans enough of the 250mV input range on the data logger to yield sufficient measurement precision with a voltage reading resolution of $66.7\mu V$. This translates to a current resolution of $6.67mA$.

The laboratory system uses an Eagle PCI 730 DAQ card to make voltage measurements. The smallest input range on this card is $\pm 2.5V$ with 14bit resolution. This corresponds to a voltage resolution of $153\mu V$ and a current resolution of $15.3mA$. While higher resolution on the current would be possible with larger shunts, it was decided that the increase in precision did not justify the increased energy losses caused by the measurement system. All shunts were calibrated by measurement of IV curves. The slope of the line fitted to the data represents the inverse of the resistance of the shunt.

Alternatives A notable alternative to shunt current measurement is the Hall effect transducer. The Hall transducer measures the current passing through a closed loop with little effect on the system being measured. It does however add to system cost and more significantly in the case of mobile systems, requires an external power source. For these reasons, Hall effect transducers were not used [8].

4.3 Voltage Measurement

Voltage measurements, along with currents, allow for the calculation of power and also provide information on battery state and the operating voltage of the PV module. Monitoring of voltage drops in the system also indicate sources of power losses. Voltage can usually be measured more directly than current because most measurement instruments are designed to measure voltages. It is not completely trivial however because most data

acquisition systems will not accept voltages as high as those in SHSs. It is therefore required to reduce the signal voltage for measurement. This is most simply done with a voltage divider.

Voltage Divider A voltage divider, seen in figure 4.1, is a simple circuit designed to reduce voltages by a fixed factor. The voltage across resistor R_2 in figure 4.1 is given by

$$V_{out} = V_{in} \cdot \frac{R_2}{R_1 + R_2}. \tag{4.5}$$

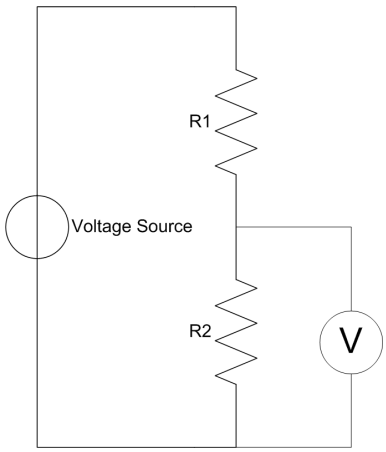

Figure 4.1: Voltage Divider

The maximum voltage we should ever expect to measure in a SHS is the open-circuit voltage of the PV module. The open-circuit voltage of the Siemens solar SM55 solar module is $21.7V$ and the maximum input voltage of the CR1000 data logger is $5V$. The maximum value for $R_2/(R_1 + R_2)$ should then be $5V/21.7V = 0.23$. To allow for possible higher values of V_{oc} at lower temperatures a smaller reduction factor should be chosen (although in normal condition with a series charge controller the module should never operate at V_{oc}).

At the same time, to maintain precision of measurements, the reduction factor should not be too small so that the signal fills out the voltage input range. For the laboratory and mobile logger systems, voltage dividers with $R_1 = 22.1k\Omega$ and $R_2 = 100k\Omega$ were selected giving a reduction factor of about 0.181. Before system deployment, the voltage dividers were calibrated to determine to greater accuracy the measured voltages.

The size of the resistors chosen is also important. In order to avoid power dissipation through the voltage divider, the resistances should be large enough that the current draw is negligible. If the resistance is too large, the effects of data logger input resistance cannot be neglected. In actual fact, the resistor R_1 is connected in parallel with R_{dl}, the

data logger input resistance. The equivalent resistance of this circuit is

$$R_{equiv} = \frac{R_{dl} \cdot R_1}{R_{dl} + R_1}. \tag{4.6}$$

If $R_{dl} \gg R_1$, equation 4.6 reduces to

$$R_{equiv} = \frac{R_{dl} \cdot R_1}{R_{dl} + R_1} \approx \frac{R_{dl} \cdot R_1}{R_{dl}} = R_1 \tag{4.7}$$

The input resistance of the CR1000 is $\sim 1G\Omega$ which is much greater than R_1 [48]. The voltage divider should be accurate and draw current on the order of $10^1 V/10^5\Omega = 10^{-4}$A, less than $1mA$.

Data logger resolution on voltage measurements in the mobile system are $\pm 1.333mV$ on the $\pm 5V$ range. With a voltage divider coefficient of $22000k\Omega/122000k/Omega$, this corresponds to a voltage measurement error of $\pm 7.4mV$. For the mobile system, a $\pm 5V$ range with 14bit resolution means a voltage resolution of 0.305mV and a voltage measurement error of 1.7mV.

Alternatives Other devices for reducing voltage for measurement do exist with the added benefit of signal isolation. These transducers however require external power and are not necessary in these applications.

4.4 Power and Energy Measurement

Power is not measured directly in either of the monitoring systems. It is calculated by taking product of corresponding measurements of voltage and current. The errors in measured power are thus related to current and voltage measurement errors by

$$\partial P = V \partial I + I \partial V. \tag{4.8}$$

This yields, for example, a power measurement error of

$$0.227W = 14.36V \cdot 0.0153A + 4.143A \cdot 0.0017V \tag{4.9}$$

for the measurement of PV power at MPP at STC for the laboratory SHS PV module. This translates to a relative error of about 0.4%. For the mobile logging system, the power measurement error on the Tyefu SHS PV array at MPP at STC is 163mW with a relative error of 0.1%.

Energy is calculated as the time integral of power. Energy measurement error will then

be the time integral of the power measurement error. The errors discussed here are errors resulting from the limited precision of the measurement devices. A significant power and energy measurement error occurring during PWM charge control will be discussed separately in the following chapter.

4.5 Temperature Measurements

As has been previously discussed, temperature has a significant effect on the performance of both batteries and solar cells. It is thus important to understand and monitor the thermal conditions under which the SHS is operating.

Battery Temperature Battery temperature can have important effects on system performance as was discussed in chapter 2. The battery temperature of the laboratory based SHS was monitored with a K type thermocouple attached to the side of the battery casing. Due to a shortage of data logger inputs, it was decided to leave out the measurement of battery temperature in the mobile system. It was not believed that battery temperature would deviate significantly from the optimal battery temperature of about 25 °C. During monitoring of the laboratory system, battery temperature averaged about 21 °C. It is expected that the operating conditions would be slightly but not significantly warmer in Tyefu than in Port Elizabeth.

Ambient Temperature In order to understand the general environmental condition during monitoring, the ambient temperature was also monitored. The ambient temperature of the laboratory based system was made in a shaded area protected from the wind located behind the PV module. For the mobile system, measurement was made outside the house under the roof overhang to protect it from wind and direct exposure to solar radiation. These measurements were also made with K-type thermocouples.

Solar Array Temperature As discussed in chapter 2, temperature measurement of the solar array is very important as cell temperatures can vary widely depending on environmental conditions and will have a significant effect on array performance [37]. In order to estimate the magnitude of these effects, module temperature must be monitored. In both systems, the back of module temperature was measured via K type thermocouples attached with duct tape to the back of a PV module in the array directly behind a cell. It is not possible to directly measure the cell operating temperature without damaging the module. The back of module (BOM) temperature is viewed as a good approximation of the cell temperature.

4.6 Irradiation

Pyranometer Irradiance measurements were made by pyranometers mounted in the plane of array on the top of the mount to prevent shading by passers by. The global POA irradiance was monitored in both systems. The laboratory system used an Apogee SP-110 pyranometer with a rated absolute accuracy of ±5%. The mobile system used a Li-Cor Li-200 pyranometer also with a rated accuracy of ±5%. Both models consist of a silicon photovoltaic sensor mounted in a cosine-corrected head [51, 52].

4.7 Logged Values

During data acquisition not every scan is recorded. In the systems monitored in this study, data logging channels are scanned every $500ms$-$2000ms$. During a scan, measurements are made an all channels. If every scan in a day was recorded, this would amount to 43,200 - 172,800 data points per channel. This would create an enormous amount of data that would be difficult to analyze and store. Instead, average values over a recording interval are recorded in the data logger memory or in a file on the PC, in this study, every 5 minutes.

4.7.1 Logged DC Parameters

Mobile System A large number of measured and derived DC parameters were logged in the mobile data logging system. The most important are the battery current, voltage and power, load current, voltage and power and the PWM corrected values of PV voltage, current and power. These corrections will be discussed in the following chapter on PWM measurement.

Other values logged for diagnostic or other interest are the maximum and minimum values on the record interval of the previously mentioned parameters. The non-corrected values of PV voltage, current and power were also recorded for comparison to corrected values. The duty cycle and period of PWM is also determined from DC measurements.

Laboratory System The same essential DC parameters were measured in the laboratory system as in the mobile system. Other values logged are the short-circuit current and voltage during PWM, PWM duty cycle and period, non-corrected PV and battery current, voltage and power.

4.7.2 Logged Environmental Parameters

Both the laboratory and mobile systems logged the plane of array irradiance, BOM temperature and ambient temperature. The laboratory system also logged battery temperature. A shortage of data logging channels meant that battery temperature was sacrificed in the mobile system. These parameters were recorded as averages over record intervals. In the mobile system, irradiance maximum, minimum and standard deviation were also recorded over each record interval. This data provides information on the short term variability of sky conditions. This information was used in the analysis of PWM measurement errors in the mobile logging system which will be discussed in chapter 5.

4.8 Monitoring System Power Supply and Consumption

The power from the SHS consumed by the monitoring system must be kept to a minimum. Consumption by measurement instruments will distort results. The data logger in the mobile system is powered by an external battery and thus effectively draws no power from the SHS. The laboratory system DAQ equipment is powered from the mains and also draws power from the SHS. The connection of the power supply in the mobile system however is important because the input signals are not isolated.

4.8.1 Monitoring System Power Supply

The mobile monitoring system data logger is powered by a 12V lead acid battery. The manner in which the battery is connected to the data logger and SHS is important. If the voltage at any data logger input is not within $5V$ of the data logger ground, erroneous measurements will occur often resulting in a returned value of NAN indicating an error in the measurement process [48].

Figure 4.2 shows the connection of the data logger power supply to the data logger and SHS charge controller circuit. Because all of the positive terminals of the Solarix charge controller are connected, measurements should be made on the positive lines of the system. The negative lines are connected during normal bulk charging but are interrupted by MOSFETs acting as switches during PWM, LVD and night time operation [33].

Figure 4.2 depicts MOSFETs as switches. During LVD, a MOSFET not seen in the figure, opens the circuit on the load. During PWM, switches S1 and S2 alternate between open and closed states whereby they are always in opposite states. This prevents the battery from discharging through the shunt while the PV module is in a short-circuit

state. During night time operation, S2 is open to prevent battery discharge through the PV module.

The current and voltage measurements must be made on the positive lines to maintain the signals within $5V$ of the data logger ground reference. If the data logger is connected to the charge controller circuit on the negative side, the interruption of the circuit shifts the voltage of inputs relative to the data logger ground resulting in measurement errors.

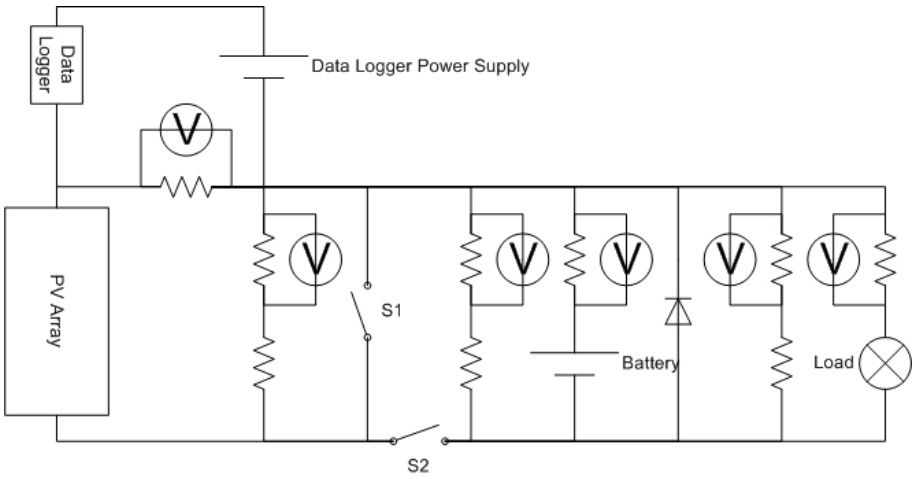

Figure 4.2: Monitoring System Circuit

4.8.2 Monitoring System Power Consumption

As discussed previously, the shunts and voltage dividers will dissipate some energy from the system. The power dissipated by shunts will not be greater than

$$
\begin{aligned}
P_{dis_{shunt}} &= R_{shunt} \cdot (I_{PV}^2 + I_{BT}^2 + I_{LD}^2) && (4.10)\\
&= R_{shunt} \cdot (I_{PV}^2 + (I_{PV} + I_{LD})^2 + I_{LD}^2) && (4.11)\\
&= 2 \cdot R_{shunt} \cdot (I_{PV}^2 + I_{PV} \cdot I_{LD} + I_{LD}^2) && (4.12)\\
&\leq 6 \cdot R_{shunt} \cdot Max(I_{PV}^2, I_{LD}^2) && (4.13)
\end{aligned}
$$

where I_{PV} is the PV current, I_{BT} is the battery current and I_{LD} is the load current. The relation $I_{PV} + I_{BT} + I_{LD} = 0$ was used with the sign convention that any current entering the charge controller is positive and current leaving is negative. This also neglects the small amount of current consumed by the charge controller itself. For the mobile system this is $3.43W$ and $1.98W$ for the laboratory system. Relative to the power flowing in the system, the shunts will dissipate about

$$P_{dis_{percent}} = \frac{R_{shunt} \cdot I^2}{V \cdot I} = \frac{I \cdot R_{shunt}}{V}. \qquad (4.14)$$

Using the nominal system voltage, the shunt resistance and short-circuit current of the PV array in the mobile system, equation 4.14 gives an expected a loss of not more than 0.53% of the PV power for the mobile system. For the laboratory system we can estimate an upper limit of 0.48% using the maximum load current, which in this case is larger than the PV module short-circuit current, at the nominal system voltage.

Voltage dividers will draw power less than

$$P_{dis_{voltdiv}} \leq 3 \cdot \frac{V_{PV_{max}}^2}{R_{voltdiv}} \tag{4.15}$$

which comes to, if overestimating by using V_{oc}, $0.011W$ for the laboratory system and $0.012W$ for the mobile system for each voltage divider. Unlike the shunt losses, voltage dividers will dissipate energy even when no power is flowing in the system but they are two orders of magnitude smaller than maximum shunt losses.

The voltage divider losses are negligible compared to shunt losses therefore we can expect the logging system to consume less than 0.96% for the mobile system and 1.06% for the laboratory system of the energy produced by the SHS. These values are double the loss calculated from equation 4.14 because all current is measured both when entering the charge controller and when exiting.

4.9 Summary

The design of SHS monitoring systems must balance cost and technical considerations. The number of parameters that can be monitored will be limited by cost. In this study, power flows in the system were monitored requiring logging of both voltage and current. Some remote monitoring programs have elected to monitor only current flow, reducing by half the required inputs for power monitoring. In doing so, information on system voltages, power and energy are lost.

Voltage dividers and shunts were selected to measure voltage and current respectively. These accurate, low cost and low power methods are well suited to remote monitoring. Voltage dividers and shunts in particular do, however, dissipate some energy from the system. The size of these losses must be considered so that the measurement process does not significantly impact the performance of the system being monitored. Energy losses for both the mobile and laboratory monitoring systems are estimated to be around 1% or less.

Other important parameters provide information on the operating conditions in which the system is performing. These environmental parameters include the POA irradiance and BOM, ambient and battery temperatures. Due to the limited number of inputs on

the mobile logging system's data logger and the desire to monitor AC power consumption, logging of battery temperature was sacrificed in this system.

The selection of monitored parameters will ultimately depend upon the goals of the monitoring program and cost and technical constraints. PC based data acquisition can monitor and log a large number of parameters at a much reduced cost compared to mobile systems utilizing data loggers but is not practical in the field where SHSs are used under typical conditions.

Chapter 5

PV Power Measurement under Pulse Width Modulation

As mentioned in the preceding chapter, a measurement error occurs when using typical data logging equipment to measure PV power under pulse width modulation. To obtain an accurate measurement of PV power, correction techniques must be applied. The techniques used in this study will be developed in this chapter. This work is based on work that has been accepted for publication in the Journal of Solar Energy Engineering [53]. First, an understanding of the how pulse width modulation (PWM) works and how it combines with the data logger measurement process to cause measurement errors is required.

5.1 PWM Measurement and Data Logger Programming

5.1.1 How PWM works

Modern charge controllers for small SHSs without maximum power point tracking typically utilize pulse width modulation to regulate charge current as a battery reaches it's full state of charge. Because excessive charge current can be harmful to a lead-acid battery, when the battery approaches gassing voltage the controller begins to send pulses of current to the battery. This is accomplished by rapidly alternating the PV module between a short-circuit and charging state using MOSFETs depicted as switches in Fig. 4.2. The electronics in the charge controller adjust the charge current according to battery state and available PV power by altering the pulse duty cycle [32]. The duty cycle in this case is the ratio of the pulse duration to the pulsing period. The pulsing frequency/period

is fixed although it has been observed to drift within a small range. Figure 5.1 shows current and voltage PWM waveforms acquired by an oscilloscope.

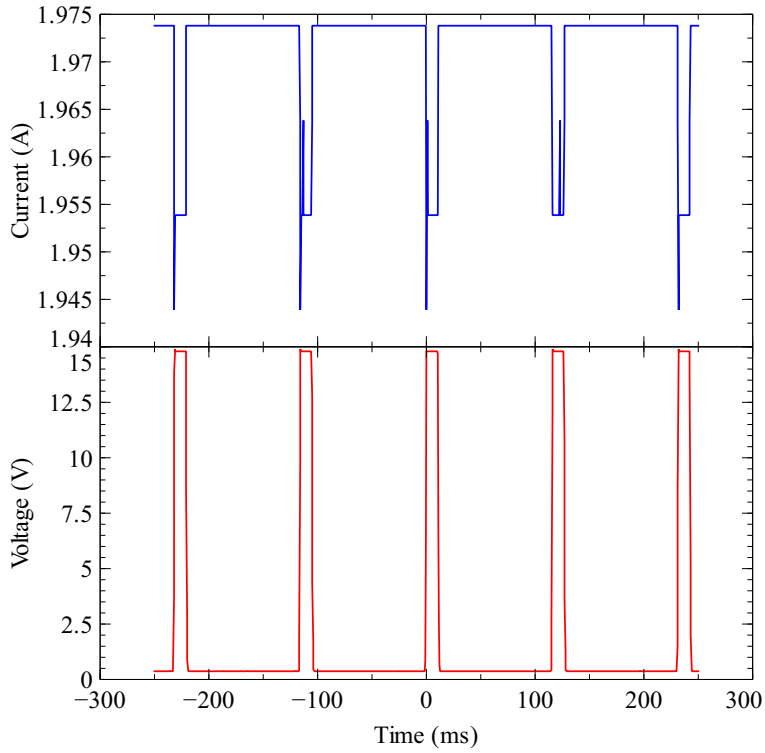

Figure 5.1: During PWM PV voltage peaks correspond to PV current valleys creating two square waves of identical period and duty cycle.

5.1.2 How PWM and data logging work together to create monitoring challenges

The measurement process, described in the preceding chapter, and PWM can interact in a way that is counter productive to the acquisition of accurate monitoring data. Figure 5.2 demonstrates the effects of sequential scanning of data logger channels in the mobile system. While all high voltage states and low current states correspond and vice versa, it is often the case that current and voltage, due to non-simultaneous measurement, are measured in different states resulting in an erroneous calculation of power. Additionally, when the charge controller short-circuits the PV module it is not exactly at I_{sc} resulting in a non-zero power measurement even though no power is delivered to the system. While this power is real, it is not a loss due to the charge controller but rather to the limited storage capability of the batteries. This loss falls into a different category which can be determined with information on the PWM duty cycle and should not be considered as PV power delivered to the system.

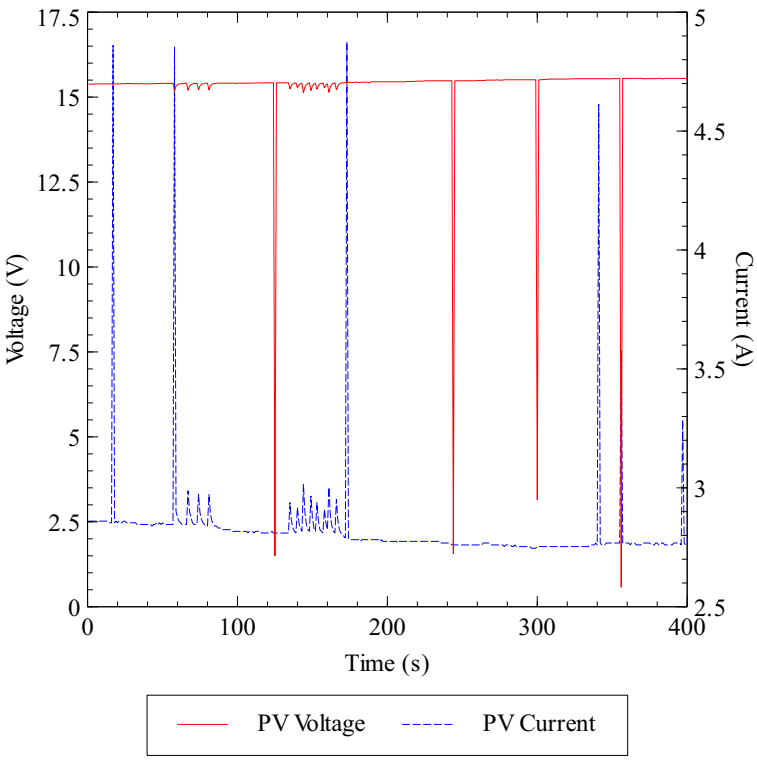

Figure 5.2: Data logger scans at the beginning of PWM. Mismatch of current and voltage peaks is particularly prevalent at very high and very low duty cycle. In this example at high duty cycle, several mismatched peaks can be seen as well as partial peaks integrated over pulse edges.

Consideration must also be made when programming the scan rate of the data logger. Poor pairings of scan frequency and PWM frequency can result in an alignment of pulse and scan which causes measurements to get "stuck" on peak or off peak resulting in erroneous power measurement. In measuring the duty cycle of the PWM, the relationship between data logger integration time and PWM frequency also comes into play. To overcome these challenges it is required to understand the measurement process well. Figure 5.3 demonstrates the dependence of measured PV current and voltage on scan rate.

These measurement errors were observed by Muñoz et al. [54] who found the relative error under heavy PWM to be up to 18%. The proposed solution by Muñoz was to eliminate the calculation of energy altogether in favor of system analysis based on charge parameters. Several monitoring studies have also chosen to monitor charge parameters rather than energy parameters in part due to the reduced number of channels required on data logging equipment [27, 46, 47].

It is however apparent that the study by Muñoz was conducted using series type PWM controllers that open the circuit on the PV module rather than short-circuiting

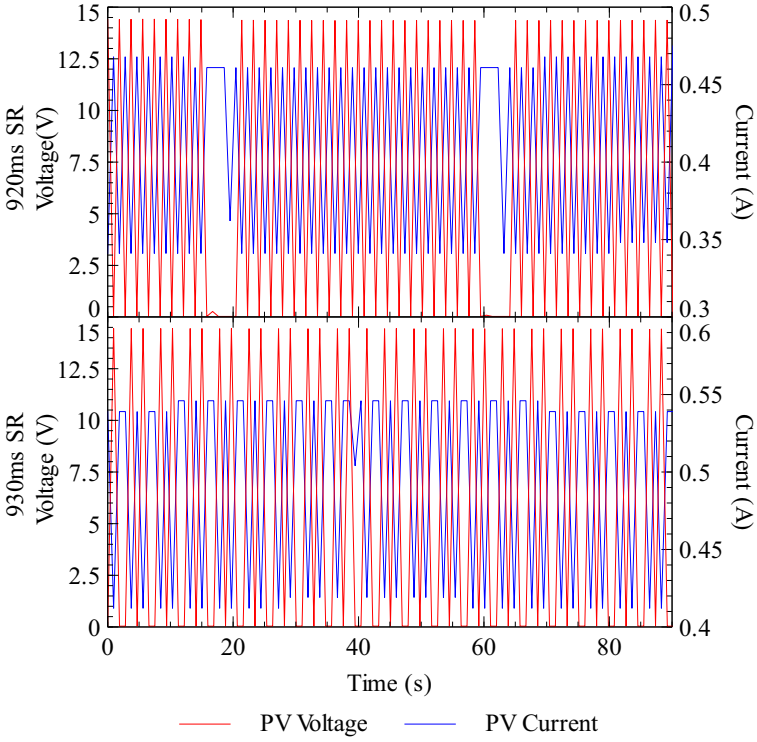

Figure 5.3: Series of scans of PV current and voltage under PWM made by the data logger. The combination of duty cycle, scan rate and PWM frequency cause distinct patterns in measurements demonstrating that the relationship between scan rate and PWM frequency can produce a non-representative sample of measurements. In the upper graph the scan rate was 920ms, the PWM frequency was 9.25Hz and the duty cycle was 44%. The lower graph has a scan rate of 930ms, PWM frequency 9.25Hz and duty cycle 43%.

it (as with the shunt type controller used in this study) [31]. This allows for the easy calculation of average PV current which is not possible with shunt type controllers.

Another approach to compensate for this error is required for systems using shunt type controllers. Furthermore, important information on the operation of the system is lost when voltage measurements are neglected, particularly with regards to battery state and the operating voltage of the PV module with respect to its maximum power point. Joint Research Centre (JRC) and International Energy Agency (IEA) guidelines [10, 11, 8] and International Electrotechnical Commission (IEC) standards [9] for the performance monitoring of photovoltaic systems are also based on energy parameters. This study seeks to fill a gap in the literature regarding power measurement errors arising due to PWM charge controllers which dominate today's market of directly coupled controllers.

5.2 Modelling PWM

In order to better understand the measurement process a model was developed using Mathematica (a technical computing software package). In the model two square waves $I(t)$ and $V(t)$ are defined by equation (5.1) and equation (5.2)

$$V(t) = \begin{cases} V_{MAX} & \text{if } 0 < Mod(t, 1/f_{PWM}) < d/f_{PWM}, \\ V_{MIN} & \text{if } d/f_{PWM} < Mod(t, 1/f_{PWM}) < 1/f_{PWM} \end{cases} \tag{5.1}$$

and

$$I(t) = \begin{cases} I_{MIN} & \text{if } 0 < Mod(t, 1/f_{PWM}) < d/f_{PWM}, \\ I_{MAX} & \text{if } d/f_{PWM} < Mod(t, 1/f_{PWM}) < 1/f_{PWM} \end{cases} \tag{5.2}$$

where V_{MAX}, V_{MIN}, I_{MAX} and I_{MIN} represent the extreme values of the current and voltage pulses with V_{MAX} and I_{MIN} occurring simultaneously, d being the duty cycle and f_{PWM} the PWM frequency. The measurement process is then simulated by choosing a random point on the PWM period t_0 as a starting point and creating a list of voltage and current measurements defined by equation (5.3) and equation (5.4)

$$V_i = \int_{t_i}^{t_i + t_{integration}} \frac{V(t)}{t_{integration}} \mathrm{d}t \tag{5.3}$$

and

$$I_i = \int_{t_i + t_{integration} + t_{settle}}^{t_i + 2t_{integration} + t_{settle}} \frac{I(t)}{t_{integration}} \mathrm{d}t \tag{5.4}$$

with

$$t_{i+1} = t_i + 1/f_{scan} \tag{5.5}$$

where $t_{integration}$ and t_{settle} are the integration time and settling time respectively. The number of elements in each list will correspond to the number of scans in one record interval. The power is then given by equation (5.6)

$$P_i = V_i \cdot I_i. \tag{5.6}$$

Taking the averages of these values yields the measurement that will be recorded for one record interval.

Figure 5.4 shows model-simulated measurements based on the average duty cycles, scan rates and PWM frequencies from Fig. 5.3. It can be seen from comparing Fig. 5.3 and Fig. 5.4 that the model successfully reproduces the measurement pattern observed with the data logger. Variations of current and duty cycle over the record interval which

are not taken as time dependent variables in the model are responsible for some slight deviations. The random variable t_0 also plays a role particularly when frequencies are poorly paired.

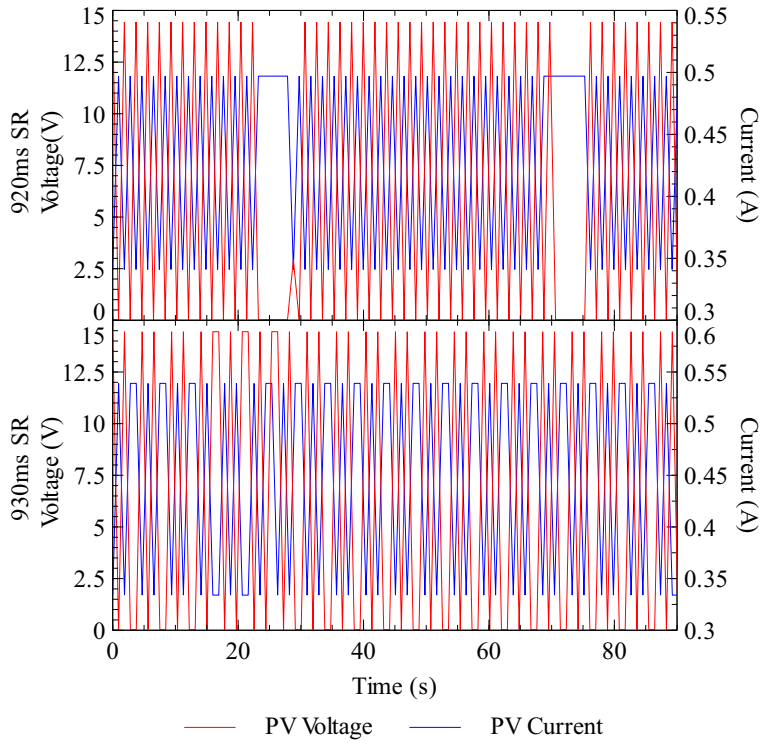

Figure 5.4: Using duty cycle, scan rate and PWM frequency data in the examples in Fig. 5.3, the developed model successfully reproduces the patterns observed in measured data.

The relationship between scan frequency and PWM frequency is also very important to consider. Frequencies with small common integer multiples create "nodes" on the scan interval resulting in a poor distribution of pulses across the scan interval. Figure 5.5 demonstrates this effect.

Figure 5.5 plots the positions of the pulse edges occurring during a 5 minute record interval on a one second scan interval with PWM frequencies of $9.2505Hz$ and $9.25Hz$. It can easily be seen that with a PWM frequency of 9.25Hz and scan frequency of 1Hz pulse edges are concentrated on 37 nodes. As the frequency deviates from 9.25Hz the nodes broaden into bands. By 9.26Hz the bands have begun to overlap giving good coverage of the record interval. When pulses are concentrated around these nodes the samples cannot be considered random and the values obtained will be highly dependent upon the location of the measurement on the scan interval. If one imagines the pulse edges expanded to square waves with width depending on the duty cycle it can be seen that for a sufficiently small integration time and duty cycle it is quite possible that no peaks at all will be measured during the record interval.

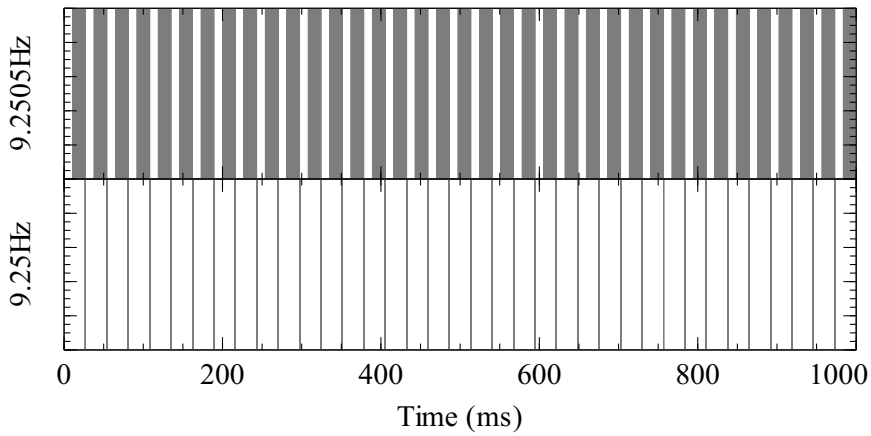

Figure 5.5: By placing the pulse edges over one record interval on a one second scan interval, we can see that with a frequency of 9.2505Hz, 37 broad bands are formed in the upper half of the figure leaving gaps on the scan interval which, with small enough duty cycle, will be left empty and result in a constant low measurement of power. At 9.25Hz, seen in the lower half of the figure, the bands shrink to single pointed nodes. This results because 37 is divisible by both 1 and 9.25.

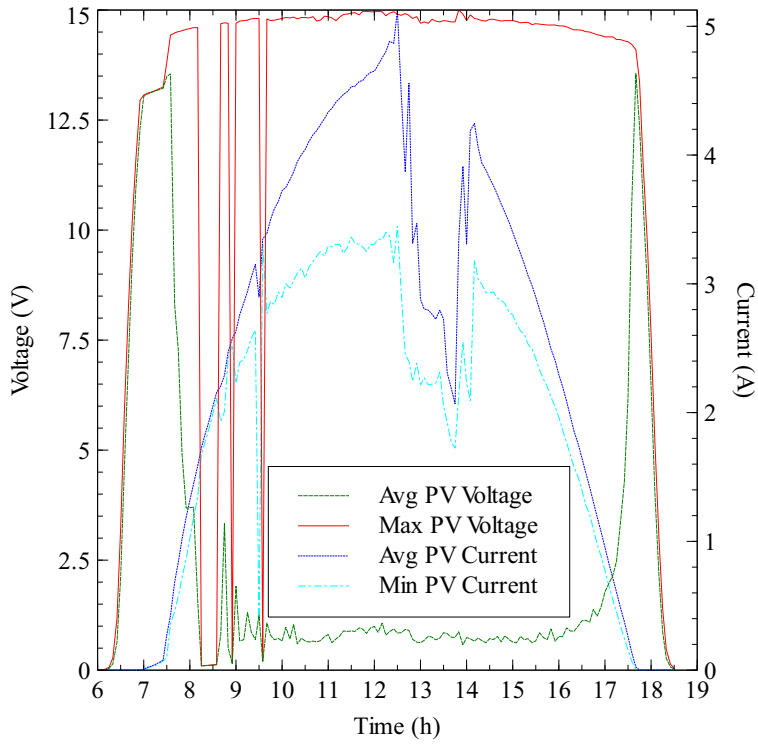

Figure 5.6: Matching of PWM frequency and scan frequency can cause periods of false measurement of both PV voltage and PV current.

This effect was observed and can be seen in figure 5.6. With a scan rate of 1 second and PWM frequency of approximately 9.25Hz, as was the case in figure 5.6, there is a risk of getting stuck making measurements in the PWM short-circuit state. It can be seen that maximum voltage (solid red) and average voltage (dashed green) correspond in a short-circuit state for a period of about 25 minutes around 8:15 and then again during two shorter intervals around 8:55 and 9:35 indicating that no peaks where measured. Similarly, the average current (dotted blue) and minimum current (dot-dashed cyan) also correspond at an elevated level on these intervals indicating measurement at short-circuit. Because the frequency of the PWM is not exactly constant, it is possible to drift in and out of this state.

To aid in the determination of an appropriate scan rate a simple algorithm, described in Fig. 5.7, was designed using Mathematica to minimize gaps on the scan interval. The idea is to reduce the gaps between pulse edges on the scan interval thus spreading edges over the interval and increasing the likelihood of a representative sample of measurements over the record interval. The tool first creates a list of the positions of pulse edges on the scan interval over one record interval with an initial scan rate and PWM frequency. The list is then sorted, the differences of adjacent elements calculated and the maximum extracted. This represents the largest gap on the scan interval. This is repeated over the range of PWM frequencies observed for the charge controller creating a new list of the largest gap for each frequency. The maximum value from the generated list is then recorded along with the corresponding scan rate. The entire procedure is repeated over a range of acceptable scan rates, in this case with a step size of $10ms$ as this is the scan rate resolution of the data logger. The list of pairs generated can then be sorted by maximum pulse gap to determine the scan rate with the lowest possible maximum gap on the scan interval for the given range of PWM frequencies.

The study using the Solsum controller with a PWM frequency range of $9.24Hz$-$9.26Hz$ and a scan rate range of $500ms$ to $2000ms$ generated a sorted list with the following top 10 and bottom 10 pairs: (650, 3.07), (860, 5.07), (760, 5.20), (1300, 5.83), (1400, 6.26), (700, 6.31), (750, 6.76), (870, 7.59), ... (1940, 104.68), (1730, 105.60), (1620, 105.87), (970, 106.23), (1080, 106.58), (1510, 106.72), (540, 107.29), (1190, 108.09). When choosing the scan rate one must also consider that the record rate should be divisible by the scan rate. In this case the lowest maximum gap was found at a scan rate of $650ms$ however one might opt for $750ms$ instead, if one prefers to work with record intervals of even integer minutes. The smallest such interval for $650ms$ would be 13 minutes whereas one minute is divisible by $750ms$. One can also see from the bottom of the list that a poor choice of scan rate can result in a very poorly covered scan interval.

The PWM correction algorithm was developed using the Solsum charge controller.

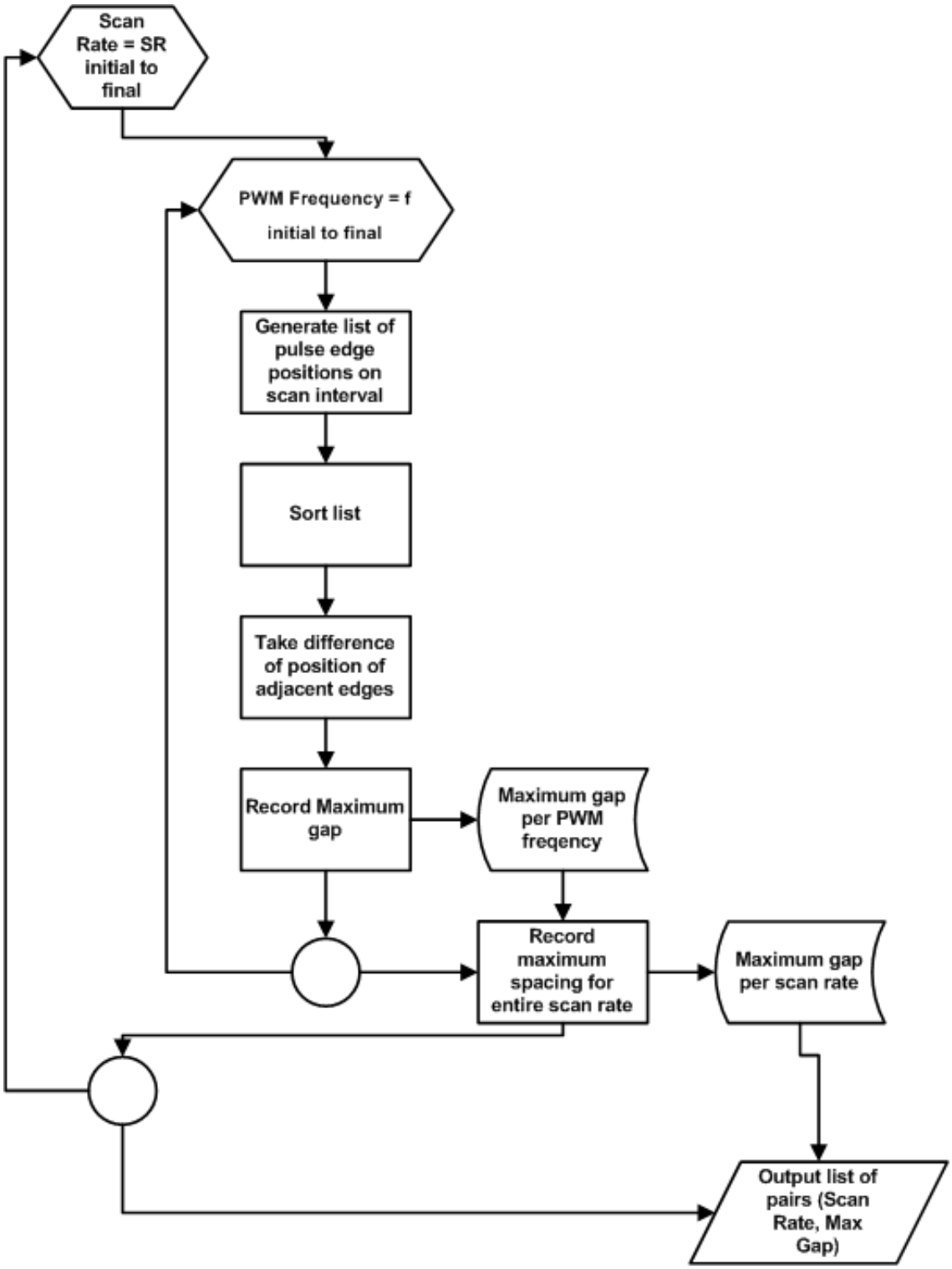

Figure 5.7: Scan Rate Optimization Algorithm

The mobile system was used to log the Tyefu SHS which utilized the Solarix charge controller with a PWM frequency range of $10.14Hz$-$10.25Hz$. A ranked list of the scan rates between $500ms$ and $2000ms$ that can be used with a five minute record interval with the Solarix controller can be found in table 5.1. The best rate was found to be $500ms$ however the data logger was not able to execute the program at that rate. The second on the list, $600ms$, was found to be the best possible scan rate.

Table 5.1: Solarix Charge Controller Best Scan Rates

Scan Rate (ms)	Maximum Interval Gap (ms)
500	10.6
600	13.9
800	15.6
1000	19.6
1200	23.3
2000	30.8
1500	31.6
1250	31.7
750	32.1

5.3 Power Estimation and Measurement Methods under PWM with the Mobile System

In order to overcome the challenges described above, techniques were developed to more accurately measure the power from the PV modules in the SHS. A first step for some of these techniques is determination of the PWM duty cycle. This information is interesting to have as it can give an idea of how much energy is being "thrown away" during charge regulation.

5.3.1 Duty Cycle Estimation Methods

Two techniques were developed to estimate PWM duty cycle. Method one relies on the measurement of minimum, maximum and average PV voltage over a record interval and assumes that the square wave pulse is approximately constant over the record interval. It is clear that when these conditions hold we have equation (5.7)

$$V_{AVG} = d \cdot V_{MAX} + (1 - d) \cdot V_{MIN}. \tag{5.7}$$

Solving for d yields

$$d = \frac{V_{AVG} - V_{MIN}}{V_{MAX} - V_{MIN}}. \tag{5.8}$$

Alternatively, with method two, one can create a variable d in the data logger program assigning it a value of 1 if the voltage is more than half peak height (in this study $7.5V$ was used as the typical peak PV voltage was approximately $15V$) and zero if below. The average value of the variable d over the record interval will give a good estimate of the average duty cycle.

5.3.2 Power Estimation Methods

Two methods of power estimation relying on the duty cycle estimate have been developed. They both require the measurement of basic parameters such as maximum, minimum and average voltages and currents over the record interval and both assume the pulses are approximately constant across the record interval.

The V_{MAX} I_{MIN} method relies on the assumption that V_{MAX} and I_{MIN}, representing the voltage and current values on a pulse, are approximately constant over the record interval. The power can then be calculated by equation (5.9)

$$P_{EST1} = d \cdot V_{MAX} \cdot I_{MIN}. \tag{5.9}$$

A more involved calculation for I_{MIN} can be made using the current equivalent of equation (5.7) which when solved for I_{MIN} gives equation (5.10)

$$I_{MIN} = \frac{I_{AVG} - (1-d) \cdot I_{MAX}}{d}. \tag{5.10}$$

Using equation (5.9) we find

$$P_{EST2} = V_{MAX} \cdot (I_{AVG} - (1-d) \cdot I_{MAX}). \tag{5.11}$$

Both methods have their drawbacks. The first estimation P_{EST1} is susceptible to error when sudden temporary changes in irradiance occur. A passing cloud, for example, would create a short downward spike in PV current resulting in a low measurement of I_{MIN} and an underestimation of PV power. Method two can smooth out such sudden spikes because PWM typically takes place during periods of clear skies when I_{MAX} is not at risk of spikes. However, constant variation of pulse characteristics, for example in the late afternoon when irradiance drops steadily, results in significant deviation of P_{EST2} from actual power.

The relationship between integration time and pulse width can also create problems. An accurate measurement of V_{MAX} and I_{MIN} is impossible when the duty cycle is smaller than $t_{integration} \cdot f_{PWM}$ because the pulse width then becomes smaller than the integration

time. The probability of measuring these parameters accurately decreases quickly as one approaches this duty cycle. Similar problems occur with the measurement of V_{MIN} and I_{MAX} around duty cycle of $1 - t_{integration} \cdot f_{PWM}$.

Problems also occur at large and small duty cycles in the calculation of duty cycle itself. It is not possible to measure a non-zero duty cycle if pulse width is less than half the integration time using method two. At this point integration over the pulse will not yield half peak height value or greater. The situation is similar in the other extreme near a duty cycle of 1. Method one is even more sensitive to integration time as it relies on measurement of V_{MAX}.

5.3.3 Data Logger Programming Solution for Power Measurement

The above power estimation methods rely on assumptions that do not always hold true. Taken together they can provide good estimates of PV power in many situations but it is desirable to have a more accurate and reliable measurement. This is possible with highly programmable data loggers such as the Campbell Scientific CR1000. Though solutions will depend on the capabilities of each data logger, the algorithm described below works well with the CR1000. This algorithm would be easy to implement with similar data loggers with an equivalent level of programmability.

Using the data logger function PeakValley to measure peaks and valleys of the current measurement, the most recent valley measurement is retained in a variable and used as the value of current in the calculation of PV power. When no pulse width modulation is detected in the system the power is calculated in the normal manner. The PV voltage used in the calculation is not corrected except when the voltage falls below a certain threshold level below which it is considered zero. This automatically corrects for duty cycle and eliminates error associated with non-zero short-circuit voltage. The threshold voltage will depend on the resistance in the lines carrying current from the PV module, the resistance across the short in the charge controller and IV characteristics of the PV module.

Figure 5.8 shows the deviation of measured power from the discussed estimation methods and the programmed solution. On the bottom of the graph is the standard deviation of the irradiation over the record interval as calculated by the data logger which demonstrates the estimation methods' dependence on steady irradiation and waveform amplitudes. It can be seen that all methods follow closely when PWM is not present. P_{EST1} is susceptible to sudden drops in irradiation as evidenced by the correspondence of irradiation standard deviation peaks to P_{EST1} valleys. Variability of irradiation during

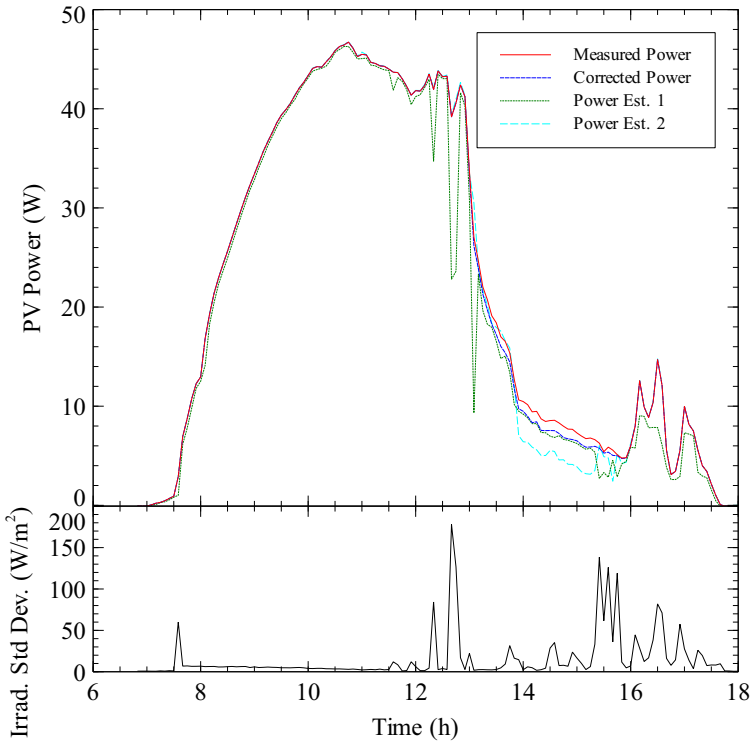

Figure 5.8: Power Calculation Methods Comparison

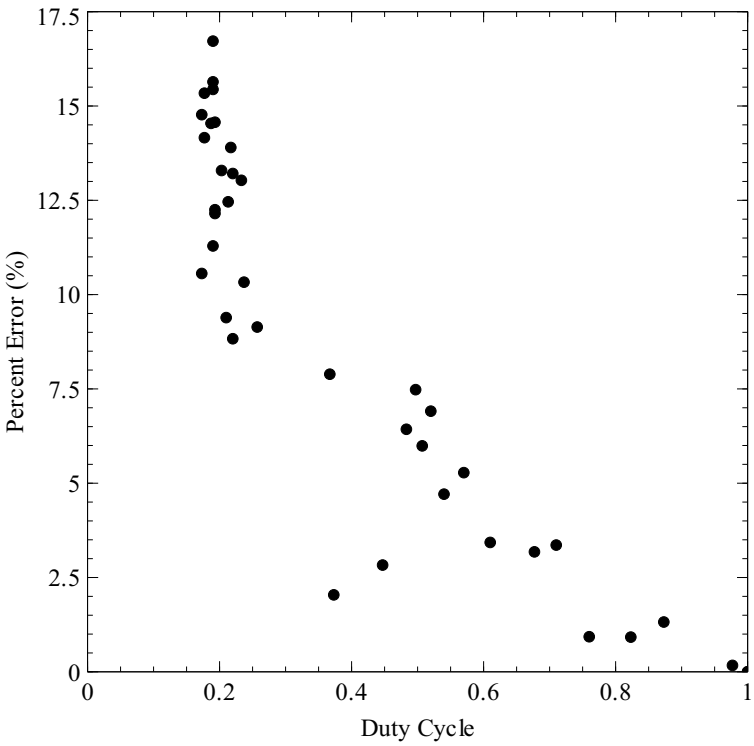

Figure 5.9: Using the same data as in Fig.5.8, we can see that the error in measured PV power depends highly on duty cycle.

pulse width modulation has an effect on P_{EST2} with it's value significantly underestimated in the late afternoon. The deviation of the measured PV power from the corrected PV power is significant and depends largely on duty cycle as can be seen in Fig. 5.9.

Table 5.2 shows the relative error of each calculation method under different duty cycles and irradiance conditions. The values were obtained through simulations of the measurement process as previously described. Five simulations under each set of conditions were carried out and the resulting power values averaged and percent errors from the actual power calculated. The simulations assumed a PWM frequency of $9.26Hz$ with a scan frequency of $1Hz$. PV voltage on peak was $14.4V$ and off peak 0.1Ω multiplied by the PV current. PV current under constant irradiance was $4.5A$ at short-circuit and $3A$ on charge. During decreasing irradiance, current values were modeled to decrease at $30mA$ per minute. The dip in irradiance condition used the same current values as under constant irradiance conditions but dropped by 25% for one minute in the middle of the five minute record interval. Initial duty cycles of 75%, 50% and 25% were taken and varied with charge current to maintain a constant average charge current.

Table 5.2: Simulated Power Measurement Error

Initial Duty Cycle	75%	50%	25%
	Percent Error (%)	Percent Error (%)	Percent Error (%)
	Constant Irradiance		
P_{EST1}	0.8%	0.0%	2.4%
P_{EST2}	1.7%	0.0%	3.7%
D.L. Algorithm	0.7%	0.0%	3.7%
Measured	0.9%	5.2%	12.9%
	Decreasing Irradiance		
P_{EST1}	2.8%	2.5%	3.4%
P_{EST2}	1.1%	2.2%	9.5%
D.L. Algorithm	0.0%	0.3%	0.7%
Measured	1.8%	5.2%	14.1%
	Dip in Irradiance		
P_{EST1}	20.1%	20.0%	19.2%
P_{EST2}	0.0%	5.2%	18.1%
D.L. Algorithm	0.0%	0.0%	1.2%
Measured	1.9%	5.0%	15.3%

The estimation methods obviously perform well under constant irradiance when the model assumptions hold perfectly. The programmed solution also performed well. Under both changing irradiance conditions the programmed solution produced the best results. The estimation methods also performed better than the uncorrected values under steadily decreasing irradiance. The dip in irradiance proved to be very troublesome for estimation method one and also for method two at low duty cycle. From this we can conclude that

the data logger algorithm provides the best results across a range of duty cycles and irradiance conditions.

The scale of the effect over a typical day will depend on several factors. The relationship between PWM frequency and scan rate will affect the quality of the sample of measurements acquired and can have an upward or downward affect on the resulting data. The amount of time the system is in a PWM charge state, which in turn depends upon system design, will also have a large affect.

Table 5.3 shows the measured and corrected measurements of PV energy on two days. Both days represented in table 5.3 were similar in terms of insolation. The measured plane of array insolation was $6.6kWh/m^2$ and $6.5kWh/m^2$ respectively for April 19th and 26th. The rated power of the mono-crystalline silicon PV module was $70W_p$. On the 19th, the battery was already in a high state of charge at the beginning of the day. No load was put on the system so it remained in a high state of charge under pulse width modulation throughout the day. The data on the 26th was taken after the system had undergone a period of typical cycling under a load of about $220Wh$ per day. It had been under load the night of the 25th and thus began the day with the $96Ah$ battery in a state of discharge and was subjected to periods of light load during the day. Pulse width modulation did not begin until around 13:00.

Table 5.3: Energy Measurement Error

	April 19th	April 26th
PV Energy Measured	$25.1Wh$	$244.2Wh$
PV Energy Corrected	$17.0Wh$	$241.7Wh$
Percent Error	47.6%	1.0%

It can be seen from the large difference in error described in table 5.3 that the scale of the measurement error depends largely on the state of the system and the loads and irradiance to which it is exposed. With little or no load, the system remains in a high state of charge therefore remaining under pulse width modulation at low duty cycle where the measurement error is most extreme. This is reflected in the higher energy measurement error observed on the 19th of April as opposed to the 26th both in absolute and relative terms. This suggests that oversized systems that maintain the battery in a high state of charge will have larger errors in PV power and energy measurement.

5.4 PWM Errors on other Logged Parameters

The same error caused by PWM on the PV array power will occur to some extent on the battery power and even the load power. These effects will be small and have been

neglected here. In the case of the battery, because the battery current oscillates between charge current and zero current, there is no analogous problem to the "non-zero" short-circuit voltage found on the PV side. Peak mismatch is mitigated by the small scale of the effect of pulsing on battery voltage. There will also be some traces of pulsing on the load side as well as due to the small variations of battery voltage but are small enough to be neglected.

5.5 PWM Measurement in the Mobile system

Several factors must be considered when designing a system to monitor a solar home system using pulse width modulation in the field. Appropriate care should be taken when selecting a data logger. More sophisticated loggers may be able to make simultaneous measurements of current and voltage or directly measure duty cycle but will likely come with added expense. Even in this case care must be taken to eliminate the measurement of energy in the short-circuit state.

Integration time must be considered with regards to measurement of V_{MAX} and the duty cycle. Scan rate, as it has been seen, should also be considered with respect to the PWM frequency to avoid the effects of matched frequencies. If price is an issue, there are estimation methods which can be used with limited data logger functionality and programmability.

The scale of the effect may or may not be considered important depending on the system being monitored and the kind of information that one wants to extract from the data. As has been shown, the effects are potentially large under certain conditions and should be considered during the design of the monitoring system.

For the mobile logger in Tyefu, a scan rate of $600ms$ was selected. Correction for PWM errors on the PV array power were made with the data logging algorithm previously described.

5.6 PWM Measurement in the Laboratory System

The correction procedure in the laboratory system is simpler than for the mobile system because of the increased functionality of the LabView programming environment. Instead of capturing data points, the laboratory system is capable of capturing and processing waveforms. In this way, more direct measurement can be made of charge current and voltage and duty cycle.

Using the LabView waveform analysis virtual instruments (VIs), the duty cycle, PWM period and maximum and minimum PV voltage and current can be measured directly.

Because of noisy waveforms, low pass digital filters were applied to the waveforms before measurement. With these values, calculation of actual PV power simplifies to

$$P_{PV} = I_{MIN} \cdot V_{MAX} \cdot d. \tag{5.12}$$

A similar procedure is performed to correct the battery power but the deviation is small because the variation of battery voltage is small and the current varies from zero to charge current. The small variation of battery voltage limits the mismatch error while the fact that the battery current drops all the way to zero between pulse eliminates the analogue to the non-zero short-circuit voltage problem.

5.7 Summary

Typical measurement methods using data loggers to monitor stand-alone PV systems utilizing PWM charge control techniques cause errors in the calculation of the power and energy from the PV array. Under certain conditions, such as sustained operation at low duty cycle or poor matching for PWM frequency and scan frequency, can result in significant measurement errors. In an extreme case, the energy measurement error over the course of a day was found to be nearly 50%. Simulations show that under typical operating conditions with a duty cycle of 25%, power measurement errors exceed 10%.

The design of the SHS will have an effect on the size of this error in terms of energy. Systems with oversized PV arrays will show larger PWM measurement errors resulting in overestimations of PV energy. A simple algorithm, developed in this study, can be applied to the calculation of PV power that greatly reduces the size of PWM errors. When data logger programmability is limited, estimation methods have been developed which can reduce power measurement errors using simple parameters such as the maximum, minimum and average PV current and voltage measured during a record interval.

Chapter 6

Modeling of PV System Performance

In designing PV systems, it is important to be able to accurately predict array output. Several models exist of varying complexity. Many models require detailed information on module characteristics and can be difficult to implement. A relatively simple model proposed by Zhou et al. [55] was adopted and adapted in this study to estimate PV module power at maximum power point (MPP). This information can then be used in the analysis of monitoring data to approximate losses due to the lack of maximum power point tracking (MPPT).

6.1 PV Performance Model

The model proposed by Zhou et al. [55] utilizes models of fill factor in combination with temperature and irradiance compensated expressions for the open-circuit voltage and short-circuit current to predict module performance at maximum power point. The fill factor of a PV array or module is a measure of the quality of the electric generator and is giving by

$$FF = \frac{V_{MPP} \cdot I_{MPP}}{V_{oc} \cdot I_{sc}}. \tag{6.1}$$

The power at maximum power point is then given by

$$P_{MPP} = V_{MPP} \cdot I_{MPP} = FF \cdot V_{oc} \cdot I_{sc}. \tag{6.2}$$

Zhou proposes a general non-linear model for I_{sc} whereby I_{sc} is given by

$$I_{sc} = I_{sc0} \left(\frac{G}{G_0} \right)^{\alpha_{nl}} \tag{6.3}$$

where α_{nl} is a dimensionless parameter responsible for any non-linear effects. However I_{sc} is known to be to good approximation proportional to the incident irradiance and can be predicted by

$$I_{sc} = \alpha \frac{G}{G_0} \tag{6.4}$$

where G is the irradiance, α is a constant with units of amps and G_0 is the irradiance at standard test conditions (STC). This is viewed as the more widely accepted model.

V_{oc} has important temperature and irradiance dependences. The irradiance dependence is of the form

$$V_{oc} = \frac{V_{oc0}}{1 + \beta \ln(\frac{G_0}{G})} \tag{6.5}$$

where β is a dimensionless coefficient [56] and V_{oc0} and G_0 are the open-circuit voltage and irradiance at STC. Zhou again took a non-linear approach with regards to temperature dependence and proposes

$$V_{oc} = \frac{V_{oc0}}{1 + \beta \ln(\frac{G_0}{G})} \left(\frac{T_0}{T}\right)^{\gamma_{nl}} \tag{6.6}$$

where γ_{nl} is a dimensionless coefficient that accounts for a non-linear temperature dependence of V_{oc}. Temperature dependence of crystalline silicon modules is generally taken as linear giving a final expression of

$$V_{oc} = \frac{V_{oc0}}{1 + \beta \ln(\frac{G_0}{G})} - \gamma(T - T_0) \tag{6.7}$$

where γ is the module temperature coefficient for V_{oc} with units of V/ °C and T_0 is the module temperature at STC. In this model for a 36 cell crystalline silicon module, γ has been theoretically calculated to be 0.0828V/ °C [37].

The fill factor can be determined as a function of T (module temperature), I_{sc}, V_{oc} and the parasitic resistances R_s (series resistance) and R_{sh} (shunt resistance). Zhou neglected shunt resistance in his model giving the fill factor as

$$FF_s = FF_0 \cdot \left(1 - \frac{R_s}{V_{oc}/I_{sc}}\right) \tag{6.8}$$

where v_{oc} is the thermal voltage normalized to the open-circuit voltage

$$v_{oc} = \frac{V_{oc}}{n_{MPP} kT/q} \tag{6.9}$$

with k being Boltzmann's constant, q the elementary charge and n_{MPP} the module ide-

ality factor at MPP. FF_0 is the ideal fill factor without parasitic resistances given by

$$FF_0 = \frac{v_{oc} - \ln(v_{oc} + 0.72)}{1 + v_{oc}}. \tag{6.10}$$

Shunt resistance can be factored into the calculation [37] with an additional term using FF_s from equation 6.8

$$FF = FF_s \cdot \left(1 - \frac{(v_{oc} + 0.7)}{v_{oc}} \cdot \frac{FF_s}{R_{sh}/(V_{oc}/I_{sc})}\right). \tag{6.11}$$

The power at MPP can then be predicted using equation 6.2 and substituting the equations for the desired open-circuit voltage, short-circuit current and fill factor models.

The model to be employed in this study will use linear models of V_{oc} temperature dependence and I_{sc} irradiance dependence. The model can be summarized as follows

$$P_{MPP} = FF \cdot \frac{V_{oc0}}{1 + \beta \ln(\frac{G_0}{G})} - \gamma(T - T_0) \cdot \alpha \frac{G}{G_0}. \tag{6.12}$$

The expression for FF will account for both the series and shunt resistance in the model.

6.2 Parameter Extraction and Model Verification

An advantage of the model presented is that the required parameters are relatively easy to determine. The required parameters are V_{oc0}, I_{sc0}, n, α, β, γ, R_s and, if included, R_{sh}. V_{oc0} and I_{sc0} can easily be determined from IV curves taken at STC or from manufacturer specifications. The temperature and irradiance coefficients can be extracted from data on V_{oc} and I_{sc} at different module temperatures and POA irradiance. Using IV curve fitting techniques, the ideality factor at MPP, n_{MPP}, and the parasitic resistances R_s and R_{sh} can also be determined.

6.2.1 Temperature and Irradiance Coefficient Determination

In order to obtain data from which module parameters could be extracted, a simple experiment was carried out. On one day the module open-circuit voltage was recorded every five seconds along with module temperature and POA irradiance. The following day, the same procedure was followed only this time measuring the short-circuit current rather than open-circuit voltage. Measurements were made with the same data acquisition system as the laboratory SHS experiment.

This data (irradiance, temperature and I_{sc} or V_{oc}) was then fit to the models presented

in the preceding section and the best fit parameters determined using the NonlinearModelFit function in Mathematica. The value of V_{oc0} used in the fits was taken from an IV curve measured under irradiance of $1000W/m^2$ in outdoor conditions with a module temperature of 25.1 °C achieved by cooling the module with water as irradiance approached $1000W/m^2$. For the purposes of modelling, $1000W/m^2$ and 25 °C will be taken as the values of G_0 and T_0. The results are summarized in table 6.1. All model fits produce coefficients of determination (R^2) greater than 0.99 indicating a high correlation to experimental data. Confidence intervals at 95% are relatively small, particularly for irradiance coefficients, giving credibility to the parameter values.

Table 6.1: PV Performance Model Parameters

Temperature and Irradiance Parameters		
Parameter	Best Fit	Confidence Interval (95%)
β_{nl}	0.0960	0.0955 - 0.0966
β	0.0969	0.0963 - 0.0974
γ_{nl}	1.122	1.097 - 1.147
γ	0.0642 V/ °C	0.0626 - 0.0658 V/ °C
Model	Best Fit	Confidence Interval (95%)
α_{nl}	1.0460	1.0445 - 1.476
α	4.705A	4.702A - 4.707A

The β values found in both the non-linear and linear temperature models are very similar at 0.0960 and 0.0969. These values are of the same order as the value obtained by Zhou, 0.058, for their modules. The non-linear irradiance coefficient for I_{sc} was found to be 1.0460 with a confidence interval of 1.0445 - 1.0476. This value shows an approximately linear relationship between I_{sc} and irradiance as is expected. Zhou [55] obtained 1.21 for their modules. The linear coefficient was found to be 4.705A with a narrow confidence interval.

The linear temperature coefficient γ is much lower than the theoretical value at 0.0642V/ °C. This comes to $-1.8mV/cell/$ °C compared to the theoretical value of $-2.3mV/cell/$ °C. The theoretical value also lies well outside of the confidence interval. This indicates weaker than expected temperature dependence of module performance on cell temperature. It should be noted however that because the temperature measurement is made at the back of the PV module and not all cell temperatures are exactly the same, it is not a precise measure of the cell operating temperature. The non-linear model produced a value of 1.122 for γ_{nl}. This value is comparable to the value of 1.15 obtained by Zhou [55].

This module assumes that all cell temperatures are the same. In obtaining the data used to extract these parameters, the BOM temperature was measured behind a single

cell. This cell should be representative of all cell temperatures. Effects like cell mismatch can cause certain cells to heat up more than others [20]. Figure 6.1 shows a thermal image of the Helios PV module used in the laboratory SHS and analyzed here. Cell temperatures vary but are mostly uniform. Several hotspots however can be observed. This must be kept in mind when measuring the BOM temperature.

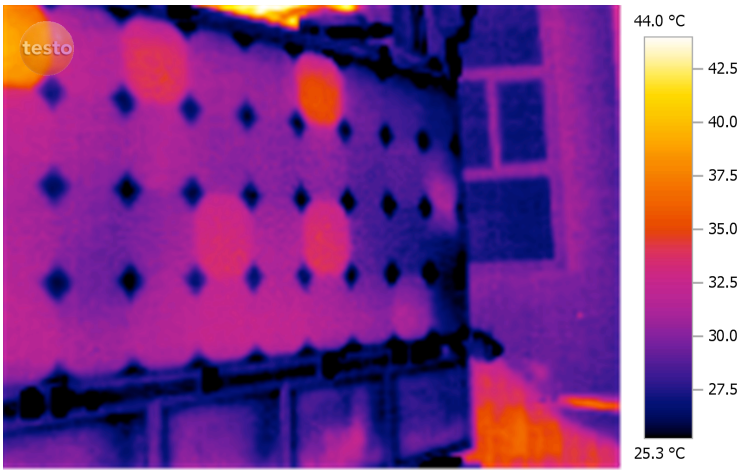

Figure 6.1: Thermal image of PV module under normal outdoor operation conditions

6.2.2 Determination of module ideality factor and parasitic resistances

Many methods exist for the determination of the module ideality factor and parasitic resistances. A review by Bashahu [57] of 12 different techniques for determining the series resistance of a mono-crystalline solar cell gave a range of values from $0.4\Omega/m^2$ to $55.1\Omega/m^2$. For our purposes, the accuracy of the values will be judged on their ability to model measured data on PV module performance. The method employed by Zhou [55] is that of Jia and Anderson [58] whereby the series resistance can be determined with knowledge of V_{oc}, I_{sc}, V_{MPP}, I_{MPP} and T by

$$R_s = \frac{V_{MPP}}{I_{MPP}} \cdot \frac{1/V_t \cdot (I_{sc} - I_{MPP}) \cdot (V_{oc} + V_t \cdot \ln(1 - I_{MPP}/I_{sc})) - I_{MPP}}{1/V_t \cdot (I_{sc} - I_{MPP}) \cdot (V_{oc} + V_t \cdot \ln(1 - I_{MPP}/I_{sc})) + I_{MPP}} \tag{6.13}$$

with the assumption that the shunt resistance is infinite. The module ideality factor can then be determined by

$$n_{MPP} = \frac{V_{MPP} + I_{MPP} \cdot R_s}{V_{oc} + V_t \cdot \ln(1 - I_{MPP}/I_{sc})}. \tag{6.14}$$

Using an IV curve from the module taken near STC (25.1 °C and $1000W/m^2$), the series resistance is found to be 3.41Ω and the ideality factor 1.43. These expressions however were developed for a single solar cell. The ideality factor for the entire module should be multiplied by the number of cells, in this case 36. This gives a module ideality factor of 51.5.

Many techniques involve the examination of module IV curves. One method employed at the CER at the NMMU involves the fitting of measured IV curves to one or two diode models of the module IV curve. This can be done visually or by a method called particle swarm optimization (PSO) via LabView programs developed at the CER [42]. The model used in this study is based on the one diode model. An IV curve taken near STC was used to fit the one diode model visually resulting in values of 0.45Ω, 120.7Ω and 67.7 for the series resistance, shunt resistance and ideality factor respectively.

These parameters can also be estimated by fitting the model developed in the previous section and fitting it to data collected on the MPP Power at various cell temperatures and irradiance levels. Data was collected in an experiment to be described in the following section. The MPP values of current and voltage were recorded along with POA irradiance and module temperature every 5 seconds. Values of the ideality factor and parasitic resistances were extracted by determination of best fits to the chosen model. The results are summarized, along with results from other methods, in table 6.2.

Table 6.2: Summary of Ideality Factor and Parasitic Resistance Values

FF Model	Method	n_{MPP}	R_s (Ω)	R_{sh} (Ω)	R^2
Series	Jia and Anderson	51.5	3.41		0.5740
Series/Shunt	IV Fit	67.7	0.45	120.7	0.9897
Series	MPP Data Fit	49.5	1.01		0.9953
Series/Shunt	MPP Data Fit	49.5	1.01	∞	0.9953

Values for the ideality factor should fall between 1 and 2 for single cells and 36 and 72 for modules of 36 cells. The values obtained here fall within that range. The series resistance obtained by the method of Jia and Anderson [58] is significantly higher than that obtained by the other methods. The R^2 value obtained indicates no correlation between the modeled and the measured data. The effectively infinite shunt resistance found by fitting of MPP data suggests a model neglecting shunt resistance is possible. This is reflected in the equivalent values of ideality factor and series resistance obtained by fits to models both with and without shunt resistance. The IV fit parameters which where obtained independent of MPP data show good correlation with an R^2 greater than 0.989.

6.2.3 MPP Data Experiment and Model Performance

In order to test the model's ability to predict module performance based on temperature and irradiance data, an experiment was carried out to monitor the MPP power, POA irradiance and module temperature over the course of three days. This data was then used to extract module parameters and compare predicted power output and energy yield with measured values.

Experimental Set-up A 70W Helios PV module was maintained at MPP with an 8A MicroCare MPPT Regulator. The battery terminals were connected to a discharged 96Ah deep cycle lead-acid battery. To prevent the battery from reaching a high state of charge when the regulator would commence charge control, it was connected to a 40W incandescent bulb. To prevent deep discharge, the connection between the battery and the load was made via a Solsum 6.6c charge controller with a low voltage disconnect feature.

Data was collected with the same data acquisition system used to monitor the laboratory system described in chapter 4. A LabView program was created to measure PV voltage, PV current, irradiance and module temperature every 5 seconds and record them in a text file.

Comparison of Modeled and Measured Power and Energy Figures 6.2.A, 6.2.B and 6.2.C plot the power measured at MPP versus modeled power using extraction methods by Jia and Anderson [58], IV curve fitting and MPP data fitting, respectively. The model used with the parameters by Jia and Anderson is the non-linear model proposed by Zhou [55]. The IV extracted parameters use a linear model with series and shunt resistance while the MPP data extracted parameters are used in a linear model with only series resistance.

The parameters extracted by the methods of Jia and Anderson produce no correspondence between measured and modeled data. Values diverge strongly with increasing power. This is due to a large overestimation of series resistance which at sufficiently high power exceeds the characteristic resistance of the module (V_{oc}/I_{sc}) leading to predictions of negative power output. The R^2 value of the fit is 0.574013.

Parameters extracted from IV curves and MPP data produced much better results. Using a linear model considering series and shunt resistance, the R^2 value for the IV fit parameters equals 0.9897132. The IV curve derived parameters tend to overestimate to some extent at higher powers. This could be due in part to maximum power point tracking errors. The MPP voltage determined by the MPPT was consistently in the region of 14.9V while IV curve measurements show a greater range of V_{MPP} under different

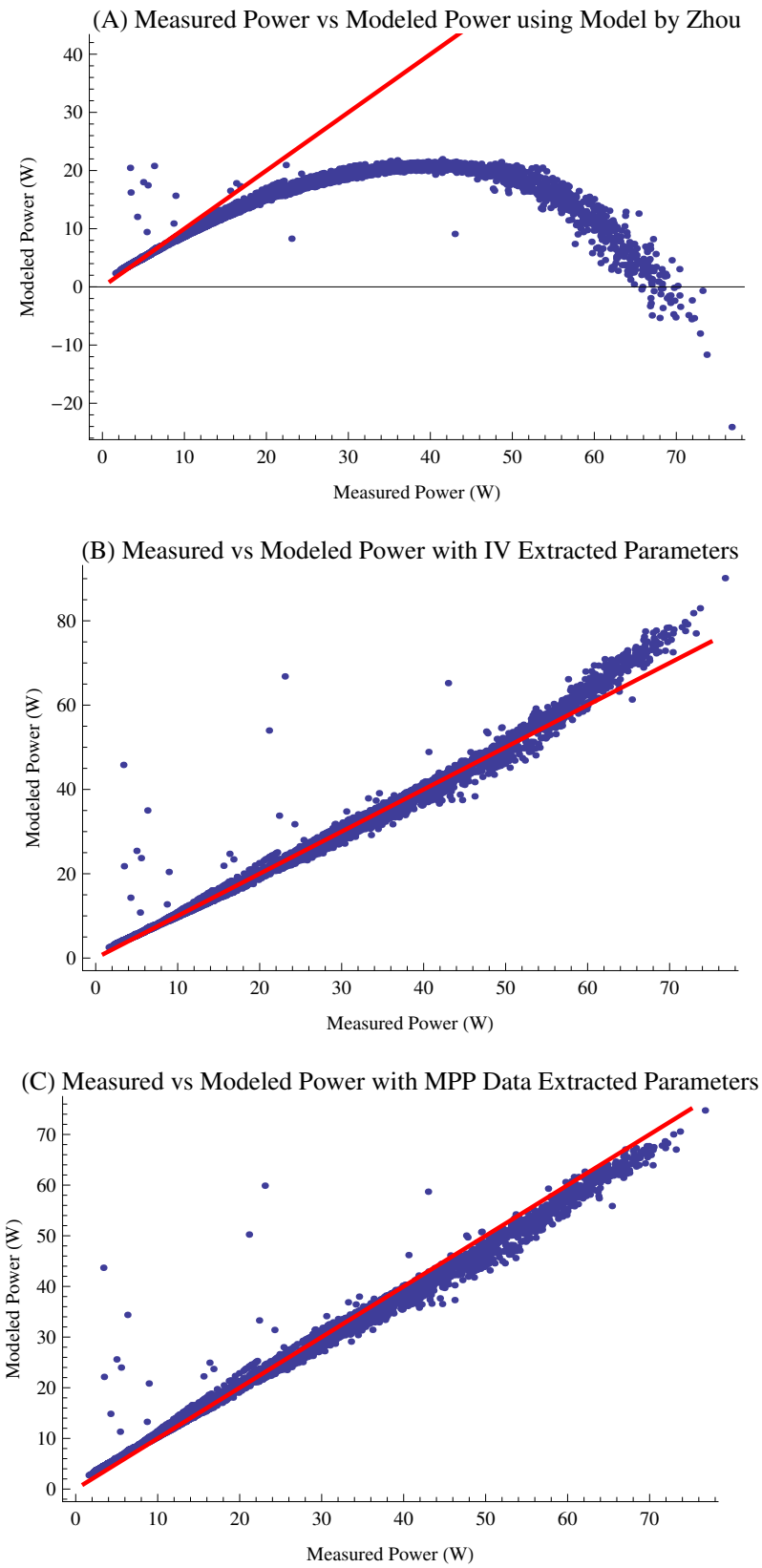

Figure 6.2: Measured MPP power versus modeled MPP power with various PV models

temperature and irradiance conditions with values at high irradiance near 13.5V. This leads to suspicion of the accuracy of the MPPT.

The operation of the MPPT also periodically brings the module to an open-circuit state while scanning for the MPP. This effect was not corrected for in the experiment and will pull down the average power measured. Some of these data points can be seen as outliers in figures 6.2.A, 6.2.B and 6.2.C, though effort was made to filter out most of them.

The parameters derived from MPP data naturally produce the best results because they were fit to the data set being examined. In terms of energy, over the monitoring period the models utilizing parameters derived from MPP and IV curve data showed good agreement with measured energy. The total measured PV energy over the monitoring period was $1158Wh \pm 10.7Wh$ using the power measurement errors discussed in section 4.4. IV curve fit parameters predict 1161Wh and MPP fit parameters give 1116Wh. These are errors of 0.2% and 3.6% respectively with the former falling within the experimental uncertainty.

6.3 Summary

The model to be adopted in the following chapter on the analysis of laboratory SHS monitoring data will utilize linear temperature-voltage and irradiance-current models with a fill factor model considering both series and shunt resistance. The IV curve parameters for ideality factor at MPP and parasitic resistances are viewed as more realistic because they are derived in a more independent manner. Modeled energy was in close agreement with the measured energy over the three day monitoring period. Furthermore, one would expect the slight overestimation of the MPP power observed with the IV curve parameters due to measurement errors which tend to underestimate the MPP power.

The final model to be used can be summarized as

$$P_{MPP} = FF_{sh} \cdot \left(\frac{V_{oc0}}{1 + \beta \ln\left(\frac{G_0}{G}\right)} - \gamma(T - T_0) \right) \cdot \alpha \frac{G}{G_0}. \tag{6.15}$$

STC values of irradiance, temperature, open-circuit voltage and short-circuit current are determined by the IV curve used to derive the temperature and irradiance coefficients. These and the other parameters are summarized in table 6.3.

With this model, monitoring data can be analyzed to predict potential module power at MPP. Comparison with measured values can give an indication of energy losses due to operation away from MPP.

Table 6.3: Summary of PV Performance Model Parameters

Parameter	Value
T_0	298K
G_0	$1000W/m^2$
V_{oc0}	19.96V
I_{sc0}	4.77A
K	$1.38 \cdot 10^{-23}$ J/K
q	$1.6 \cdot 10^{-19}$ C
n	67.7
β	0.0969
γ	0.0642
R_s	0.45Ω
R_sh	120.7Ω

Chapter 7

Laboratory System Monitoring

The laboratory based system in this study allowed for the controlled monitoring of a working solar home system. The difficulty of monitoring battery performance in the field made a laboratory based system interesting in that the system battery could periodically be tested for actual capacity. Furthermore, the more flexible PC based monitoring system allowed more data to be captured than in a remote system. The disadvantage is of course that the system usage does not represent that of an actual solar home system. While effort was made to create a realistic load profile, the variability of actual system use is not practical to simulate.

7.1 System Description

The laboratory based SHS consists of the components found in table 7.1. The Helios PV module was not new at the time of implementation and has likely suffered some performance degradation over its operational life. The load profile was simulated with three CFLs rated at 7W, 9W and 13W as well as a 40W incandescent bulb. The load profile was taken from data logged on a system in New Brighton Township, Port Elizabeth, South Africa as found in figure 2.5 and normalized to a 201Wh daily load. Figure 7.1 shows the simulated load profile as measured by the data logging system. The data acquisition system used by the system is described in chapter 4.

Table 7.1: Laboratory System Specifications

Component	Name	Quantity
PV Array	70W mono-crystalline Helios PV module	1
Battery Bank	96Ah Deep Cycle Lead Acid Battery	1
Charge Controller	Steca Solsum 6.6 (6A)	1

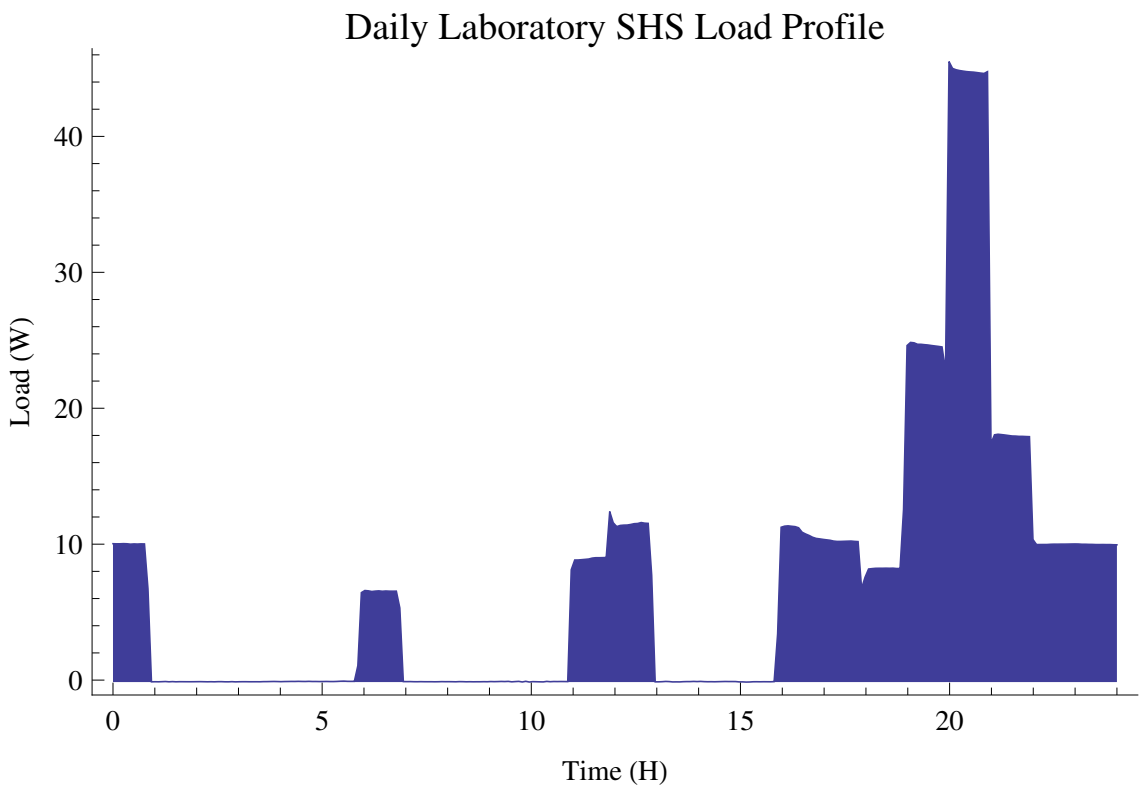

Figure 7.1: Simulated Laboratory SHS Load Profile

7.2 Meteorological Data

PV array performance depends primarily upon environmental factors such as incident POA irradiance and solar cell temperature. The availability of solar radiation depends upon solar geometry (which in turn depends upon the time of year and latitude) and atmospheric conditions. The available extra-terrestrial solar irradiance at any given time can be calculated. The fraction of that irradiance that reaches the earth is called the clearness index (CI). Figure 7.2.A describes the extra-terrestrial solar irradiation in the POA and the measured POA irradiance at the PV array.

The average daily clearness index can be calculated by taking the quotient of the measured POA insolation and the extra-terrestrial daily POA insolation. The average daily clearness index is showed in figure 7.2.B. Average daily insolation can be predicted with knowledge of the average clearness index and the extra-terrestrial irradiance.

Solar cell temperature has an important effect on array performance. The cell temperature will depend on several factors such as ambient temperature, irradiance and wind speed. In this study, irradiance and back of module and ambient temperatures were measured. The BOM temperature is measured on the back of the PV module directly behind a solar cell. This is to ensure that the temperature measured is indicative of the actual cell temperature. As discussed in chapter 6, hot spots do occur on some modules

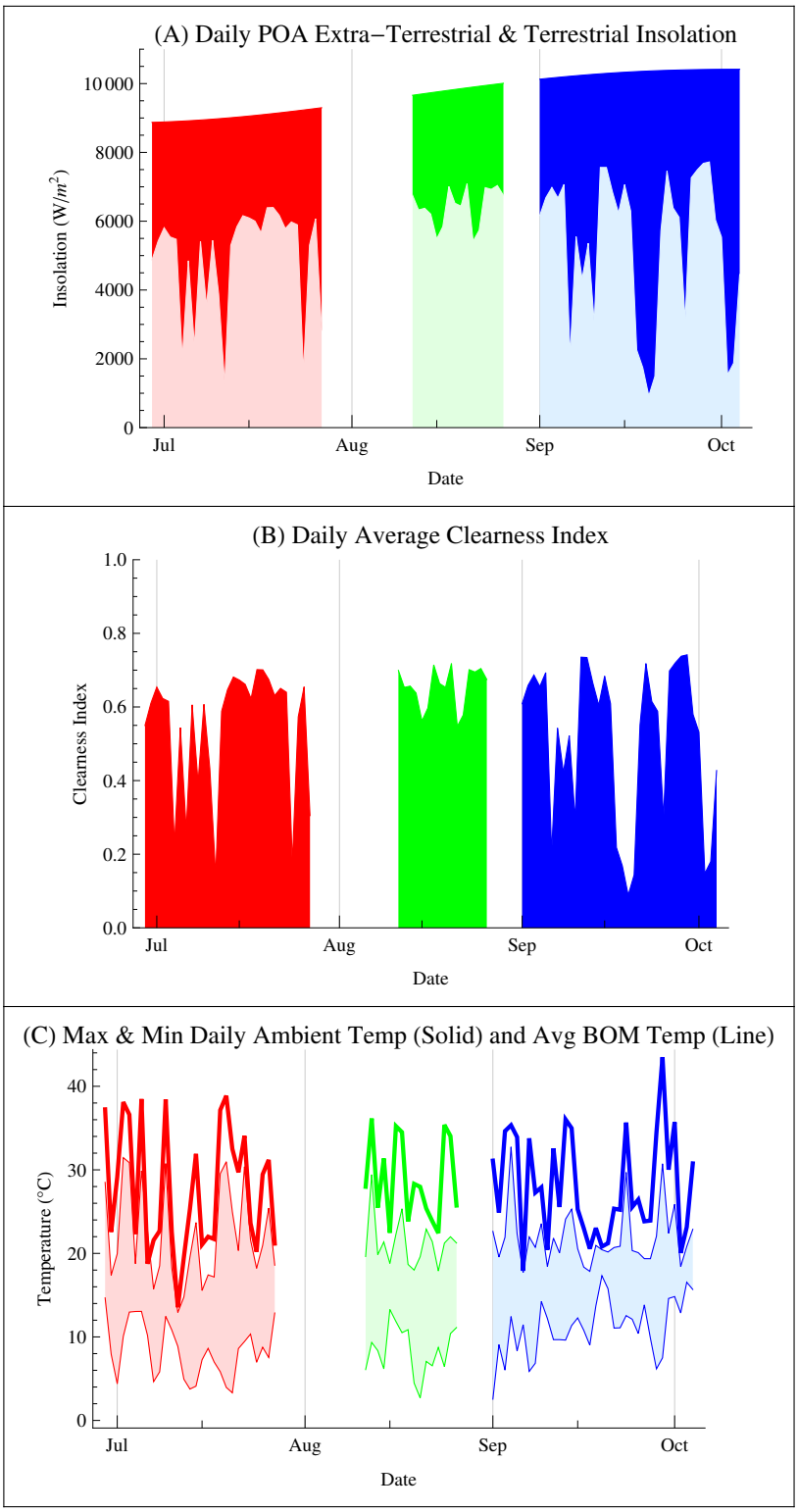

Figure 7.2: Laboratory System Meteorological Data

and not all cells are at precisely the same temperature. A cell should be chosen that is representative of the mean cell temperature. Figure 7.2.C shows the maximum and minimum daily ambient temperatures.

Figure 7.3 plots the BOM temperature versus the ambient temperature and POA irradiance. It can be seen that the BOM temperature increases with both ambient temperature and irradiance. The difference between ambient temperature and BOM temperature depends strongly upon the POA irradiance. This can be observed in figure 7.4 which plots the difference between ambient temperature and BOM temperature versus POA irradiance. The relationship is approximately linear however there is some divergence, particularly at higher irradiance. Although wind speed was not recorded in this study, it is expected that this is the cause of the divergence. High winds increase convective cooling of the module and so it is expected that data collected during higher wind speeds is represented on the lower edge of the band in figure 7.4 and lower wind speeds at the higher edge.

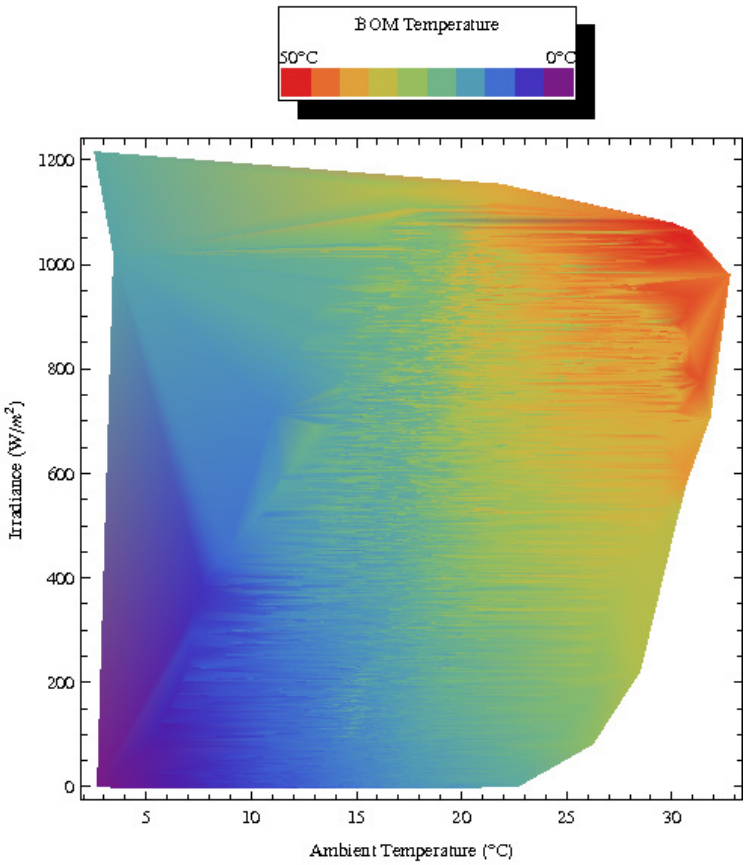

Figure 7.3: Back of module temperature versus plane of array irradiance and ambient temperature

Taking the average BOM temperature does not provide a good basis for estimation

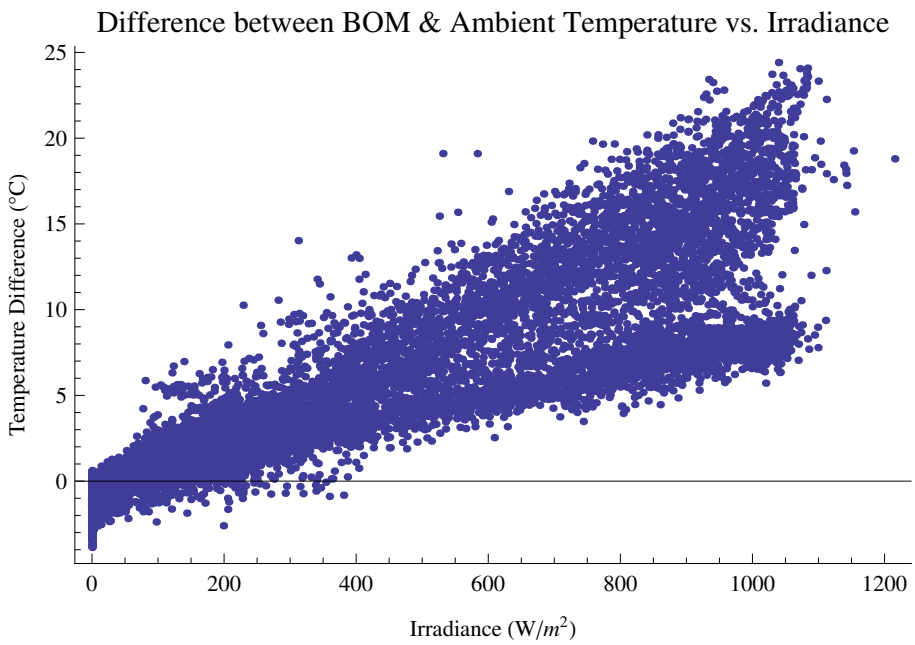

Figure 7.4: Difference between back of module temperature and ambient temperature versus POA irradiance

of temperature effects because higher temperatures typically correspond to higher levels of irradiance and thus higher temperature losses in absolute terms. A better indication can be acquired by taking the irradiance weighted average BOM temperature calculated by

$$\int (G \cdot T_{BOM})dt / \int Gdt. \tag{7.1}$$

Because the power output of PV modules, neglecting low irradiance effects on PV voltage, is linear, this irradiance weighted average temperature provides a good estimation of the BOM temperature that should be used in determining the temperature losses that will be incurred by a PV array.

For the three monitoring periods, June 29th to July 27th, August 11th to August 26th and September 1st to October 4th, this produced temperatures of 28.9 °C, 28.9 °C and 29.6 °C. The daily average irradiance weighted BOM temperature is plotted as a line in figure 7.2.C. On average it tracks about 6 °C above the daily maximum ambient. On one occasion the average BOM temperature was actually lower than the daily maximum ambient temperature. The net temperature effect on module performance relative to the STC rating will be slightly negative since the average irradiance weighted BOM temperatures over the entire monitoring periods are near but higher than the STC temperature of 25.0 °C. Slightly higher temperature losses are expected during the third monitoring period.

Battery Temperature stayed relatively steady throughout the monitoring period av-

eraging 20.1 °C and recording extreme values of 16.2 °C and 24.8 °C. High operating temperatures of lead-acid batteries can cause rapid deterioration of battery performance however the battery in this system is operating at temperatures well below those considered detrimental [29].

Summary of Meteorological Data During the monitoring periods from June 29 to July 27, August 11 to August 26 and September 1 to October 4 the average daily POA insolation was found to be $4.9kWh/m^2$, $6.4kWh/m^2$ and $5.3kWh/m^2$ respectively. The corresponding clearness index values are 0.55, 0.65 and 0.51. Average insolation values for Port Elizabeth from long term monitoring on an equivalent array tilt are $5.0kWh/m^2$, $5.4kWh/m^2$ and $5.7kWh/m^2$ respectively for the months of July, August and September. Clear skies during the August monitoring period produced higher than normal insolation values while September was slightly below average.

The moderate climate of Port Elizabeth kept ambient and BOM temperatures relatively low. The average daily maximum temperature during the monitoring periods were 22.2 °C, 21.2 °C and 21.9 °C respectively. Daily BOM temperature profiles indicate relatively low module temperatures. The net temperature effect on array performance is expected to be slightly negative. Battery temperatures are not expected to have significant effect on system performance.

7.3 System Performance and Loss Analysis

The objectives of PV systems analysis are typically to either compare the performance of different systems or to analyze system losses in order to improve performance. For the comparison of different PV systems and their operating environments, several normalized performance parameters have been established by the IEC, IEA, the JRC of the European Commission and others in published standards and guidelines [12, 9, 10, 11]. These parameters, normalized to the nominal array power, allow for the comparison of system performance between systems of different sizes but similar type (stand-alone or grid-connected).

To better understand where losses in systems occur, a thorough loss analysis is required. This involves looking at the performance of individual system components and quantifying energy losses due to the applicable loss mechanisms. This sort of analysis is more in-depth and requires more information than that required to calculate standard performance parameters.

7.3.1 Normalized Performance Parameters

The normalized PV system performance parameters applicable to SHSs are defined in table 7.2. The array, reference and final yields are in units of hours per days. This can be interpreted as the number of hours per day, on average, that the system operates at its rated capacity. An array yield of 3h/d for a 100W PV array for example means that the PV module produced energy equal to that which would be produced during 3 hours operation producing its rated 100W power. The final yield, in the case of a stand-alone system, is simply the energy consumed by the loads normalized to the PV array size. Reference yield measures the number of "sun-hours" during the day in the POA. 5 sun-hours indicates insolation equivalent to 5 hours irradiation at STC, $1000W/m^2$.

Table 7.2: Summary of Normalized System Performance Parameters

Parameter	Symbol	(Units)	Definition
Array Yield	Y_A	(h/d)	$E_{array/day}$
Final Yield	Y_f	(h/d)	$E_{load/day}$
Reference Yield	Y_r	(h/d)	$\int_{day} G_I \mathrm{d}t / G_{STC}$
Array Capture Losses	L_C	(h/d)	$Y_r - Y_A$
System Losses	L_S	(h/d)	$Y_A - Y_f$
Performance Ratio	PR		Y_f/Y_r
Usage Factor	UF		$E_{array}/E_{array,pot}$
Mean Array Efficiency	$\eta_{A,mean}$	(%)	$E_{array}/\int G_I \cdot A_{array}\mathrm{d}t$
Mean System Efficiency	$\eta_{S,mean}$	(%)	E_{load}/E_{array}
Overall Efficiency	η_{tot}	(%)	$E_{load}/\int G_I \cdot A_{array}\mathrm{d}t$

Array capture losses and system losses are also in units of hours/day. Array capture losses are the difference between the reference yield and the array yield. In other words it is what the array should have produced had it operated in all conditions as rated at STC minus what the array actually produced. The reasons for these losses will be examined in more detail in the following section. System losses are the difference between the array yield and the final yield. This translates to the losses incurred between the production of the energy by the PV array and the consumption of the energy by the loads. In stand-alone systems, the value of the system losses will also be effected by differences in initial and final battery SOC as well as initial and final battery capacity.

The most often quoted performance parameter is the performance ratio (PR). This represents the ratio of the energy consumed by load on the system (the final yield) to the array's rated energy production (the reference yield). Another important parameter for stand alone systems is the usage factor (UF). The limited storage capacity of batteries means that when batteries are full, some energy will have to be "thrown away" during charge control. The usage factor is the ratio of the energy realized by the PV array to the

energy that could have potentially been realized had there been no need for charge control. A high usage factor during the critical design month means the PV array size is optimal for the size of the loads on the system. In order to maintain battery health however, usage factors less than one are necessary to assure that battery the receive proper charging. Furthermore, since stand alone systems are designed to to ensure adequate energy supply during the worst insolation months, usage factors during high insolation periods will be low.

Efficiencies are somewhat self-explanatory. The mean array efficiency refers to the average efficiency at which the PV array converts solar energy in the form of radiation into electrical energy. The mean system efficiency is the average efficiency at which the electrical storage and transmission system delivers energy from the PV array to the system loads. The overall system efficiency is then the combined array and system efficiency.

Table 7.3 summarizes the normalized system performance parameters obtained from monitoring data during the monitoring periods. The data shows strong isolation during the August monitoring period which resulted in above average array yield. The increase, however, was not proportional to the increase in insolation due to the limited capacity of the battery. The battery was kept in a high state of charge resulting in long periods of charge control. This potential PV power was lost and resulted in a low usage factor of 0.62. The low usage factor resulted in a low performance ratio of 0.38. This is also reflected in elevated array capture losses. Higher system losses are due to decreased battery efficiency in high states of charge and to a smaller extent larger line losses due to higher current flows in the system.

Table 7.3: Summary of Laboratory System Normalized Performance Parameters

Parameter		Jun 29 - Jul 27	Aug 11 - Aug 26	Sep 1 - Oct 4
Y_A	(h/d)	2.77	2.89	2.77
Y_f	(h/d)	2.44	2.42	2.45
Y_r	(h/d)	4.95	6.43	5.30
L_C	(h/d)	2.18	3.54	2.54
L_S	(h/d)	0.33	0.46	0.32
PR		0.49	0.38	0.46
UF		0.75	0.62	0.71
$\eta_{A,mean}$	(%)	5.8	4.6	5.4
$\eta_{S,mean}$	(%)	88.1	83.9	88.5
η_{tot}	(%)	5.1	3.9	4.8

Final yields are, as expected, very similar during all monitoring periods since the daily load is fixed by the load simulator. Array yields also deviate little due to the constant load demands. In a stand alone system, when the incoming PV energy exceeds the load

demand, the battery is maintained constantly in a high state of charge. This results in more charge control which reduces the array yield and usage factor and increases array capture losses. This is in contrast to a grid connect system that utilizes the grid as an effectively infinite storage reservoir. The July and September monitoring periods were similar in array yield, final yield and system losses. Slightly stronger insolation in September pushed down the September usage factor and performance ratio relative to July.

Array efficiency is much lower than its 10.3% rating. This is due in part to the low usage factor as well as efficiency reduction due to temperature and low irradiance effects and non-MPP tracking. The potential array efficiency, calculated by correcting measured PV power for duty cycle, was 7.7%, 7.5% and 7.6% respectively. These efficiencies correct for the usage factor. Further reductions of efficiency will be discussed later in this chapter.

System efficiency, comprising all system components except the PV array, was high. These values are not entirely accurate because they do not account for differences in initial and final battery state of charge. As such they likely overestimate the efficiency of the DC system. The lower system efficiency during the August monitoring period is, like the corresponding rise in system losses, due to battery operation at higher states of charge and increased line losses. The total system efficiency is equal to the product of the array efficiency and system efficiency.

Low usage factors indicate that the system is oversized for its load and local insolation. The usage factor is low even during July which is on average the second worst month of the year in terms of insolation. Furthermore, the July monitoring period showed insolation slightly lower than average. This means that the system's performance ratio can be improved by reducing the size of the PV module. If the size of the PV module is reduced too much, the system's battery will not regularly receive a full charge. This will result in faster degradation of battery performance leading to shorter battery life cycles and higher system life cycle costs. A balance must be found between maximizing battery life and reducing PV array size. The decision should be made in a way that minimizes the life cycle cost of the system.

7.3.2 Loss Analysis

In order to improve system performance, one must first identify system inefficiencies limiting the system. The laboratory based system utilizes a solar module rated at 70W under $1000W/m^2$ irradiance. Neglecting all capture losses, one would expect the module to produce a quantity of electrical energy per day on average equal to 70W multiplied by the reference yield (the sun-hours). Modules do not always perform as they are rated and degrade to some extent over time. A de-rated module power can be obtained by

measuring the IV curve at STC of the module to extract the maximum power point.

This is the actual maximum power at STC, however, modules in solar home systems do not operate at STC or in most cases at MPP. This further reduces the energy supplied by the module. When a battery is in a high SOC, it will not be able to accept all the available energy from the PV array. This will again reduce the useful energy produced by the system. Furthermore, not all of the energy produced by the array will end up being consumed by system loads. Losses due to charge controller inefficiencies, line losses and battery losses with further reduce the useful energy that the system can provide [59].

Figure 7.5 describes the energy yield at different loss levels for the monitoring periods in this study. The rated energy is the energy that would be produce by a module performing as rated, operating at STC and having been exposed to the average daily insolation for the given period. The de-rated energy is calculated in the same manner only using the actual maximum power at STC as determined from an IV curve measured at STC. The modeled energy is the energy production at MPP predicted by the model described in the preceding chapter using measured module temperature and irradiation data. Potential PV energy is obtained by correcting measured PV power for duty cycle and integrating it. The actual PV energy is the integrated PV power as measured during monitoring. Consumption is the energy consumed by loads on the system. The definitions of these energy quantities are summarized in table 7.4.

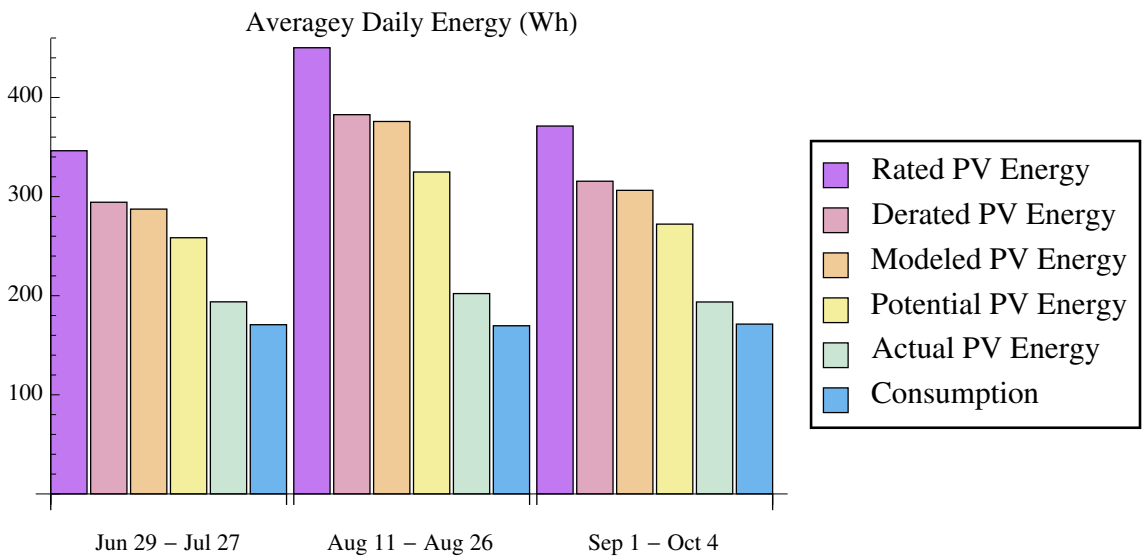

Figure 7.5: Average Daily Energy Yield

The differences between bars on the chart in figure 7.5 represent energy losses at various stages of energy production, storage and distribution. The difference between the rated energy and de-rated energy represent losses due to inaccurate module rating and module degradation. The difference between de-rated energy and modeled energy repre-

Table 7.4: Energy Quantity Definitions

Quantity	Definition
Rated Energy	$P_{STC,rated} \cdot \int G_I \, \mathrm{d}t / G_{STC}$
De-rated Energy	$P_{STC,meas} \cdot \int G_I \, \mathrm{d}t / G_{STC}$
Modeled Energy	$\int P_{PV,model} \, \mathrm{d}t$
Potential Energy	$\int P_{PV,meas} \, \mathrm{d}t$
Actual Energy	$\int P_{PV,meas} / DC \, \mathrm{d}t$
Consumption	$\int P_{load} \, \mathrm{d}t$

sents losses due to low irradiance and temperature losses. These losses can be separated by modelling the PV power at a constant STC temperature of 25 °C and calculating the energy yield. The difference between this and the de-rated energy gives the low irradiance losses and the difference between the constant temperature modeled energy and the normally modeled energy gives the energy losses relate to temperature (referred to as temperature losses).

Taking the difference between modeled energy at MPP and the potential PV energy gives the losses due to non-MPP tracking. Charge control losses are obtained by taking the difference between potential and actual PV energy. Charge controller losses, due to charge controller inefficiency and energy consumption, can be calculated directly from monitoring data by taking the difference between energy flowing into the controller from the energy flowing out. The actual PV energy minus the load energy consumption and less the charge controller losses can be attributed to the battery. Note that battery losses do not account for differences between initial and final battery states and are thus not complete. These values are almost certainly underestimations since new monitoring periods follow battery testing after which the battery is fully charged. Final battery state of charge can be deduced from battery tests but because tests and trial runs often precede the commencement of monitoring periods, it is difficult to determine the exact state of charge at the beginning of a monitoring period. A closer look at battery losses and efficiencies will be taken later in this chapter.

These calculations depend largely on the accuracy of the PV performance model that has been adopted. Line losses are also not taken into account and are lumped into other categories of losses. Since measurements are taken on the lines near the charge controller, these losses will affect the measured performance of the loads, the battery and the PV array. In the case of the PV array, since IV curve measurements used to derive model parameters were taken at the ends of the lines carrying current to the measurement system, the line losses will appear as an extra series resistance on the PV module causing a slight de-rating of the module power. Line losses to and from the battery will decrease the apparent battery efficiency and the lines to the load will slightly increase the energy

consumed by the loads. These losses are considered to be small in comparison to the losses they are attached to during their calculation.

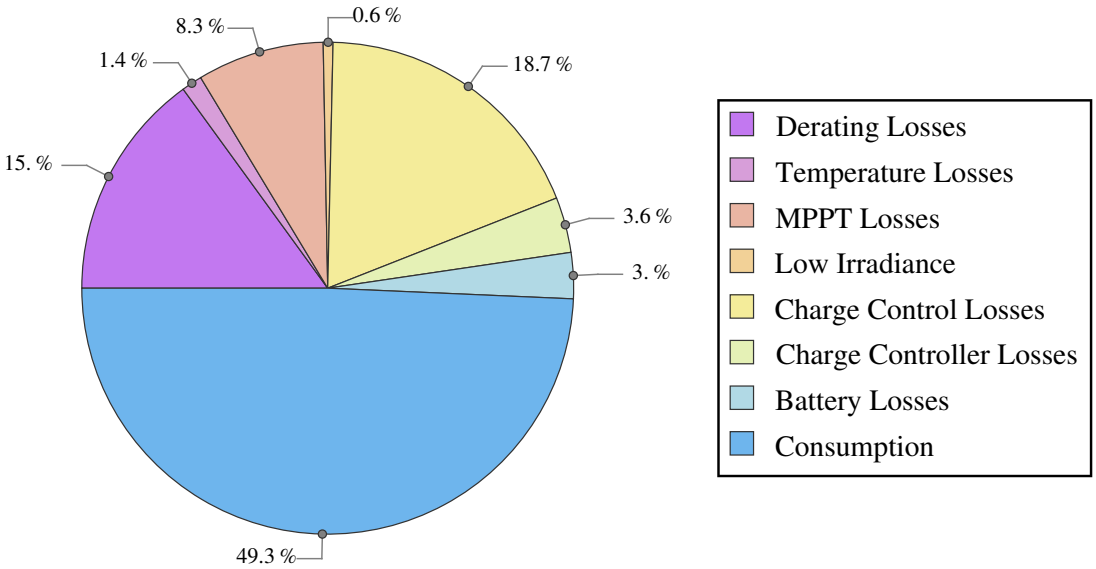

Figure 7.6: Energy losses and consumption during the July monitoring period

June 29 - July 27 Figure 7.6 shows losses calculated for the July monitoring period. Just under 50% of the rated energy is consumed by the loads. This corresponds to the system's performance ratio. The largest single loss is due to charge control. As discussed in the previous section, the system is oversized resulting in high levels of charge control and a low usage factor. The PV module, as seen in chapter 3, performs well below it's rated power due in large part to a high series resistance. This is the second largest loss during this period.

A further 8.3% of the rated energy was lost due to operation away from the module's MPP. This is a significant loss of energy which could be mitigated with the use of a MPPT charge controller. Low irradiance and temperature losses are low at 0.6% and 1.4%. System losses, defined as all losses occurring after production by the PV array, are also low although as previously mentioned, battery losses are underestimated.

August 11 - August 26 Figure 7.7 summarizes the losses during the August monitoring period. During this period, only 37.7% of the rated energy yield was consumed by loads. High insolation lead to 27.2% of this energy being thrown away during charge

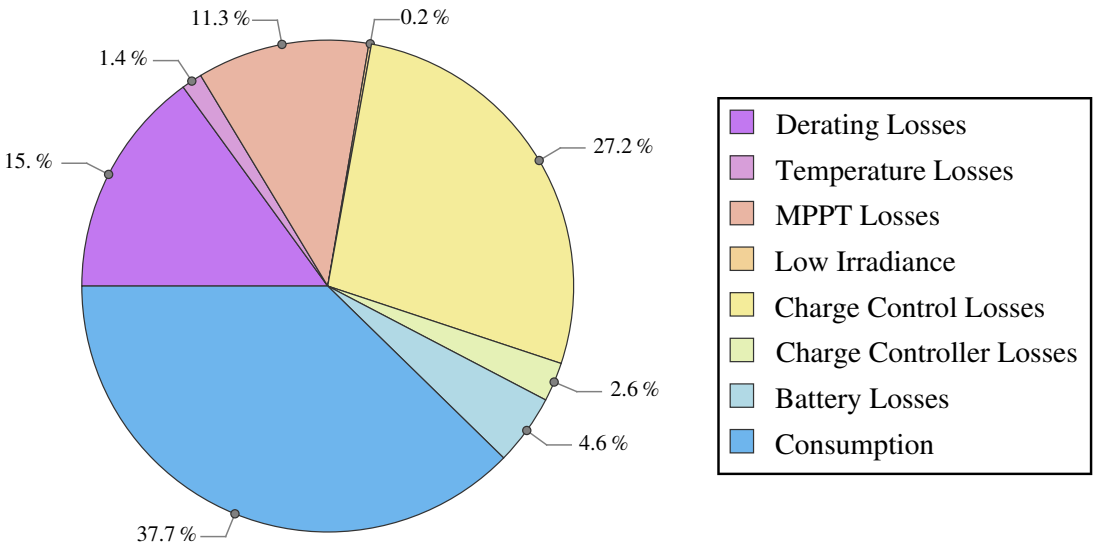

Figure 7.7: Energy losses and consumption during the August monitoring period

control. The de-rating losses are the same during all monitoring periods as the module is assumed not to have degraded in performance significantly during the study. MPPT losses are higher than the previous monitoring period at 11.3%. With the battery operating at a high state of charge, module operating voltages were higher than in the previous period. Normally, PV modules operate below their MPP voltage however IV curves show that this module has an MPP voltage of 14.4V at STC. This low MPP voltage means that the system often operates above MPP, particularly when the battery is in a high state of charge. In this region of the IV curve, module power drops rapidly as current falls. Battery losses are significantly higher than in other monitoring periods due to lower battery efficiency in high states of charge.

September 1 - October 4 Losses during the September monitoring period found in figure 7.8 show a slightly lower usage factor than the July period accompanied by higher charge control losses. Module de-rating and MPPT losses are again the two most significant losses other than charge control. Temperature losses are slightly higher during this period than the previous, as was expected because of the higher average irradiance weighted BOM temperature. This period also has the highest low irradiance losses which is consistent with the lower clearness index for this period which results in longer periods under low irradiance.

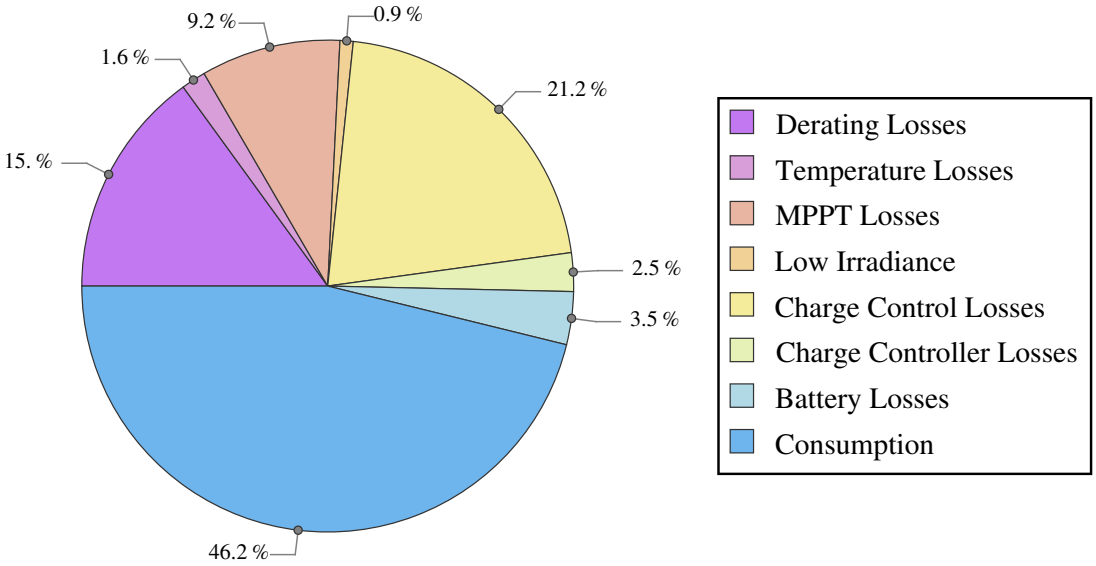

Figure 7.8: Energy losses and consumption during the September monitoring period

Losses Summary Loss analysis indicates possible system over-sizing as we found when looking at normalized performance parameters. After charge control, the largest loss is due to module under-performance. Had the module performed as rated, the charge control losses would have been greater. The cost of the system could have been reduced by selecting a module with a lower power rating. Care should be taken, if possible, to verify the power rating of the module with an IV test at STC. Losses due to non-MPP tracking are found to be significant with losses on the order of 10%. If a 10% reduction in module size decreases module cost by more than the increased cost of purchasing an MPPT, it may be advisable to do so. Low irradiance losses are relatively low.

Temperature losses are also low in the windy and temperate climate of Port Elizabeth. Based on loss analysis and the irradiance weighted average BOM temperature, temperature decreases module performance by 0.35%/ °C. Adjusting for module de-rating gives 0.42%/ °C. Various methods of active and passive cooling could reduce temperature losses but are not likely to be economical. Charge controller losses are low in comparison to others. Because most of these losses are due to voltage drops which are in part ohmic, charge controller losses, as well as line losses, could be reduced by employing a higher system voltage. The lower currents drawn at higher voltage incur smaller losses. Battery losses will be explored further in the final section of this chapter.

7.4 Performance under various conditions

We have thus far examined the performance of the SHS in terms of energy over the time scale of about a month. In order to better understand system dynamics and different operating modes, a look should be taken at short term performance in terms of power. This section will examine system performance in different operating conditions through a more direct analysis of data rather than time integrated parameters.

7.4.1 Performance under clear skies

The ideal operating condition for a solar energy system is of course clear skies. Figure 7.9 shows the irradiance, power, temperature and duty cycle profiles in sub-figures A, B, C and D, respectively, for the 19th of July 2010. The irradiance profile found in figure 7.9.A shows an almost perfectly clear day. There is a small indentation in the early afternoon due to passing clouds and slight deviation in the early morning due to shading from a nearby building. Otherwise, the irradiance profile is perfectly symmetric with a peak irradiance of $963W/m^2$ at solar noon. The total POA insolation on this day was $6.4kWh/m^2$. The maximum module temperature recorded during the course of the day was 50.3 °C with an irradiance weighed average of 27.9 °C. In figure 7.9.C, the BOM temperature can be seen to vary with ambient temperature but is scaled by irradiance. The module is heated by the solar irradiation and the rate at which this heat is dissipated into the surrounding environment is regulated by the ambient temperature.

The power profiles in figure 7.9.B for the PV, load and battery power show good correspondence. Battery power is defined as negative when the battery is discharging and positive while charging. In the absence of PV power, the load power is a mirror image of the battery power. The battery power mimics the PV power under no load conditions with small losses due to charge controller voltage drops observable. When a load is switched on at 11:00, a portion of the PV power is delivered directly to the load, reducing the power delivered to the battery.

The early morning dip in PV power occurring around 8:00 is most likely due to shading that did not occur on the pyranometer. At around 12:20 the potential PV power and measured PV power split, indicating charge control. The large area between these curves is equal to the amount of energy lost during charge control. The usage factor during this day was 0.70. There is also a large gap between the potential PV power and the modeled PV power. This results from operation of the module beyond its MPP voltage. As previously noted, the Helios module has a very low MPP voltage, particularly at high irradiance due to increased module operating temperatures. Because the PV power drops very quickly at voltages greater than V_{MPP}, large MPPT losses will occur when operating

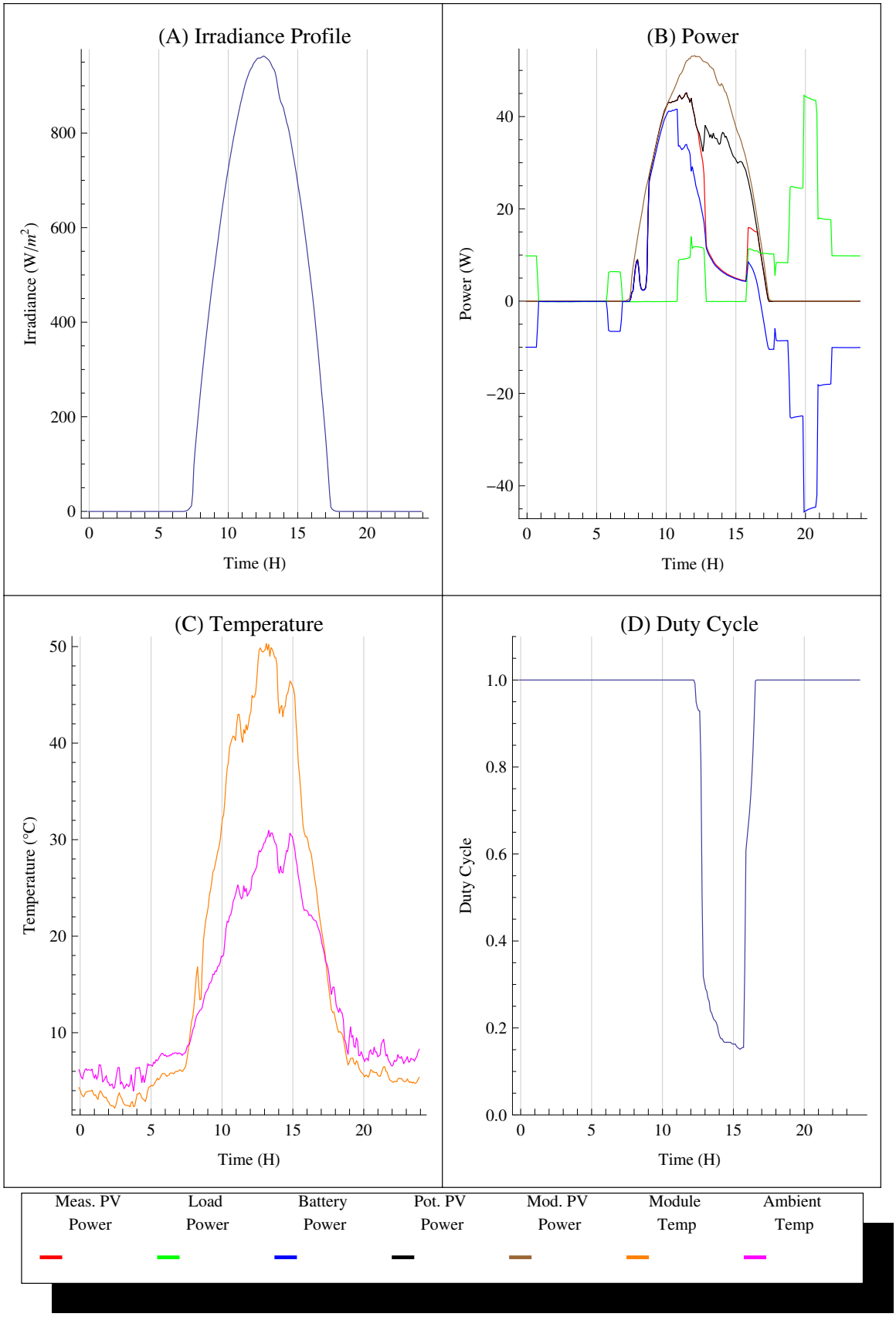

Figure 7.9: July 19, 2010 Laboratory System Monitored Parameter Profiles

in this region.

The charge controller PWM duty cycle profile in figure 7.9.D illustrates the manner in which the charge controller maintains the battery voltage. Around 12:20, the duty cycle dips slightly from one and remains in a range from 0.9-1.0 for a period of about 40 minutes to maintain the battery voltage at the set point until the load on the system is disconnected. After load disconnect, the current to the load is diverted to the battery. In response, duty cycle drops drastically to reduce the current to the battery and maintain the battery voltage. The duty cycle gradually falls as battery SOC rises until 16:00 when a new load is put on the system. Current from the PV array to the battery is diverted directly to the load and the duty cycle of PWM is reduced accordingly. In the evening when the available PV current is no longer sufficient to maintain battery voltage, the duty cycle goes to one.

During the course of the day, the PV array produced 202Wh and the system fed 170Wh to loads. MPPT losses were very large relative to the potential PV energy at 19.5% but the low usage factor makes this rather inconsequential. This highlights the limitations of energy storage in stand-alone systems which severely limits system performance. Storage capacity limitations in combination with the need to design systems for periods of low insolation forces the utilization of over-sized PV arrays.

7.4.2 Performance under mostly clear skies

Figure 7.10 shows the irradiance, power, temperature and voltage profiles in sub-figures A, B, C and D, respectively for the 9th of September, 2010. On a mostly clear day with some passing clouds the irradiance profile, found in figure 7.10.A, is not as smooth as on the clear day just examined. Solar energy incident on the POA was measured at $5.4kWh/m^2$. Several periods of passing clouds are evident in the morning and early afternoon, particularly around noon. The temperature profiles found in figure 7.10.C again show the dependence of BOM temperature on ambient temperature and irradiance. Wind, which was not measured, could explain the larger difference between BOM and ambient temperature in the late morning as compared to the early afternoon despite similar irradiance. This effect was seen in figure 7.4 and discussed in section 7.2. Higher winds in the afternoon would have increased convective cooling of the module resulting in lower operating temperatures.

The power profiles in figure 7.10.B lead to similar observations made for the 19th of July. Large deviations of potential PV power to modeled PV power under high irradiance reflects the PV module's low MPP voltage at high irradiance. Charge control appears to have begun around 13:00 when the load on the system was disconnected and skies began to clear. This is reflected in figure 7.10.D which plots the system voltage profiles. Around

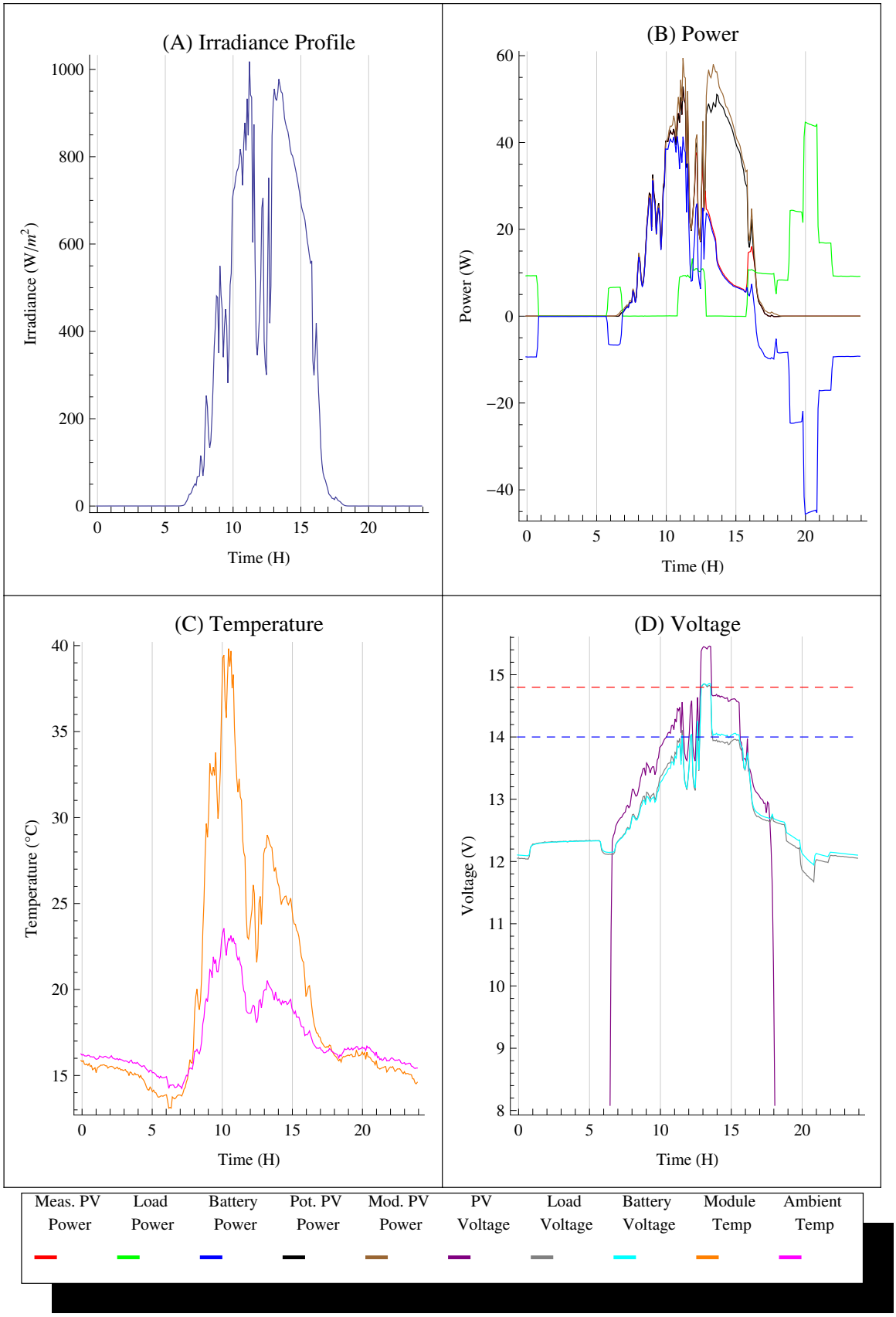

Figure 7.10: September 9, 2010 Laboratory System Monitored Parameter Profiles

13:00, the battery voltage reached its gassing voltage at 14.8V. The charge controller then maintained the battery at this voltage for one hour before reducing it to the end of charge voltage at 14.0V. This voltage is maintained until the available PV current is no longer sufficient to do so and is achieved by variation of the PWM duty cycle.

The voltage drops from the PV array to the battery that are responsible for maintaining the PV array well above its MPP voltage are also clearly visible in figure 7.10.B. While maintaining the battery at 14.8V, the PV array operated at 15.4V, well above its measured MPP voltage of 14.4V. The total PV energy collected on the day was 195Wh with a total load of 167Wh. The usage factor for the day was low at 0.67 while losses of potential PV energy due to non-MPP tracking amounted to 7.2%. The sometimes cloudy skies, particularly during peak irradiance, resulted in lower operating voltages during the day which served to reduce MPPT losses.

7.4.3 Performance under overcast skies

Overcast skies severely limit the performance of any solar energy system. Figure 7.11 shows the irradiance, power, temperature and voltage profiles in sub-figures A, B, C and D, respectively for the 19th of September, 2010. The 19th of September saw a total POA insolation of only $920Wh/m^2$. Five minute averages of irradiance only briefly surpassed $300W/m^2$ as can be seen in figure 7.11.A. Temperatures on this day, plotted in figure 7.11.C, were low with the maximum BOM temperature on the day being 24 °C. This would serve to enhance slightly the energy yield compared to the rated power at STC although the low irradiance would severely limit or cancel any gains due to low irradiance losses.

The power profile in figure 7.11.B shows very low array yield. In this case, potential PV power is equivalent to the measured PV power because no charge control occurred on this day. The modeled PV power also follows the measured PV power very closely. Low system voltages caused by low irradiance reduce the PV array's operating voltage below the module's MPP voltage. Power drops more slowly in this region resulting in array operation close to MPP power.

It can be seen in figure 7.11.D that the battery voltage did not approach the gassing voltage, achieving a maximum of 12.6V. PV voltage only briefly surpassed 13.0V. The smaller voltage drops from PV array to battery are the result of low currents which serve to reduce ohmic voltage drops.

The total PV energy collected during the course of the day was 45.5Wh. This was far exceeded by the daily load of 164Wh. This load is the lowest daily energy consumption of the three days examined. Despite the fact that the simulated load profile is exactly the same on all days, the energy consumed is lower due to lower operating voltages.

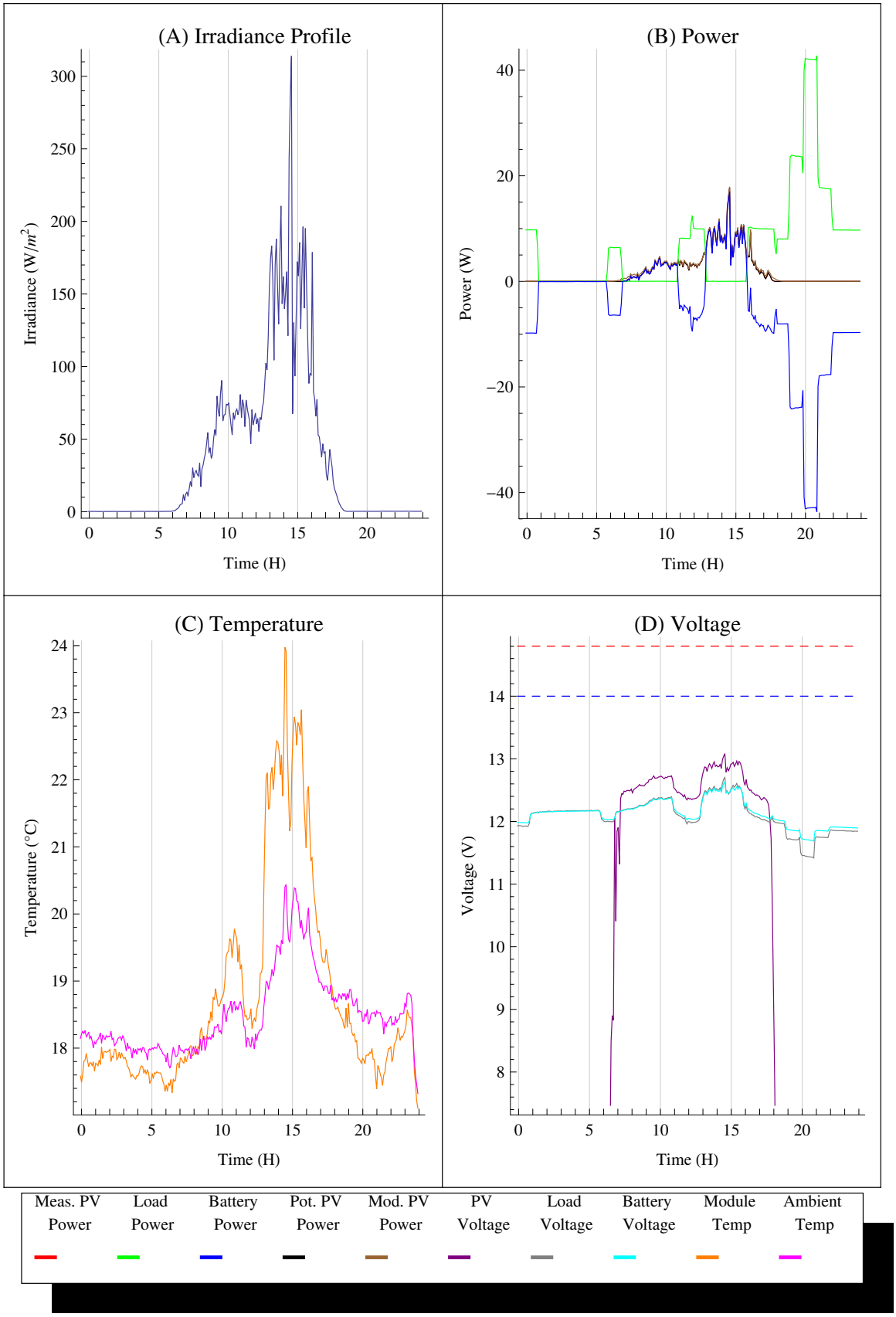

Figure 7.11: September 19, 2010 Laboratory System Monitored Parameter Profiles

For ohmic loads, the power consumed by loads varies with V^2. A constant current load's consumption is proportional to voltage. This means that higher system operating voltages lead to higher energy consumption by loads, particularly for ohmic loads. The load energy consumption was reduced by about 4% from the 9th of September due to system operating voltage.

7.5 Component Performance and PWM Error Analysis

This section will examine in more detail the performance of individual components of SHSs. It is important that all components of SHSs operate optimally to prevent bottlenecks on the system performance. A PV array that does not perform as rated will not be compensated for by an extremely efficient charge controller or storage device. Likewise, an exceptionally high performing PV array will not be able to power loads at night when the system battery is not effectively storing the energy produced.

7.5.1 PV Array

The process of generating the energy required to power loads begins with the PV array. If the PV array does not provide enough energy to power the loads on the system, the system will most certainly fail. The PV module used in this study is a 70W mono-crystalline module of 36 series connected cells manufactured by Helios. A laboratory analysis of the performance of this module has been documented in chapter 3. This section will examine the module performance in the field. Module performance is characterized by its efficiency in converting sunlight into electrical energy. Table 7.5 defines the efficiencies discussed in this section.

Table 7.5: PV Array Efficiency Definitions

Efficiency	Definition
Rated Efficiency	Manufacturer specified efficiency at STC
De-rated Efficiency	Measured efficiency at STC
Modeled Efficiency	Model predicted efficiency in the field
Potential Efficiency	Measured efficiency in the field corrected for duty cycle
Actual Energy	Measured efficiency in the field

The module's efficiency in converting solar irradiation at STC into electrical energy is rated at 10.3% as calculated from manufacturer specifications of peak power and measured module dimensions. Recalculated with the measured maximum power near STC gives a

de-rated efficiency of 8.8%. This assumes operation at MPP and neglects low irradiance and temperature losses. The actual efficiency over the 3 monitoring periods was calculated at 5.8%, 4.6% and 5.4% respectively. These measured efficiencies are limited largely by the system usage factor as discussed in section 3 of this chapter. Taking into account duty cycle gives efficiencies of 7.7%, 7.5% and 7.6%. These efficiencies cover a smaller range of values than the uncorrected values. The remaining variance can be attributed to the higher average operating voltages that, in this system, push the module further from MPP thus reducing array efficiency. The modeled array efficiencies were steady at 8.6%, 8.6% and 8.5%. The difference between the modeled efficiency and de-rated efficiency of 8.8% can be attributed to low irradiance and temperature losses.

The PV module in the SHS performs well below it's rated power. This is largely due to an oversized array which resulted in large amounts of charge control. The approximately 1% difference between potential array efficiency and modeled MPP array efficiency means about a 13% increase in potential PV energy could be obtained with the use of a MPPT charge controller. Taking the July period as the worst case month with a usage factor of 75%, it can be deduced that an array of $61.2W \times 0.75 \ = 45.9W\%$ would be sufficient to power the system. An increase of 13% efficiency due to MPP tracking would further reduce the required array power by $45.9W/1.13 = 40.6W$. This reduction in PV array size would lead to increased battery operation at low SOC causing low voltage disconnect during periods of low insolation and an increased rate of battery degradation. An array size of 50W-55W gives an A:L ratio of 1.23-1.35 and would be a good compromise.

7.5.2 Charge Controller

The charge controller efficiency can be estimated by the ratio of energy measured going out of the charge controller to the energy measured going in. Energy losses are due to voltage drops in the charge controller and the energy consumption of the charge controller itself. Charge controller self-consumption is rated at less than 5mA.

The voltage drops in the charge controller are both ohmic and constant diode voltage drops in the case of the Steca Solsum 6.6c. The energy into the charge controller is the sum of the integrated PV power and the integrated positive measurements of battery power. The energy out is the sum of the integrated negative battery power and the integrated load power. During a 5 minute record interval, it is possible for the battery power to take on both positive and negative values. The recorded value will be the average battery power. Because of this, some information is lost on exactly how much energy went into the charge controller from the battery and how much power went into the battery from the charge controller. This can happen when loads are switched on or off during a record interval or when the system is under load during charge controller.

In the former case, the pulses oscillate between charge and discharge rather than charge and no charge.

All this means that the calculated charge controller efficiency is a lower limit. Average charge controller efficiencies over the monitoring periods were found to be 96.3%, 96.6% and 97.2% in chronological order. Analysis of data on the voltage drop from PV array to battery and PV current suggests a diode voltage drop of about 0.3V and an ohmic drop due to a resistance of around 0.08Ω. The relative small diode voltage drop is characteristic of a Schottky diode which responds quickly to the rapidly changing voltages such as those occurring in PWM charge controllers [60]. This is the most significant source of energy loss in the charge controller due to the larger diode voltage drop in addition to ohmic losses.

7.5.3 Battery

Battery performance is more difficult to monitor in an automated manner. Periodic battery tests, described in chapter 3, were carried out to monitor changes in battery performance over time. The results of these tests are summarized in table 7.6. A significant drop in battery efficiency and particularly capacity is observed between the initial test on March 1st when the battery was acquired and the second test after the first monitoring period on July 28th. A long period of storage without charge or discharge is most likely responsible for the majority of capacity loss. This underlines the need to store batteries under a float charge to prevent capacity loss due to sulfation.

Table 7.6: Battery C_{20} Capacity Test Results

Period	March 1	July 29	August 27	October 5
Capacity (Ah)	96.2	63.7	65.3	58.8
Capacity (Wh)	1148	749	768	688
Coulombic Efficiency (%)	93.5	84.6	84.6	81.7
Energy Efficiency (%)	80.5	69.5	69.8	66.6

Ideally, another battery test would have taken place just before the start of monitoring but due to a technical fault in the battery testing system, this was not possible. The initial battery test shows excellent correspondence of the battery's tested capacity and its rated 96Ah capacity. Energy and coulombic efficiencies were also high. The August 27th test revealed a small recovery of battery capacity after a period of cycling. This is to be expected since periods of cycling can reverse the sulfation that occurs during periods of non-use. The October 5th test shows a reversal of this trend with a 6.5Ah loss in battery capacity.

Battery energy efficiency varied with battery capacity as can be seen in table 7.6. The initial test showed an excellent energy efficiency of 80.5% but dropped sharply with the battery capacity to 69.5% on the second test. Battery energy efficiencies of around 70% are typical. At the end of the last monitoring period, the battery energy efficiency had dropped to 66.6%. It should be noted that the battery energy efficiencies listed in table 7.6 are calculated from data obtained from the charge-discharge test described in section 3.2.2. The energy efficiency of a battery varies as a function of its state of charge. The average battery energy efficiency in a typical SHS will likely be slightly different from the value obtained during the charge-discharge test.

Assuming that the energy efficiency obtained in the charge-discharge test is similar to the average energy efficiency during normal operation in the SHS, we can estimate the size of the energy losses due to the battery. The measured energies delivered by the battery to loads during the monitoring periods were 4219Wh, 2183Wh and 4762Wh, respectively. Multiplication by one over the corresponding measured battery energy efficiencies minus one gives the approximate energy losses associated with the battery. As a percentage of the rated PV energy, for the sake of comparison with the values obtained in section 7.3.2 on the energy loss analysis, the energy losses due to the battery are 18.4%, 13.2% and 18.9%, respectively. This makes battery losses on of the largest in the system.

The tested capacity from the final battery test of 58.8Ah is only 61% of rated capacity. Despite this loss in capacity, no load shedding occurred during the monitoring period. The minimum load voltage achieved was 11.34V on the night of September 20th, above the tested LVD voltage of 11.2V. Figure 7.12 plots the estimated minimum SOC of the SHS battery during the monitoring periods. The low load voltage described above on September 20th is easily observable. The SOC values are estimated using the open-circuit battery voltage after a period of rest following the disconnect of all loads. The fixed load profile makes this easy to measure. The battery voltage at 5:00AM each day was used to estimate SOC. At this time the battery has been in a resting state for about 4 hours. The relationship between SOC and open-circuit voltage is approximately linear and can be estimated by

$$SOC = \frac{V_{oc,bat,SOC(100\%)} - V_{oc,bat}}{V_{oc,bat,SOC(100\%)} - V_{oc,bat,SOC(0\%)}} \tag{7.2}$$

where $V_{oc,bat}$ is the measured open-circuit battery voltage and $V_{oc,bat,SOC(X\%)}$ is the open-circuit battery voltage at X% SOC [61]. Typical values of $V_{oc,bat,SOC(100\%)}$ and $V_{oc,bat,SOC(0\%)}$ are 12.65V and 11.85V. These voltages were used in calculating the SOC in figure 7.12. Typical DOD during monitoring was about 40%. The load on the system represents about 20%-25% of measured battery capacity.

Most SHS are not capable of bringing the system battery to 100% SOC because of the

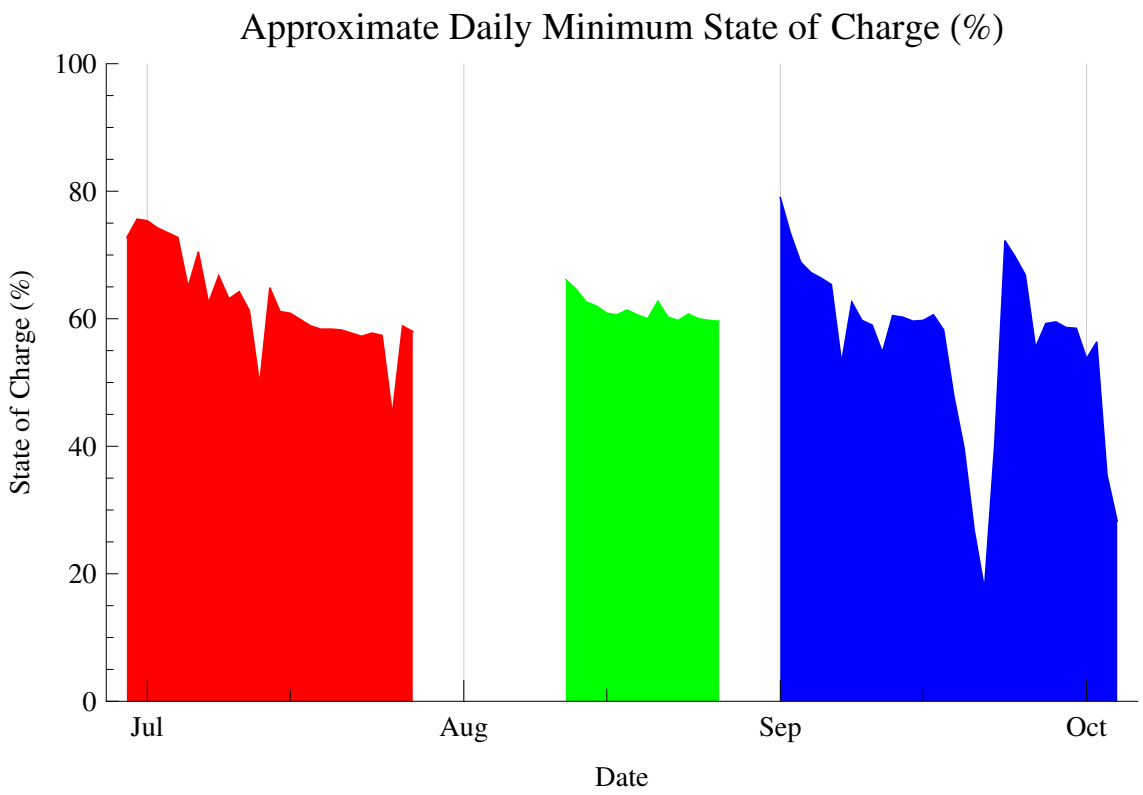

Figure 7.12: Approximate Daily Battery Minimum SOC

long duration of constant voltage charging required. A more typical maximum SOC in a stand-alone solar system is around 80% [61]. This agrees well with the estimated 40% DOD (equivalent to a 60% minimum SOC) under a load of 20% storage capacity. The maximum DOD observed was 82% on the night of September 20th. This is a bit of an overestimate of DOD on this day because battery voltage begins to drop more rapidly at low SOC. As discussed in chapter 2, the A:L ratio is an indicator of the PV array's ability to provide sufficient charge to the battery to maintain battery health. The A:L ratios for the monitoring periods were, in chronological order, 1.5, 1.9 and 1.6 and indicate that the PV array is sufficiently large to maintain battery health. A:L ratios of around 1.3 or higher are usually considered to be acceptable. The July A:L ratio is in line with the A:L ratio of 1.5 predicted during system design for the worst case month (expected to be June).

Actual battery capacity in the SHS fell short of the designed capacity due to capacity loss from a period of storage. Batteries purchased for SHS purposes in rural areas are often kept in this state for long periods until sale so in some way this effect inadvertently simulated the situation in the field.

Despite the capacity loss, no load shedding was observed. This could be due in part to periodic battery tests which restored the battery to a full SOC. On one occasion, the

battery came very close to LVD. Without the roughly one third reduction in battery capacity due to a period of storage, this would not have occurred. The battery sizing of the system was appropriate but costs could be cut from the system by reducing the designed battery capacity without risk of significant load shedding.

Capacity loss between the August and October battery tests was significant after a period of capacity recovery. Continued capacity loss at this rate, about 7% of rated capacity/month, would results in load shedding and a short battery lifetime. This would significantly affect the life-cycle cost of the system. Due to the limited life spans of lead-acid batteries, the development of an affordable, efficient and long lasting energy storage device would result in the most significant reduction in the life-cycle cost of SHSs.

7.5.4 Load Profile

It does not make so much sense to speak of load "losses" because it is the purpose of the entire system to create energy to be consumed by loads. But loads typically have power ratings. These power ratings are then used to estimate load requirements. The loads used in this system to simulate a typical rural household load were three low power CFLs and one 40W incandescent bulb. Because the load was simulated, the precise amount of energy that should have been consumed by the loads had they performed as rated can be calculated. The ratio of measured load energy to rated load energy can then be calculated. For the monitoring periods analyzed here, this ratio ranged from 0.84-0.85. This means the loads actually consumed only about 85% their rated power. This directly effects the amount of energy thrown away during charge control. Had the loads consumed their rated power, energy consumption would have increased by about 18%. On the pie charts in figures 7.6, 7.7 and 7.8, this energy could have come out of the sector for charge control losses. So in some sense it can be said that the array was not oversized as much at it appears, rather the loads were overestimated. The value that is truly important is the A:L ratio, or the ratio of the array energy yield to the load on the system.

7.5.5 PWM Error Analysis

In addition to recording PWM corrected PV power, uncorrected values were also computed and recorded to give an idea of the scale of the PWM error. The errors in energy measurement found during the August, September and October monitoring periods were overestimations of 3.0%, 5.2% and 3.8%, respectively. The errors, as expected, are negatively related to the usage factors during the monitoring periods. More charge control of course leads to larger PWM errors.

The measurement method utilized in the laboratory system is particularly susceptible

to PWM errors. A long integration time was selected in order to obtain full waveforms so that duty cycle and high and low states could be accurately determined. This long integration time means that normally computed power will be the product of the average current and average voltage over a full pulse. The averaging of charge current with short-circuit current will result in high measurement of current while the averaging of charge voltage with short-circuit voltage will result in low measurement of voltage. In general, the product of averages is not equal to the average of products which leads to measurement errors by this method. In this case the high current had a greater effect resulting in significant overestimations of power.

7.6 Summary

Analysis of the laboratory SHS monitoring data reveals that the largest source of energy loss in the system is charge control. This is due in part to an over-sized PV array, however, it has also been seen that the loads on the system require significantly less power than their rated power. Other significant limitations to system performance were found to be PV module degradation and performance below rated power and MPPT losses. It is estimated that a 10% increase in potential PV energy could be produced with the use of a MPPT charge controller. Overall, the cost of the system could be significantly reduced by decreasing the size of the PV array and employing a MPPT charge controller. It is estimated that a 25% reduction in the size of the PV array could still power the system loads and maintain the battery in a healthy state under the conditions found during monitoring.

The loss analyses do not fully take into consideration energy losses in the battery. Battery tests show significant losses of battery capacity and efficiency. This was, however, in large part due to a long period of disuse before deployment in the system highlighting the importance of proper battery storage. Despite the capacity loss, no load shedding occurred during monitoring. Battery energy losses can be estimated using measured battery efficiencies obtained from charge-discharge tests. These estimates suggest that battery losses are on par with MPPT losses at around 10% of rated PV power.

Chapter 8

Remote System Monitoring

The remote solar home system allowed for the monitoring of a typical system under use in the field. Remote monitoring poses more challenges and has more limitations than laboratory monitoring but allows an examination of how systems are used and perform in the field.

The challenges involve the limited resources available at the site and the time and cost involved in visiting the site to collect data and ensure proper operation. For example, a broken resistor during system installation required a 90 minute round trip drive to the the nearest large town to replace it. Inadvertent system disruption by users can also cause problems with monitoring and solar home systems in general.

During the first site visit six weeks after installation, it was discovered that a wire connecting the PV array to the charge controller had been pulled loose about eight days after monitoring began. The system went into a permanent state of low voltage disconnect but the system users never communicated the problem. This resulted in five weeks of lost data and lost system usage that could have been fixed with a screwdriver. Because of this, only four weeks of reliable data were available at the time of publication of this study.

8.1 System Description

The remote solar home system was installed at a household in a village called Tyefu near the town of Peddie in the Eastern Cape of South Africa. The home is located in a semi-arid region at 33° 10' 50" S, 26° 58' 32" E. The home is occupied by an elderly woman and her granddaughter who is a high school student. The home is also visited on occasion by relatives visiting from outside the village.

The system design, described in chapter 2, provided for two 55W mono-crystalline Siemens solar modules, two 65Ah deep-cycle lead-acid batteries and a 12A Steca Solarix

Table 8.1: Mobile System Specification

Component	Name	Quantity
PV Array	55W mono-crystalline Siemens PV module	2
Battery Bank	65Ah Deep Cycle Lead Acid Battery	2
Charge Controller	Steca Solarix Gamma (12A)	1

charge controller as summarized in table 8.1. System design was based on insolation data from Port Elizabeth and an estimated average daily load of 306Wh.

8.2 Meteorological Data

Specific meteorological data for the site in Tyefu was lacking. Estimates of solar insolation may be obtained from satellite data or by interpolation of data from nearby sites. In designing the system, interpolated insolation data for the site generated with the Meteonorm software package was corrected for array tilt and used for the purpose of system sizing. The average daily POA insolation during the period from October 19, 2010 to November 15, 2010 was measured at $4.1kW/m^2$ with an average clearness index of 0.48. The average irradiance weighted BOM temperature, discussed in chapter 7, was 34.5 °C.

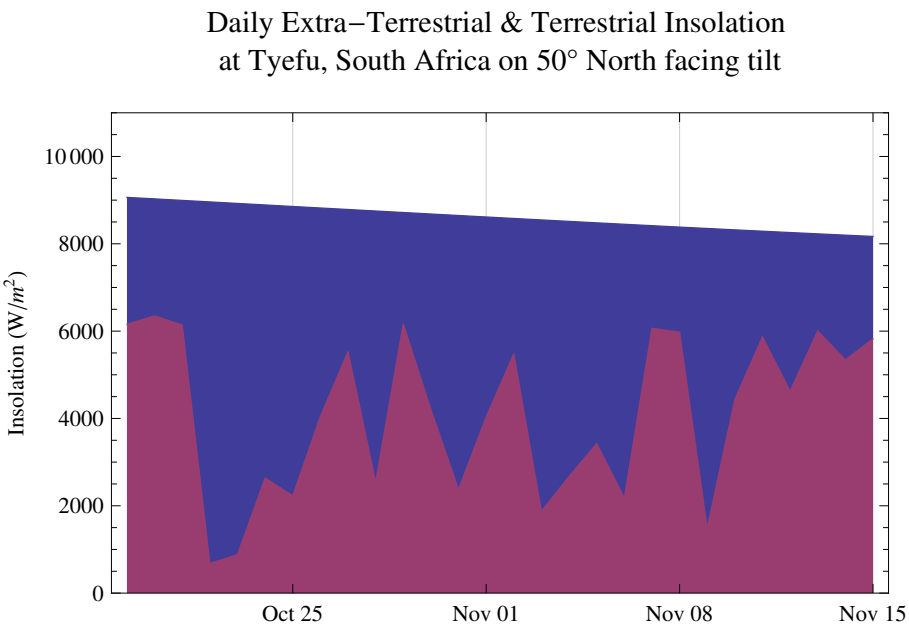

Figure 8.1: Daily POA Insolation and Extra-Terrestrial POA Insolation

The average extra-terrestrial POA solar insolation and daily POA insolation during monitoring is plotted in figure 8.1. It shows the available POA extra-terrestrial solar insolation decreasing from October into November because the array tilt is optimized for

the winter. Clearness index can be deduced by taking the ratio of measured insolation to extra-terrestrial insolation. Sky conditions were quite variable throughout the period.

The daily maximum temperatures ranged from 17.7 °C to 37.2 °C. Figure 8.2 plots the daily maximum and minimum ambient temperatures. BOM temperature is of course dependent on incident irradiance, ambient temperature and wind speed which was not monitored. The relationship between the incident irradiance and the difference between ambient and BOM temperature is plotted in figure 8.3. The relationship is approximately linear within a wide band. This band is due to wind, the speed of which affects the rate of conductive heat transfer from the module to the surrounding air. This was also seen in the laboratory system and can be observed in figure 7.3.

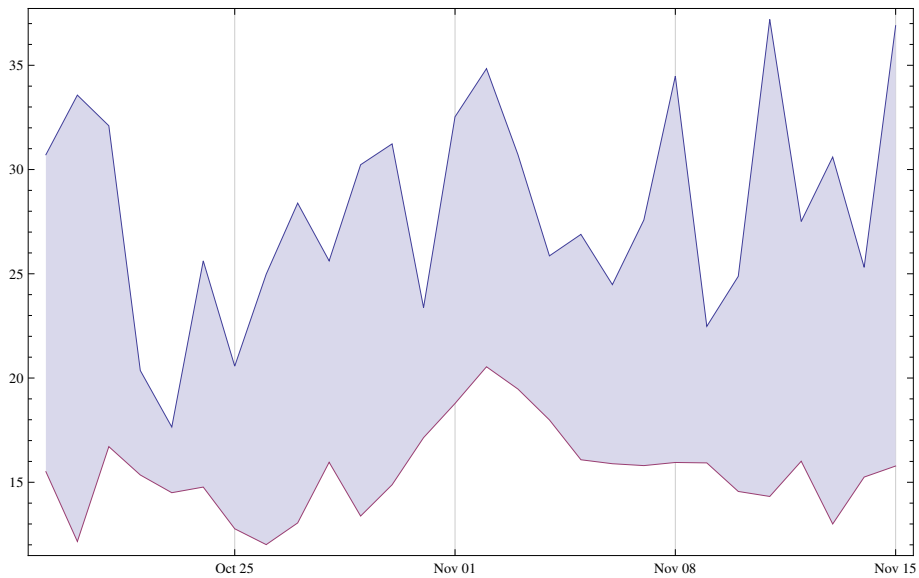

Figure 8.2: Maximum and Minimum Daily Ambient Temperature

The meteorological conditions under which the system operated during monitoring were poor. The average daily insolation was only $4.1kWh/m^2$ while the system was designed assuming a worst month average of $5.1kWh/m^2$. The average irradiance weighted BOM temperature was 9.5 °C higher than the STC temperature which, assuming a temperature de-rating of PV power of about 0.5%/ °C, suggests temperature losses from the PV array of around 5%. This is, however, still smaller than the temperature losses accounted for in the sizing of the PV array. The periods of low clearness index will also increase low irradiance losses. With respect to data used during system design, the operating conditions of the system fell short of expectations. The data obtained, however, represents long term averages of meteorological data and are expected to vary from year to year.

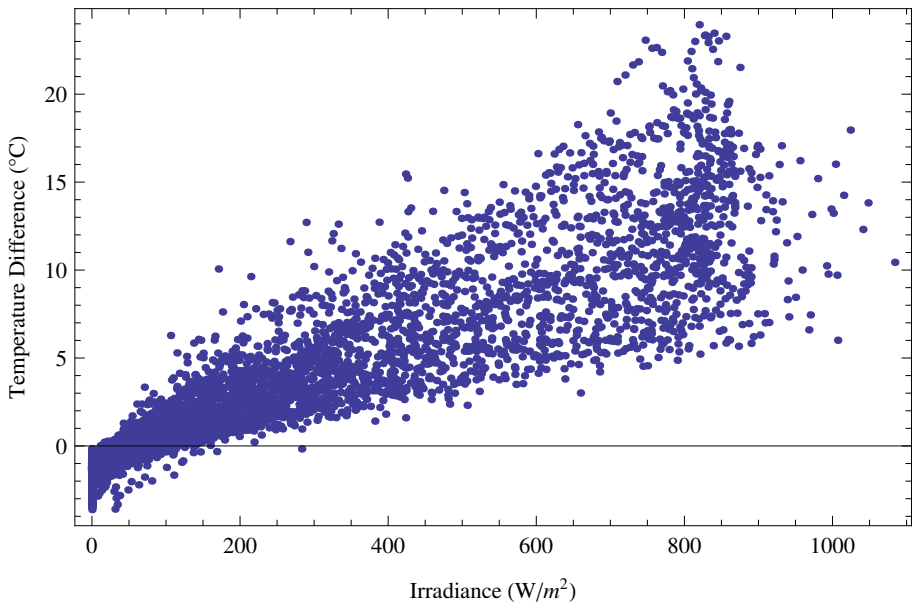

Figure 8.3: Difference of BOM and Ambient Temperature versus POA Irradiance

8.3 System Performance

Table 8.2 gives the performance parameters of the Tyefu SHS normalized to the nominal system PV array power during the monitoring period from October 19, 2010 to November 15, 2010. The definitions of these parameters can be found in table 7.2. The performance ratio of 0.46 is similar to that found for the laboratory based system. Because the monitoring period began while the battery was in a low state of charge after a long period of load disconnect and the reference yield was lower than expected, the usage factor was significantly higher than in the laboratory system at 0.78. This is higher than what it would have been had the system load not been significantly smaller than estimated.

The load on the system normalized to the nominal array power, represented by the final yield for stand-alone systems, was estimated to be 2.78h/d during system design. The measured final yield was only 1.91h/d. The measured load profile will be examined in more detail in section 5 of this chapter. Array performance was poor in comparison to the laboratory system despite a larger usage factor due to the lower than expected reference yield and higher BOM temperatures.

Capture losses for the remote system were much smaller than for the laboratory system even when accounting for the smaller reference yield. Array efficiency was significantly higher than that of the laboratory system at 8.2%. System losses were however nearly twice as large for the remote system compared to the laboratory system at 0.71. The mean system efficiency was found to be 73% compared to efficiencies in the mid-eighties for the

Table 8.2: Summary of Remote System Performance Parameters

Parameter		
Y_A	(h/d)	2.62
Y_f	(h/d)	1.91
Y_r	(h/d)	4.12
L_C	(h/d)	1.50
L_S	(h/d)	0.71
PR		0.46
UF		0.78
$\eta_{A,mean}$	(%)	8.2
$\eta_{S,mean}$	(%)	73.0
η_{tot}	(%)	6.0

laboratory system. This is due to the low initial state of charge of the system batteries. The system efficiency here is calculated by taking the ratio of the energy consumed by loads to the energy provided by the PV array. A significant portion of the PV energy went towards charging the system batteries. This energy is stored in the batteries but by the standard method is considered an energy loss in this case. Because monitoring of the laboratory system started with the battery in a high state of charge and most probably ends the monitoring period in a lower state of charge, the system efficiency will typically be somewhat inflated. The problem of initial battery SOC becomes less significant with longer monitoring periods.

The total system efficiency of 6.0% compares favorably to the laboratory system due to greater array efficiency. This is due in part to the larger usage factor resulting for the low initial battery SOC. Even while accounting for the larger UF, the PV array in the remote system still out performed the laboratory system as will be examined in section 5 of this chapter.

It was not possible to extract the device parameters necessary to apply the model used in the preceding chapter before the system was deployed in the field. Therefore the depth of loss analysis used in chapter 7 is not possible here without interrupting the system in the field to extract these parameters. Figure 8.4 shows a simplified loss analysis illustrating the proportion of array capture and system losses to the energy consumed by the loads on the system. Just under half of the rated array energy was consumed by the loads. About two-thirds of the energy lost was due to array capture losses while the remaining third is credited to system losses.

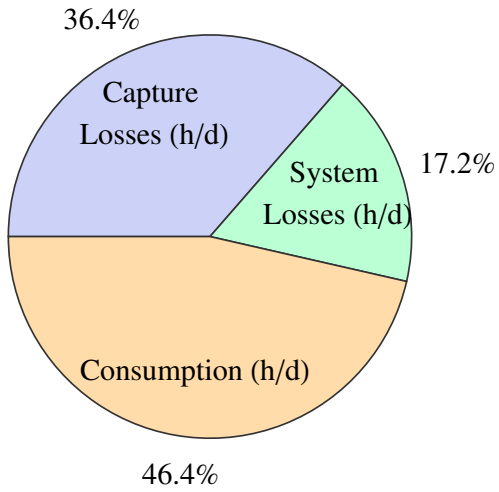

Figure 8.4: Tyefu SHS Performance Losses and Energy Consumption

8.4 Performance under various conditions

Thus far we have only examined the long term performance of the system in terms of energy. To shed more light on what happens in SHSs on short time scales, power parameters can be examined over the period of a day. In this section, system performance under different environmental conditions will be examined.

8.4.1 Performance under clear skies with no charge control

Figure 8.5 shows the irradiance, power, current and voltage profiles in sub-figures A, B, C and D, respectively, for the 20th of October 2010. Under normal operating conditions clear skies usually leads to charge control. As such, the PV power profile found in figure 8.5.B is rare. October 20th was the first clear day after monitoring began on the Tyefu SHS which was initially in low-voltage disconnect. The low state of charge of the battery allowed it to accept all the potential charge from the PV array. The battery power followed the PV power closely with ohmic losses increasing with increasing currents.

The load power profile shows energy consumption only during the night as would be expected for a system powering only lighting. There is an 11W base load throughout the night that is the 15W rated outdoor CFL with a day/night sensor. It was seen in chapter 7 that CFLs often consume significantly less than their rated power. Indoor lights were used from 18:30 to 22:00 indicating an earlier than predicted bedtime in the household.

The clean irradiance profile in figure 8.5.A indicates clear skies. The BOM temperature was high particularly in the late morning when it briefly surpassed 50 °C. The

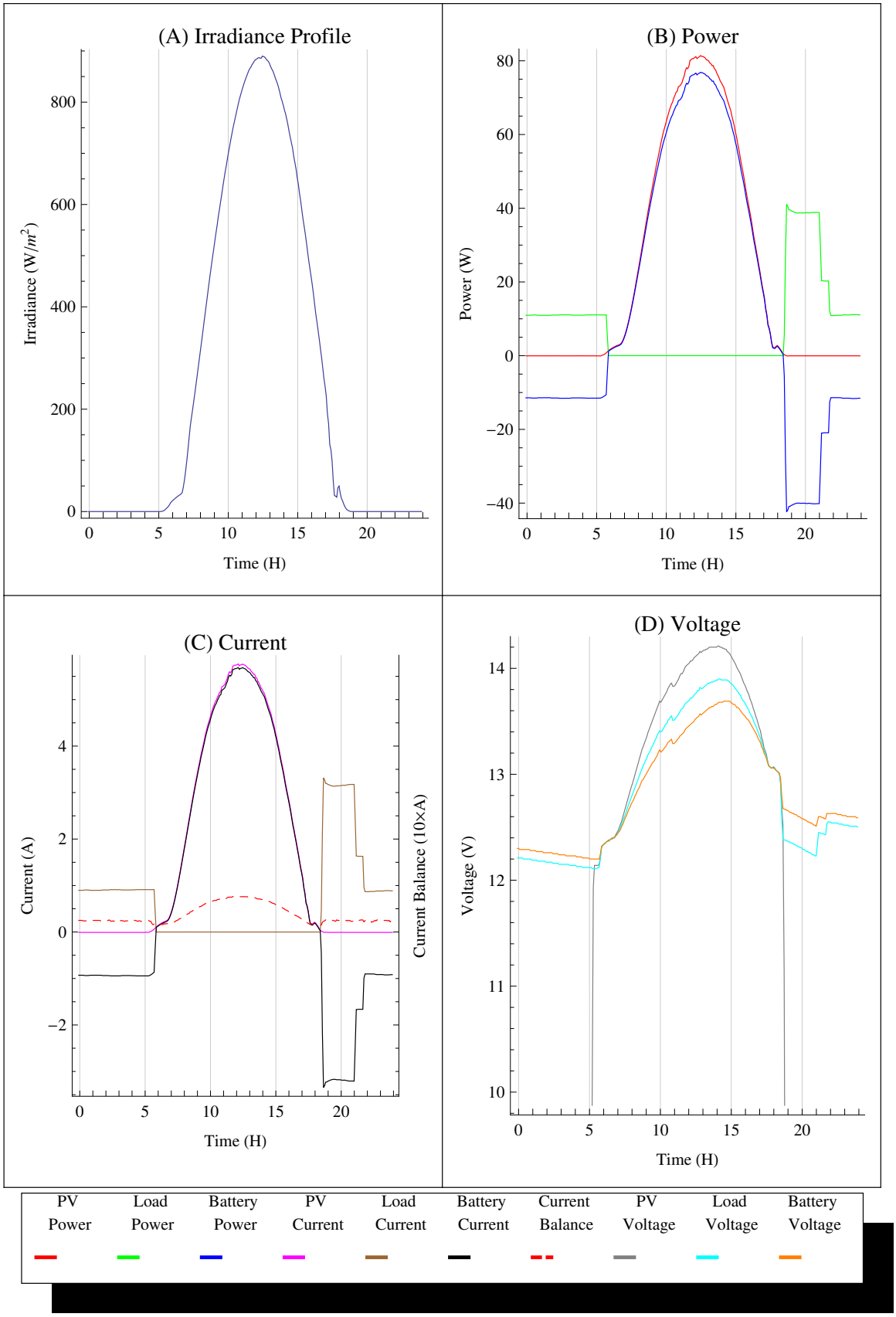

Figure 8.5: October 20, 2010 Remote System Monitored Parameter Profiles

maximum ambient temperature was 33.6 °C. The average irradiance weighted BOM temperature was well above STC rating at 38.8 °C.

Figures 8.5.C and 8.5.D depict the current and voltage profiles of the PV array, battery and load. The voltage drops behave qualitatively as expected with voltage drops between system components increasing with increasing currents and the sign of the drops being dictated by the direction of the current. Voltage drops from the PV array to the battery when current is flowing from the array to the battery, while the drop occurs from the battery to the load when current is flowing to loads.

The current flows in the system should be balanced minus the small self-consumption of the charge controller. The dotted line in figure 8.5.C shows the current balance throughout the day and shows small deviations of battery current from PV current during peak charge currents. This is likely due to small errors in the shunt calibrations which are magnified at higher currents. The current balance over the day indicates a loss of 0.9Ah compared to the total array charge of 40.6Ah. This amounts to an average current of 37mA, much higher than the 5mA charge controller self-consumption rating. Examination of the current balance profile indicates an underestimation of battery current or an overestimation of PV and load current. This is evident from the current balance which should be nearly zero but shows that PV and load currents are greater than the battery current, the difference increasing with increasing current.

October 20th had a total POA insolation of $6.3kWh/m^2$ and an average irradiance weighted BOM temperature of 38.8 °C. The energy produced by the PV array was 563Wh with a total daily load of 200Wh. Average PV array efficiency was 10.4% compared to the rated efficiency at STC of 12.9%. Adjusting for temperature effects using manufacturer specified thermal parameters gives an efficiency of 11.2%. The remaining loss of efficiency is due in large part to operation away from MPP.

8.4.2 Performance under clear skies with high module temperature

The following two days to be analyzed are similar in that they received high POA insolation and had low usage factors but different in terms of BOM temperature. The first to be considered had a high irradiance weighted average BOM temperature of 44.0 °C while for the second day it was only 31.8 °C.

Figure 8.6 shows the irradiance, power, temperature and voltage profiles in sub-figures A, B, C and D, respectively, for the 11th of November 2010. Figure 8.6.A shows the POA irradiance profile on November 11, 2010 at the site of the Tyefu SHS. Irradiance was high with some clouds in the afternoon. The total insolation for the day was $5.9kWh/m^2$.

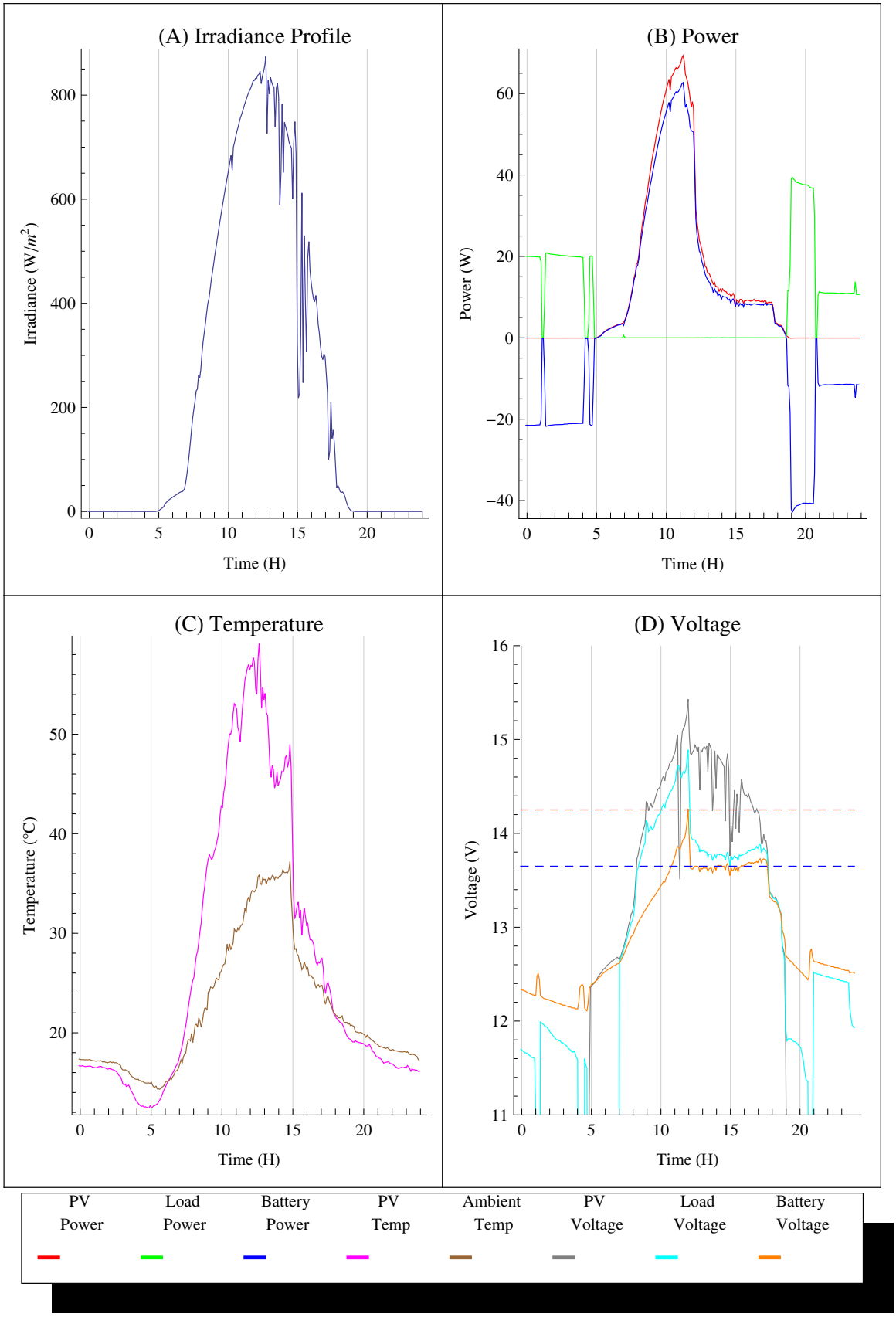

Figure 8.6: November 11, 2010 Remote System Monitored Parameter Profiles

The power profiles in figure 8.6.B are as expected with load power mirroring battery power during the night and battery power mimicking PV power during the day with larger power losses at higher powers due to increased voltage drops. The sudden drop in PV and battery power at around 11:15AM indicates the start of charge control. The long period of charge control lead to a low usage factor of 0.61.

Voltage profiles in figure 8.6.D give an indication of charge controller set points. Charge control began when the battery reached about 13.9V however the battery voltage continued to rise to a value of 14.25V around 12:05PM. The charge controller then reduced the battery voltage to 13.65V where it was maintained during the rest of the day. This is near to the manufacturer specified end of charge voltage of 13.7V. This set point is temperature compensated by -4mV/K/cell. The compensation temperature used by the charge controller is measured within the charge controller. The temperature measured by the charge controller is unknown but the ambient temperature measured by the data logging system of around 35 °C would suggest negative temperature compensation on the 13.7V set point. This is qualitatively in agreement with the set point of 13.65V observed in the monitoring data.

High BOM temperatures can be seen around midday in figure 8.6.C with a peak of 59.1 °C. The ambient temperature reached a high of 37.2 °C and stayed within a few degrees of 35 °C for most of the afternoon until some clouds and possibly wind appear to have arrived around 3:00PM causing a sharp drop in both ambient and BOM temperatures. BOM temperatures during the day were high with an average irradiance weighted BOM temperature of 44.0 °C as previously mentioned.

The high temperatures negatively affected the PV array efficiency. The PV average array efficiency during the day was 6.1%. Adjusting for duty cycle gives a potential array efficiency of 9.9%. If manufacturer specified temperature coefficients are used, an efficiency of 11.1% is found, near to that found on October 20, as seen previously. This translates to nearly an 11% reduction of array yield demonstrating the importance of temperature effects on PV array performance.

The duty cycle reached lows near 0.17 during the day with a daily usage factor of 0.61. In terms of energy, 303Wh were collected by the PV array with a total load during for the day of 188Wh.

8.4.3 Performance under clear skies with low module temperature

November 7, 2010 was qualitatively similar to November 11, analyzed above. Total POA insolation was slightly higher at $6.1kW/m^2$ and the usage factor of slightly lower at 0.59.

The exception to the similarities is the average irradiance weighted BOM temperature which was calculated to be more than 10 °C lower than on November 11th at 31.8 °C. These lower module temperatures should result in increased array efficiency. The maximum ambient temperature during the day was 27.6 °C. The total load during the day was similar to that on November 11th at 190Wh and the total energy collected from the PV array was 330Wh.

Figure 8.7 shows the irradiance, power, temperature and voltage profiles in sub-figures A, B, C and D, respectively, for the 7th of November 2010. The irradiance profile in figure 8.7.A shows mostly clear conditions with some morning clouds. Analysis of duty cycle data indicates charge control began very early around 10:15AM. Interestingly, the duty cycle never reached the low levels observed on November 11th with a minimum value of 0.34. Furthermore, the maximum charge current on November 7th was 5.4A compared to 4.8A on November 11th. The higher charge currents, despite similar irradiance, may be due to the higher end of charge set point caused by lower ambient temperatures.

The higher duty cycle on November 7th, despite higher currents, indicates higher charge acceptance from the battery. This is also a temperature effect. High temperatures increase the charge capacity of lead-acid batteries however they also reduce the battery's gassing voltage. The temperature compensated charge controller used in the remote system raised the end of charge voltage set point allowing for higher battery voltages and thus higher battery currents. The increased end of charge voltage can be observed in figure 8.7.D. The end of charge voltage on November 7th, marked as a dotted red line in figure 8.7.D is 0.1V higher at 13.75V than on November 11th, seen in figure 8.6.D.

Figure 8.7.D also shows several losses of load voltage which are also seen with less frequency in figure 8.6.D. These drops are difficult to explain purely from monitoring data. They do not appear to be measurement errors because the voltage drops correspond to losses of load current as well. Battery voltage increases also indicate the disconnection of loads.

Of particular interest on this day is the effect of the low BOM temperature relative to the high insolation. The temperature profile can be seen in figure 8.7.C. BOM temperatures during peak sun hours generally stayed in a range around 35 °C with a brief spike to 40.6 °C around 12:45PM. Ambient temperatures peaked at 27.6 °C. With an average irradiance weighted BOM temperature over 10 °C less than on November 11th, a significantly higher PV efficiency should be expected on November 7th.

This was exactly what was found. The average potential (duty cycle corrected) array efficiency on November 7th was 1% greater than that on November 11th (9.9%) at 10.9%. Using manufacturer specified thermal parameters, a temperature corrected efficiency of 11.2% is found for the day. The close correspondence of these temperature corrected effi-

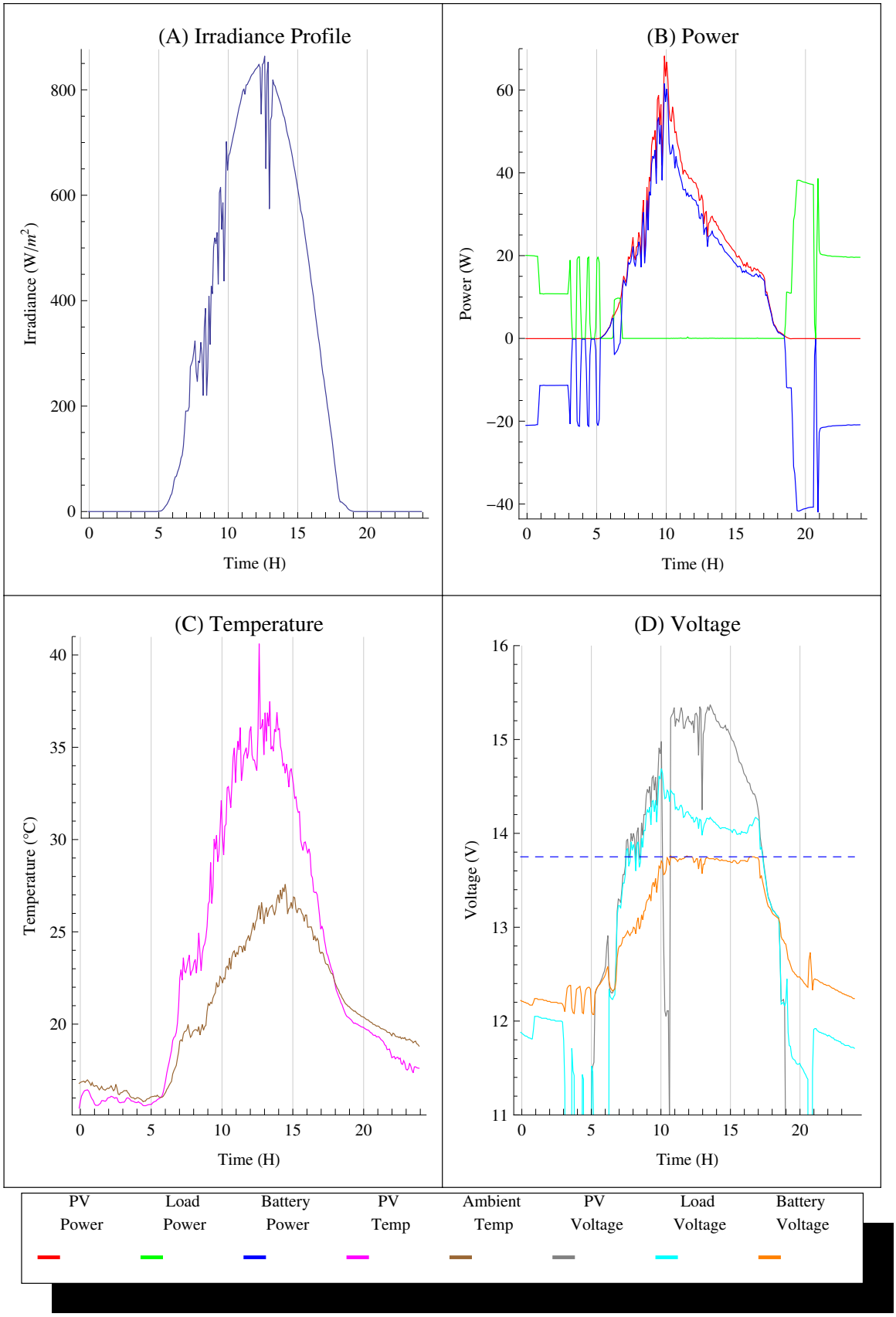

Figure 8.7: November 7, 2010 Remote System Monitored Parameter Profiles

ciencies gives merit to the manufacturer specified temperature coefficients. The efficiency values obtained on the 7th and 11th of November correspond to a 0.8% decrease in PV array performance per degree Celsius in average irradiance weighted BOM temperature.

The current profile in figure 8.8 shows good performance of the PV current correction algorithm under PWM with some small deviations, circled in blue, during periods of more variable sky conditions. Overall the method appears to work well and is certainly a vast improvement over the uncorrected current which would be a duty cycle weighted average of charge current and short-circuit current.

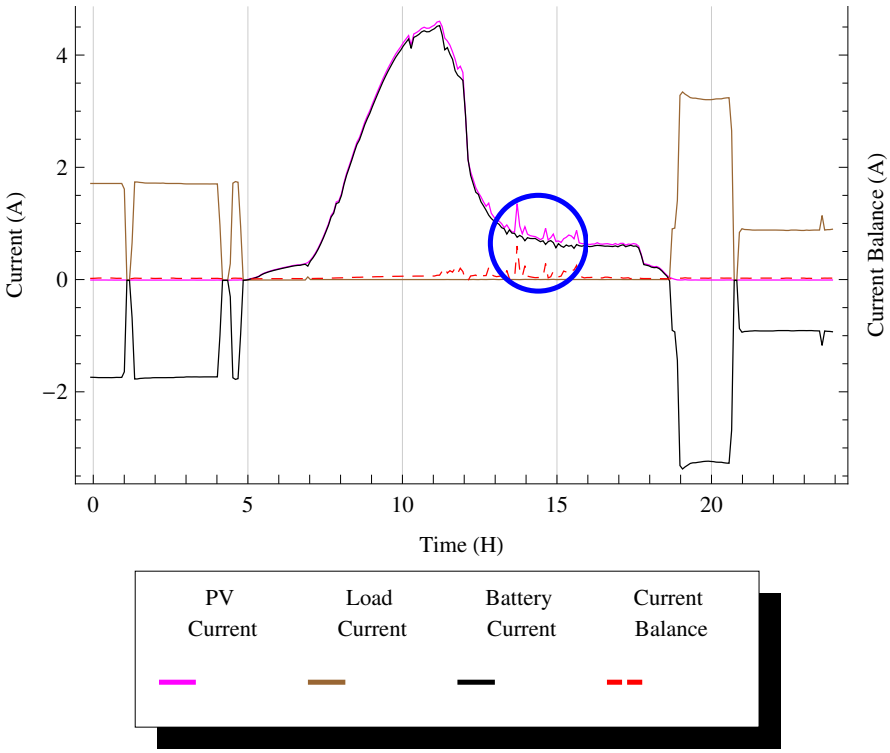

Figure 8.8: Tyefu SHS Current Profile, November 11, 2010

Summary Analysis of daily monitored parameter profiles and energy totals demonstrates the importance of the module temperature. A 9% decrease in average PV array efficiency was observed with a 12.2 °C decrease in average irradiance weighted BOM temperature. Temperature was also seen to affect the charge acceptance of the system's battery.

Some indication of the accuracy of the PWM correction algorithm can be gained as well. Some drops in PV voltage and spikes in PV current during variable sky conditions demonstrate the difficultly of obtaining accurate estimates under such conditions. These effects however tend to cancel each other out and variations of average voltage and current do not necessarily reflect directly on the average calculated power. These spikes are not

seen to the same degree in the power profile because the average power is the average of the power at individual data points and not the product of the average current and voltage. On the whole the data collected gives confidence in the power values obtained.

8.5 Component Performance and PWM Error Analysis

System performance will be a reflection of the performance of individual components. This effect can be disproportional for certain components if they under perform and limit the performance of the system as a whole. This section will examine the performance of individual system components. Without device parameters, modelling of PV performance will be more limited than for the laboratory system. Battery performance is particularly difficult to analyze with monitoring data. Analysis of loads will consist of an examination of the load profile and energy consumption patterns of the system.

8.5.1 PV Array

The PV array in the Tyefu SHS consisted of two 55W mono-crystalline Siemens PV modules connected in parallel. The rated power of the array was thus 110W at STC. The rated module efficiency can be calculated from the module data sheet [62] as 12.9%. This is already higher than the 10.3% efficiency rating of the Helios module used in the laboratory system. Performance of the Siemens modules were greater even relative to their rated efficiencies. The Siemens modules produced a combined average duty cycle corrected efficiency of 10.5% over the monitoring period. This is 81% of rated efficiency compared to the 74% of rated efficiency provided by the Helios module.

This is despite much higher BOM temperatures in the Tyefu system. Correcting for temperature using manufacturer thermal coefficients gives an average efficiency of 11.1%. The remaining 1.8% loss of efficiency is due mostly to operation away from MPP and to a lesser extent low irradiance losses. Module under performance and degradation could also play a role but obtaining accurate IV curves before deployment was not possible. The temperature effects in this case were quite strong accounting for a loss of 4.6% of potential PV energy relative to the nominal array power. This is about three times larger than those calculated for the laboratory system. Relative to the potential PV energy, this loss is 5.7% which amounts to a rather low 0.3%/ °C.

It should be noted that these temperature corrected values are obtained by correcting measured average PV voltage and current values for temperature based on manufacturer provided parameters. The average corrected PV power is then calculated as the product

of the corrected current and voltage. This assumes that the product of the average currents and voltages is equal to the average of the product of current and voltage. This is not in general true, however when comparing the average measured PV power with the product of the average PV current and voltage, the difference is found to be less than 0.1%. Based on this, it is assumed that any similar errors in the temperature corrected power will be likewise small.

PV array performance in the Tyefu SHS was found to be satisfactory, performing at greater than 80% of rated efficiency. Considering the relatively high BOM temperatures and the lack of MPPT in the system, the array performs as required by the system. The PV losses were however slightly higher than predicted during system design which predicted PV array performance at about 85% of rated power. This is almost certainly due to an underestimation of MPP losses. The temperature de-rating factor here was found to be 0.94, smaller than the 0.89 used in system design. Combined with low irradiance losses which should be comparably small, the MPP de-rating factor should be about $0.81/0.94 = 0.86$. This is a much larger de-rating than the 0.95 used in system design for MPP losses.

During system design, MPP losses were underestimated and temperature losses overestimated. During the summer months, however, temperature losses would be expected to be larger and MPP losses smaller. The opposite is true in the winter which is the critical design period. Correctly estimating MPP and temperature losses can be difficult but is important in optimizing system design. Insolation and wind speed data are important in determining approximate BOM temperatures. Wind speed data in particular is highly localized and difficult to obtain in remote areas. MPP losses will depend upon battery voltage and consequently battery SOC, charge controller design and the IV characteristics of the PV array. Lower battery voltage and SOC in winter months tends to increase these losses and the array MPP voltage moves further from the battery voltage.

8.5.2 Charge Controller

The charge controller used in the Tyefu SHS was a 12A Steca Solarix. The controller efficiency during monitoring was estimated at 94%. This is close to the value used in system design of 95% although this de-rating was to account for line losses as well. As mentioned in chapter 7, this is a lower limit on the charge controller efficiency based on average power to and from the charge controller from the battery, loads and PV array. If power flows both to and from the battery to the charge controller during a record interval, the average will be recorded and there will appear to be some power lost during this interval. The load profile that will be examined in section 8.5.4 shows very little load usage during daylight hours so this effect will be very small and the efficiency value can

be assumed largely accurate.

The Steca Solarix controller does not use a blocking diode like the Steca Solsum. It instead utilizes MOSFETs to prevent battery discharge through the PV array at night. At low currents, this should result in lower voltage drops and higher efficiencies. This was however not the case with the Solsum controller showing efficiencies greater than 96%. A possible explanation is higher self-consumption by the Solarix controller but self-consumption is small and could not account for such a reduction in efficiency.

Analysis of data on the voltage drop from the PV array to the battery and PV current gives the reason for the lower efficiency. The data shows much higher ohmic voltage drops than that in the Solsum controller discussed in chapter 7. Data suggests a resistance of about 0.17Ω between the PV and battery terminals of the charge controller. This is about double the resistance in the Solsum controller which surpasses the diode voltage drop already at around 3A PV current.

The design of the Solarix controller leads to poor efficiency in comparison to the Solsum at current greater than about 3A. The blocking diode in this case seems to be a superior method of preventing night time discharge of the battery through the PV array despite the 0.3V resulting drop in voltage.

8.5.3 Battery

Battery performance is particularly difficult to analyze from monitoring data. The proximity of the laboratory system to battery testing facilities allowed for the periodic monitoring of battery capacity which is not easily achievable in the field. Field tests of solar home system batteries have been carried out by Gustavsson and revealed significant loss of capacity after one year of use [63].

It is likely that the battery in the Tyefu SHS sustained some level of capacity loss after remaining in a low voltage disconnect mode for over one month when a connection on the distributor board to the PV array came loose. Battery losses in the system appear to be high when calculating system losses and subtracting charge controller losses. These losses, however, are due to the low initial battery SOC. The apparently “lost” energy is actually stored in the battery. The difficultly in determining the actual battery capacity makes it challenging to extract useful data on battery storage capacity. The system had a healthy A:L (array to load) ratio during the period of 1.7 which is more than enough to ensure sufficient battery charging and health.

8.5.4 Load Profile

Figure 8.9 shows the estimated load profile used in system design as a bold red line and the average measured load profile in solid blue. It is easy to see that load requirements of the system were greatly overestimated. Energy usage was confined almost exclusively to the night time as was expected for a lighting system. There was no morning peak of consumption as was estimated. Evening use picked up around the expected time and was strong in the early evening. Bedtime in the household was apparently much earlier than anticipated at around 10:00PM when the load dropped to the base load outdoor lamp.

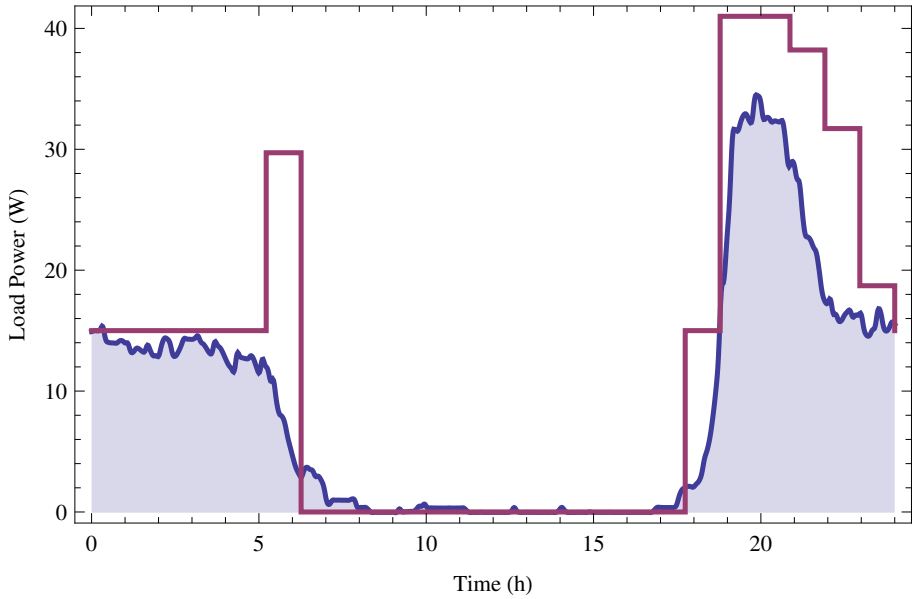

Figure 8.9: Estimated and Measured Average Load Profiles for Tyefu SHS

The average total daily load was only 210Wh. This is much less than the design load of 306Wh. Figure 8.10 shows the average daily load for the different days of the week. It was predicted that weekend loads would be higher, however, it seems the opposite was true with more consumption during the week. Friday, on average, had the highest energy consumption. Variations of consumption throughout the week were somewhat small. The AC current transducer did not operate correctly and did not provide reliable information on the AC energy consumption. Our information on the household energy consumption was therefore limited to the lighting loads on the SHS.

8.5.5 PWM Error Analysis

This section will briefly describe the size of the error between PWM corrected and uncorrected measurements of PV energy during the monitoring period. With a relatively high usage factor of 0.78, PWM errors would not be expected to be large. Over the 28

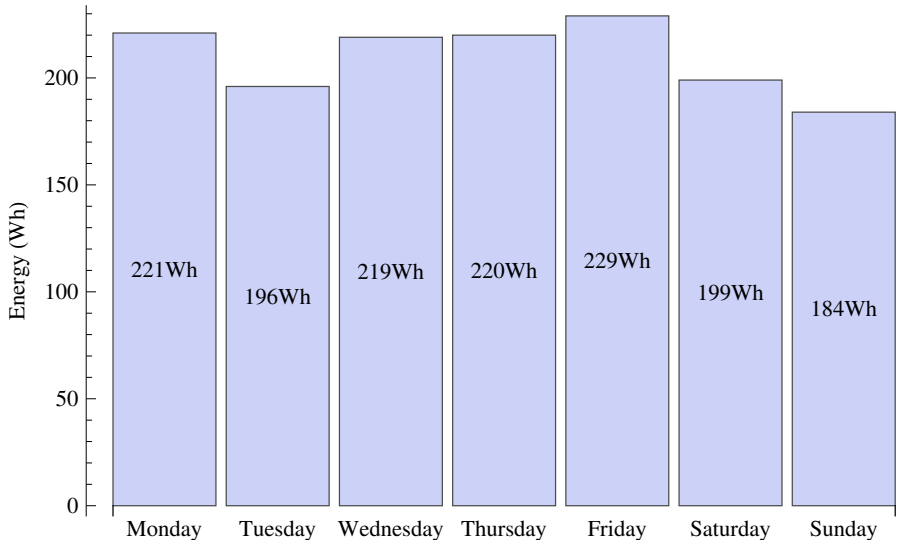

Figure 8.10: Average load on different days of the week

days of monitoring, the PV energy was overestimated by 0.8% relative to the corrected value.

The relationship between PWM error and duty cycle for the mobile monitoring system can be seen in figure 8.11. The error is related to the inverse of the duty cycle. Errors rise quickly below a duty cycle of 0.2.

By comparison to the PWM error found in the laboratory system, the mobile logger errors are quite small. During the August monitoring period in the laboratory system a usage factor of 0.75 lead to a measurement error of 3.0%, nearly four times larger than the remote system with a usage factor of 0.78. From this it can be concluded that if no corrective measures are to be made for PWM measurement errors, it is better to use short integration times as in the remote system rather than the long integration times used by the laboratory system.

8.6 Summary

The operating conditions for the Tyefu SHS fell short of expectations in terms of projected insolation. Insolation over the 28 day monitoring period averaged $4.1kWh/m^2/d$ while the expected worst month insolation used in system design was $5.1kWh/m^2/d$. Despite this, the system met all the energy demand from the loads on the system and produced a performance ratio of 0.46, similar to that of the laboratory system. This is in part due to the lower than expected load energy demand. The usage factor, however, was high at 0.78 due to the low battery SOC at the beginning of monitoring which in turn resulted in a calculation of system efficiency at a low 73.0%.

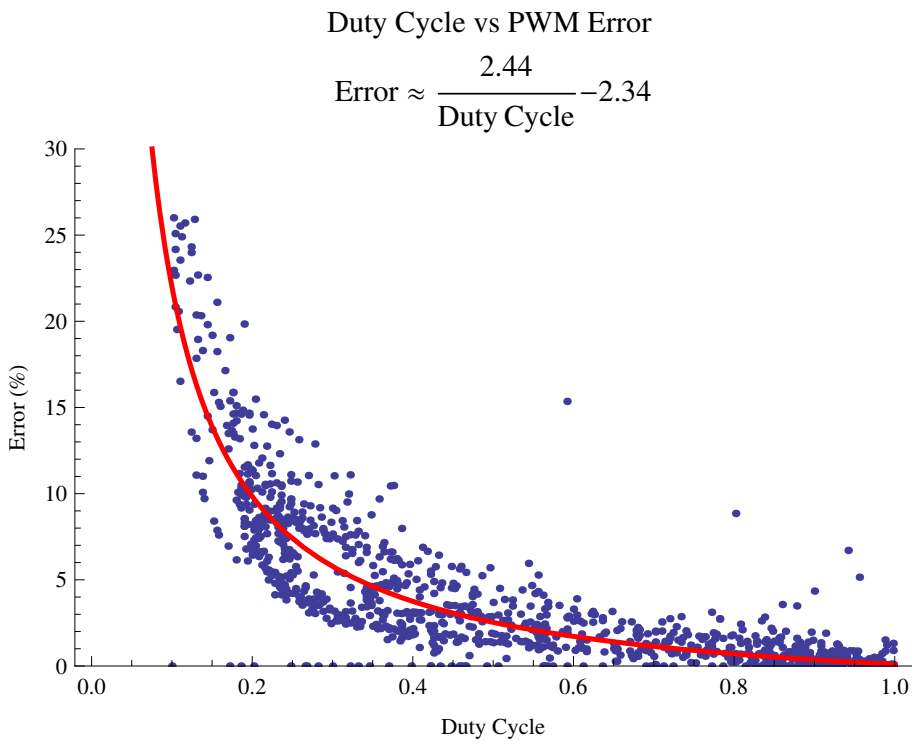

Figure 8.11: Relationship between duty cycle and PWM error in mobile monitoring system

Array performance in the remote system was superior to that of the laboratory system. The array of two mono-crystalline 55W Siemens PV modules produced an average efficiency of 8.2%. Corrected for duty cycle, the array efficiency was 10.5%, 81% of the STC rated efficiency. This is compared to an average duty cycle corrected performance at 74% of STC rated efficiency for the Helios module used in the laboratory system. This is also despite higher module operating temperatures in the remote system. The importance of module operating temperature was highlighted by the drop in average duty cycle corrected array efficiency from 10.9% to 9.9% with an increase from 31.8 °C to 44.0 °C in average irradiance weighted BOM temperature despite similar insolation.

Chapter 9

Conclusions

The aim of this study was to analyze the performance of typical rural solar home systems through a thorough monitoring program. During the course of the study a measurement error in PV power caused by PWM charge control techniques was discovered. To ensure accurate monitoring data, even during charge control, a correction algorithm was developed to reduce the effect of the measurement error. To aid in analysis and to quantify the sources of array capture losses in the laboratory based system, a PV module performance model was developed to predict PV performance at MPP given the module operating temperature and POA irradiance. A detailed analysis of energy losses in the system was then performed to estimate the size of various loss mechanisms.

Performance parameters normalized to nominal array size were computed for both the laboratory based and remote SHSs. This allows for the direct comparison of different systems. From these analyses, recommendations can be made to improve system performance while maintaining or reducing system cost.

9.1 Remote Monitoring System Development

A major research output of this study was the development of a remote monitoring system capable of correcting for PV power measurement errors caused by PWM charge control (accepted for publication in Journal of Solar Energy Engineering [53]). This measurement error arises primarily due to two causes. First, the non-simultaneous measurement of PV voltage and current coupled with a rapidly varying signal during PWM create mismatch between measured PV current and voltage states. Second, the inability of the charge controller to achieve a 0V short-circuit voltage results in the measurement of a small but significant short-circuit power which was never intended to be delivered to the system.

The scale of the problem was found to depend heavily upon the duty cycle of PWM. Low duty cycle results in large measurement errors. Over the course of one day under

consistently low duty cycle, the energy measurement error was found to be 47.6% relative to corrected values. Simulations of the measurement process under typical operating conditions show power measurement errors greater than 10% at 25% duty cycle. Monitoring data indicates that errors rise rapidly as duty cycle drops below 20%.

Correction methods developed to compensate for this problem have been proven effective by simulations. Measurement errors were predicted, by simulation, to be up to 20 times smaller than uncorrected values, depending on operating conditions.

9.2 PV Performance Model

As a way to deduce the causes and size of energy losses in the PV array, a performance model was developed to predict module output at MPP based on module temperature and incident POA irradiance. The model, based on fill factor models dependent on parasitic resistances, was adapted from a model by Zhou et al. [55]. Device parameters such as parasitic resistances and ideality factor were extracted from IV curves using methods developed at the NMMU CER [42]. Temperature and irradiance coefficients were experimentally determined based on linear models of short-circuit current-irradiance and open-circuit voltage-temperature dependence. The resulting model was tested in the laboratory and predicted module energy production at MPP over a three-day period to within 0.2%.

9.3 Energy Loss Analysis

Armed with this model, a detailed analysis of energy losses in the laboratory based system was made. It was found that the single largest source of energy loss was charge control. This energy is essential thrown away because there is nowhere to put it. This may indicate that the PV array is over-sized relative to the loads on the system. However, it is also indicative of a fundamental limitation of stand-alone PV systems. Limited storage capacity and the variability of the solar resource throughout the year means that in a well designed system there will be times when energy production exceeds energy demand. Stand-alone systems must be designed for the critical month when the solar resource is at its lowest during the year. Furthermore, to maintain battery health and extend battery life cycles, lead-acid batteries must be regularly charged to full capacity. This requires long periods of charge at constant voltage, which demands the use of charge control techniques, which limit PV array performance. Charge control losses during the monitoring periods ranged from 18-27% of the module rating.

The second largest cause of energy losses was found to be PV module under-performance.

PV module performance degrades during its useful life. There are various possible causes of these performance losses, which require a thorough evaluation of the PV module. In this particular case, IV curves of the 70W Helios module indicate a high series resistance. This caused a reduction in the MPP voltage of the module and consequentially also a 15% reduction of the MPP Power.

The other significant source of energy loss was MPPT losses. When utilizing a charge controller that directly couples the PV array with the system battery, the battery voltage will dictate the PV array's voltage. This is almost never the same as the MPP voltage of the PV array resulting in a loss of potential energy. Relative to the expected energy yield at the module's rated power, these MPPT losses were found to range from 8%-11% during the monitoring periods.

Other losses such as temperature losses, low irradiance losses and DC system losses were relatively small. Battery losses are difficult to deduce from monitoring data, however, periodic battery tests indicate loss of capacity and storage efficiencies over time. The tested energy efficiency of the battery dropped from an initial 80.5% to 69.5% after a four month period of storage followed by a month of cycling on the SHS. Two months later it had fallen to 66.6%. Based on these measured battery energy efficiencies, it is estimated that battery losses are roughly 13-18% of the rated PV energy. Capacity loss was also significant, particularly after the long period of storage, dropping from 96.2Ah to 63.7Ah. At the end of the final monitoring period, the capacity was tested at 58.8Ah.

Several recommendations for system design can be made based on the results of the energy loss analysis. PV modules should be tested to verify that they are operating according to manufacturer specifications before deployment. In the laboratory system, module de-rating resulted in an immediate loss of 15% of rated power due to module under performance.

Another way to easily increase the amount of available energy, or likewise decrease the required array nominal power, is to employ a MPPT charge controller. Gains in power from MPPT controllers will vary depending upon operating conditions but in the case of the laboratory SHS, losses were estimated at around 10%. A 10% reduction in nominal array power would quite often exceed the increased cost of a MPPT charge controller, particularly for larger systems.

The largest source of losses, charge control losses, is to some extent necessary to ensure proper battery charging and health. The important factor to consider here is the A:L ratio. More work should be done to determine which range of A:L ratios best balance the increased cost of larger PV arrays and the increase in cost resulting from shorter battery lifetime caused by smaller PV arrays. A ratio of 1.3 is often viewed as sufficient. Using this metric, the system PV array was perhaps slightly oversized for the operating

conditions during the monitoring periods. During the July monitoring period, the A:L ratio was 1.5 however June is, on average, the month with the lowest POA insolation. Had the PV array performed as rated, the A:L ratio would have been much higher.

The reason the under performance of the PV array did not cause an unacceptable A:L ratio is that the loads on the system consumed less than their rated power. The loads, consisting of three CFL bulbs of various rated powers and one 40W incandescent bulb, consumed on average only 85% of their rated power. This balances well with the 15% loss of rated power.

With efficiencies less than 70% and most energy consumption occurring during the night when all power to the loads is drawn from the batteries, battery losses are significant as well. There are not, at present, many good alternatives to lead-acid batteries for SHS applications. The development of a more robust and efficient energy storage device would perhaps go the farthest in improving the performance and life cycle cost of SHSs.

9.4 Comparison of Remote and Laboratory Solar Home Systems

In order to facilitate the comparison of different PV systems, performance parameters are often normalized to the nominal array power. Comparison of the remote and laboratory SHSs gives an idea as to the relative performance of each system. The most oft quoted parameter is the performance ratio, which represent the ratio of the energy demand on the system to the available energy at the nominal array power. By this measure, the systems performed to a similar level. It is best to compare performance ratios based upon annual data or data from corresponding seasons and months since the PR will drop in the summer and rise in the winter for stand-alone systems. The PR ratio for the laboratory system during the September monitoring period was the same as the PR ratio calculated for the remote system during a period from mid October to mid November at 0.46.

The usage factor for the remote system compares favorably to that of the laboratory system. The UF for the remote system was 0.78 and ranged from 0.62-0.75 for the laboratory system during the monitoring periods. This indicates that a larger percentage of the potential energy production of the PV array was transmitted to the remote system. This may also suggest a lower A:L ratio which could be detrimental to battery lifetime. In this case however, the low initial battery state of charge resulted in a large amount of energy being put into storage that would have been lost to charge control had the battery been in a high state of charge when monitoring began. The A:L ratio for the

remote system was 1.8. This larger A:L ratio resulted from the larger overestimation of the load on the system during system design. The PV array was over sized for the load on the system. This highlights one of the challenges of system design. Minimization of system costs requires an accurate knowledge of the loads on the system.

9.5 System Design Recommendations

The results of this study show the importance of proper SHS design. While sometimes difficult to acquire, an accurate knowledge of the loads on the system is of paramount importance when designing a stand-alone PV system. A delicate balance must be struck between minimizing PV array size and maintenance of battery health and ensuring sufficient energy production to meet the energy demand throughout the year.

If possible, the actual MPP power of PV modules should be verified before deployment to ensure proper operation. Module defects and degradation can significantly reduce system performance. Furthermore, under performance of a single module in an array can limit the performance of the entire array. A defective module will result in significant under performance of the system as a whole.

Finally, it has been seen that the use of a MPPT charge controller could significantly boost PV array power and reduce the required array size. Larger systems in particular can receive large cost reductions with the use of MPPT controllers. Battery losses were also significant but affordable alternatives to lead-acid batteries have yet to be developed.

DC system losses, including charge controller losses, are typically small in comparison to PV array capture losses. Other capture losses such as temperature and low irradiance losses were also found to be relatively small. The size of these losses will vary depending on local operating conditions. Temperature losses can become important in very hot climates but were not found to significantly limit system performance in the moderate climates found at the project sites. Array mounting will also affect temperature losses. The arrays in this study were mounted on free-standing mounts allowing for passive cooling in the wind.

Overall this study has found that the most significant improvements in SHS performance can come from optimization of PV array sizing and PV array performance. This requires an accurate knowledge of system loads, proper balancing of array size and battery health, the employment of MPPT techniques and verification of PV module performance relative to manufacturer specifications before deployment. In the case of the laboratory system, a reduction of nominal array power of 25% would be possible while still maintaining battery health and without risk of significant load shedding. This reduction would result in significant savings on the cost of the SHS.

Appendix A

PVSol Simulation Results

The following pages contain the results from the PVSol simulations of the SHS installed in Tyefu and the laboratory based SHS. Simulations were run using components from the PVSol data base of similar specifications to actual components. The hourly meteorological data used in the simulation was taken from monthly mean data in Port Elizabeth, South Africa.

Nathan Williams
NMMU - CER

Project Name:	Tyefu	2010/11/09
Variant Reference:	12V	
Designer:	Nathan Williams	

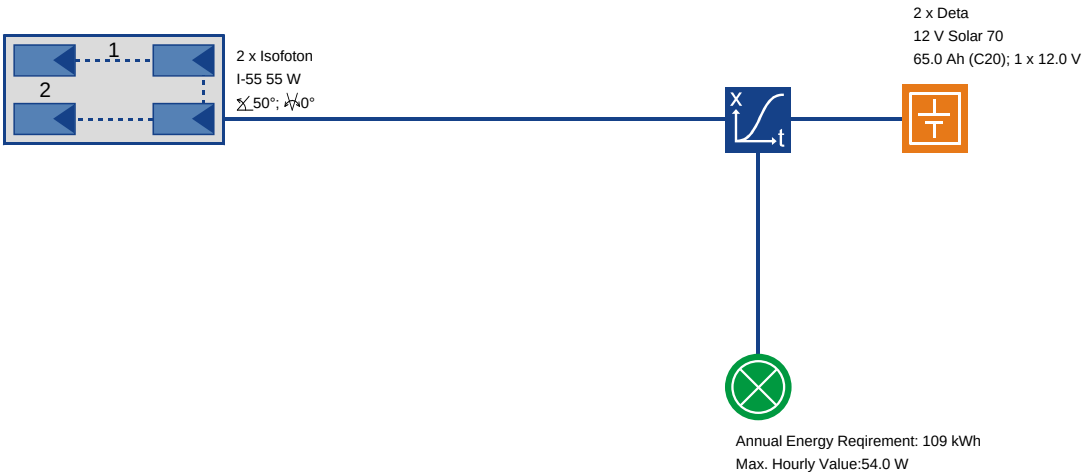

Location:	Tyefu
Climate Data Record:	PORT ELIZABETH
PV Output:	110.0 Wp
Gross/Active PV Surface Area:	0.89 / 0.89 m²

PV Array Irradiation:	1,718.1 kWh
Energy Produced by PV Array:	142.62 kWh
Consumption Requirement:	108.94 kWh
Consumption Covered by Solar Energy:	90.678 kWh
Consumption Not Covered by System:	18.3 kWh

Solar Fraction:	83.2 %
Performance Ratio:	42.5 %
Specific Annual Yield:	824.6 kWh/kWp
CO2 Emissions Avoided:	56 kg/a
System Efficiency:	5.3 %
PV Array Efficiency:	8.3 %

The results are determined by a mathematical model calculation. The actual yields of the photovoltaic system can deviate from these values due to fluctuations in the weather, the efficiency of modules and inverters, and other factors. The System Diagram above does not represent and cannot replace a full technical drawing of the solar system..

Nathan Williams
NMMU - CER

Project Name:	Laboratory SHS	2010/11/09
Variant Reference:	12V	

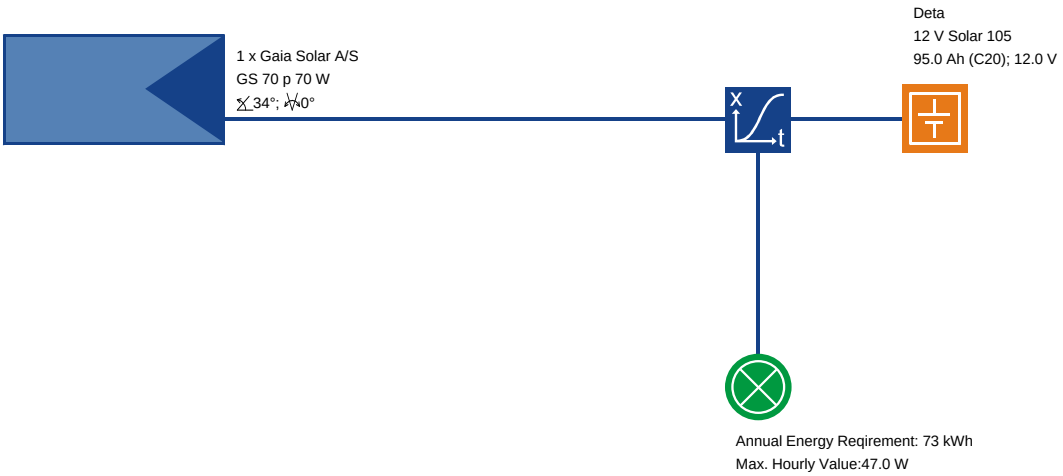

Location:	PORT ELIZABETH
Climate Data Record:	PORT ELIZABETH
PV Output:	69.97 Wp
Gross/Active PV Surface Area:	0.68 / 0.68 m²

PV Array Irradiation:	1,381.2 kWh
Energy Produced by PV Array:	101.93 kWh
Consumption Requirement:	73.365 kWh
Consumption Covered by Solar Energy:	67.001 kWh
Consumption Not Covered by System:	6.4 kWh

Solar Fraction:	91.3 %
Performance Ratio:	47.1 %
Specific Annual Yield:	957.6 kWh/kWp
CO2 Emissions Avoided:	41 kg/a
System Efficiency:	4.9 %
PV Array Efficiency:	7.4 %

The results are determined by a mathematical model calculation. The actual yields of the photovoltaic system can deviate from these values due to fluctuations in the weather, the efficiency of modules and inverters, and other factors. The System Diagram above does not represent and cannot replace a full technical drawing of the solar system..

Appendix B

Charge Controller Bench Test Procedure

The charge controller bench test discussed in chapter 3 is used to determine the accuracy of set points specified by manufacturers. The required equipment is a power supply capable of voltages up to at least 15V or more depending on the charge controller being tested, and a voltmeter. A familiarity with the charge controller indicator lights is also required and can be obtained from manufacturer documentation.

This procedure, for pulse width modulation controllers, is adapted from the procedure described in the MSc dissertation of E.L. Meyer [45] which was developed for simple on-off charge controllers.

Low Voltage Disconnect To determine the low voltage disconnect set point of the charge controller, the power supply should be connected to the charge controller battery terminals following labelled sign conventions. The voltage of the power supply should be set to 13V and decreased at fixed increments until the charge controller indicators signal low voltage disconnect. A rest period should be allowed at each voltage with the duration depending on the charge controller. This may require some experimentation to determine. Many controllers require a fixed period of time below the low voltage disconnect set point before triggering low voltage disconnect to prevent false triggers. The voltage at which the indicator light indicates low voltage disconnect is then recorded as the low voltage disconnect set point.

Load Reconnect From the low voltage disconnect voltage, the power supply voltage should then be raised following the same procedure described for the low voltage disconnect until the charge controller indicators signal load reconnect. The voltage at which the indicators show load reconnect is recorded as the load reconnect voltage.

Charge Regulation Voltage When the battery of a solar home system reaches a certain voltage, the charge controller tries to maintain the battery at this voltage for a set period of time via pulse width modulation. To determine this set point, the power supply must be connected to the PV array terminals of the charge controller. If a shunt type controller is being tested, a load may be connected in series with the charge controller to prevent short-circuiting the power supply when pulse width modulation commences. The voltmeter should be set up to read the voltage on the charge controller battery terminals.

Starting at 13V, the power supply voltage should be increased in fixed increments until the voltage on the voltmeter becomes unstable due to the pulse width modulation on the power supply. This set point can be more accurately determined by monitoring the battery terminal voltage with an oscilloscope. When pulse width modulation is detected in the system, the previous stable battery terminal voltage reading is recorded as the charge regulation voltage.

Bibliography

[1] Modi, V., McDade, S., Lallement, D., and Saghir, J., 2005. Energy Services for the Millennium Development Goals. Tech. rep., United Nations Development Programme.

[2] Gustavsson, M., and Ellegard, A., 2004. "The impact of solar home systems on rural livelihoods. Experiences from Nyimba Energy Service Company in Zambia". *Renewable Energy,* **29**, pp. 1059–1072.

[3] Schare, S., and Smith, K. R., 1995. "Particulate emission rates of simple kerosene lamps". *Energy for Sustainable Development,* **2**, pp. 32–35.

[4] Community members of Kalouba, Zambia, December 24, 2009. Personal communication.

[5] Kaundinya, D. P., Balachandra, P., and Ravindranath, N., 2009. "Grid-connected versus stand-alone energy systems for decentralized power - A review of literature". *Renewable & Sustainable Energy Reviews,* **13**, pp. 2041–2050.

[6] Ketlogetswe, C., and Mothudi, T., 2009. "Solar home systems in Botswana - Opportunities and constraints". *Renewable & Sustainable Energy Reviews,* **13**, pp. 1675–1678.

[7] Martinot, E., Cabraal, A., and Mathur, S., 2001. "World Bank/GEF solar home system projects: experiences and lessons learned 1993-2000". *Renewable & Sustainable Energy Reviews,* **5**, pp. 39–57.

[8] International Energy Agency, 2003. Guidelines for Monitoring Stand-Alone Photovoltaic Power Systems. Tech. rep., International Energy Agency.

[9] International Electrotechnical Commission. IEC Standard 61724. Photovoltaic System Performance Monitoring Guidelines for Measurement, Data Exchange and Analysis, April 1998.

[10] Commission of the European Communities. Photovoltaic System Monitoring, Guidelines for the Assessement of Photovoltaic Plants, Document A, April 1997.

[11] Commission of the European Communities. Photovoltaic System Monitoring, Guidelines for the Assessement of Photovoltaic Plants, Document B, April 1997.

[12] Jahn, U., Grimmig, B., and Nasse, W., 2000. Analysis of photovoltaic systems. Tech. rep., International Energy Agency.

[13] Jacobson, A., 2004. "Charge Controllers and Small Solar PV Systems". *Solarnet,* **5**(2).

[14] Gxasheka, A. R., 2003. "On the monitoring of current-voltage characteristics of photovoltaic modules". Master's thesis, Nelson Mandela Metorpolitan University.

[15] Florida Solar Energy Center. Test method for photovoltaic module power rating.

[16] Muneer, T., 2004. *Solar Radiation and Daylight Models.* Elsevier Butterworth-Heinemann.

[17] Parretta, A., Sarno, A., and Vicari, L. R., 1998. "Effects of solar irradiation conditions on the outdoor performance of photovoltaic modules". *Optics Communications,* **153**, pp. 153–163.

[18] Green, D., 2004. "Thailand's solar white elephants: an analysis of 15yr of solar battery charging programmes in northern Thailand". *Energy Policy,* **32**, pp. 747–760.

[19] Gxasheka, A., van Dyk, E., and Meyer, E., 2005. "Evaluation of performance parameters of PV modules deployed outdoors". *Renewable Energy,* **30**, pp. 611–620.

[20] Alonso-Garcia, M., Ruiz, J., and Chenlo, F., 2006. "Experimental study of mismatch and shading effects in the I-V characteristic of photovoltaic module". *Solar Energy Materials & Solar Cells,* **90**, pp. 329–340.

[21] Diaz, P., and Lorenzo, E., 2001. "Solar home system battery and charge regulator testing". *Progress in Photovoltaic Research and Application,* **9**, pp. 363–377.

[22] National Academy of Sciences, 1976. *Energy for Rural Development.* National Academy of Sciences.

[23] Komp, R. J., 2001. *Practical Photovoltaics: Electricity from Solar Cells.* AATEC publications.

[24] Dunlop, J. P., and Farhi, B. N., 2001. "Maximizing battery life in photovoltaic systems: A review of lessons learned". In Forum 2001 Solar Energy: The Power to Choose.

[25] Markvart, T., and Castaner, L., 2003. *Practical Handbook of Photovoltaics: Fundamentals and Applications.* Elsevier.

[26] Power Electronics and Photovoltaic Power Systems Laboratory, University of Colorado. ECEN 4517 Lecture Notes: Batteries.

[27] Reinders, A., Pramusito, Sudradjat, A., van Dijk, V., Mulyadi, R., and Turkenburg, W., 1999. "Sukatani revisited: on the performance of nine-year-old solar home systems and street lighting systems in Indonesia". *Renewable & Sustainable Energy Reviews,* **3**, pp. 1–47.

[28] *Steca Solsum Solar Charge Controllers 5.6/6.6/5.0/8.8/8.0 User's Manual.*

[29] Linden, D., and Reddy, T. B., 2001. *Handbook of Batteries*, 3rd ed. McGraw-Hill Professional.

[30] Wagner, R., and Sauer, D. U., 2001. "Charge strategies for valve-regulated lead/acid batteries in solar power applications". *Journal of Power Sources,* **95**, pp. 141–152.

[31] Dunlop, J. P., 1997. Batteries and Charge Control in Stand-Alone Photovoltaic Systems. Tech. rep., Florida Solar Energy Center.

[32] Luque, A., and Hegedus, S., 2003. *Handbook of Photovoltaic Science and Engineering.* Wiley.

[33] *Steca Solarix Solar Charge Controller Operating Instructions.*

[34] Types of lighting. http://www.energysavers.gov/your_home/lighting_ daylighting/index.cfm/mytopic=12030.

[35] Collier, J. L., 2006. *Electricity and the Light Bulb.* Marshall Cavendish Benchmark.

[36] Beggs, C., 2009. *Energy: Management, Supply and Conservation.* Butterworth-Heinemann.

[37] Green, M. A., 1982. *Solar Cells.* Prentice Hall.

[38] Endecon Engineering, 2001. A guide to photovoltaic system design and installation. Tech. rep., California Energy Commission.

[39] Lorenzo, E., 1994. *Solar Electricity: Engineering of Photovoltaic Systems.* Progensa.

[40] Chen, W., Shen, H., Shu, B., Qin, H., and Deng, T., 2007. "Evaluation of performance of MPPT devices in PV systems with storage batteries". *Renewable Energy,* **32**, pp. 1611–1622.

[41] Messenger, R. A., and Ventre, J., 2004. *Photovoltaic Systems Engineering.* CRC Press.

[42] Munji, M., Okullo, W., van Dyk, E., and Vorster, F., 2010. "Local device parameter extraction of a concentrator photovoltaic cell under solar spot illumination". *Solar Energy Materials & Solar Cells,* **94**, pp. 2129–2136.

[43] Lam, L., Ozgun, H., Lim, O., Hamilton, J., Vu, L., Vella, D., and Rand, D., 1995. "Pulsed-current charging of lead/acid batteries - a possible means for overcoming premature capacity loss?". *Journal of Power Sources,* **53**, pp. 215 – 228.

[44] Hund, T., 1996. "Battery testing for photovoltaic applications". In 14th NREL Program Review.

[45] Meyer, E. L., 1999. "Investigation of properties and energy rating of photovoltaic modules". Master's thesis, University of Port Elizabeth.

[46] Nieuwenhout, F., van de Rijt, P., and Vervaart, M., 2001. "Monitoring of Solar Home Systems in China: First Year Results". In 17th European Photovoltaic Solar Energy Conference.

[47] Gustavsson, M., 2007. "With time comes increased load - An analysis of solar home system use in Lundazi, Zambia". *Renewable Energy,* **32**, pp. 796–813.

[48] *CR1000 Measurement and Control System Operation Manual.*

[49] *PCI 725/726/730/E & PC104PLUS-26/30 PCI PnP Analog Board User's Manual.*

[50] *PCI 773 Series PCI PnP Analog Board User's Manual.*

[51] *Apogee SP-110 User's Manual.*

[52] *Li-Cor 200SA Pyranometer Sensor Datasheet.*

[53] Williams, N., van Dyk, E., and Vorster, F., 2010. "Monitoring solar home systems with pulse width modulation charge control". *Journal of Solar Energy Engineering,* **In Press**.

[54] Muñoz, F., Almonacid, G., Nofuentes, G., and Almonacid, F., 2006. "A new method based on charge parameters to analyse the performance of stand-alone photovoltaic systems". *Solar Energy Materials & Solar Cells,* **90**, pp. 1750–1763.

[55] Zhou, W., Yang, H., and Fang, Z., 2007. "A novel model for photovoltaic array performance prediction". *Applied Energy,* **84**, pp. 1187–1198.

[56] van Dyk, E., Meyer, E., Vorster, F., and Leitch, A., 2002. "Long-term monitoring of photovoltaic devices". *Renewable Energy,* **25**, pp. 183–197.

[57] Bashahu, M., and Habyarimana, A., 1995. "Review and test of methods for determination of the solar cell series resistance". *Renewable Energy,* **6**, pp. 129–138.

[58] Jia, Q., and Anderson, W., 1988. "A novel approach for evaluating the series resistance of solar cells". *Solar Cells,* **25**, pp. 311–318.

[59] Anis, W. R., and Nour, M. A. S., 1995. "Energy losses in photovoltaic systems". *Energy Conversion and Management,* **36**, pp. 1107–1113.

[60] Benenson, W., Harris, J. W., Stocker, H., and Lutz, H., 2002. *Handbook of Physics.* Springer.

[61] Rand, D., Moseley, P., Garche, J., and Parker, C., 2004. *Valve-Regulated Lead-Acid Batteries.* Elsevier.

[62] *Siemens Solar Module SM55 Datasheet.*

[63] Gustavsson, M., and Mtonga, D., 2005. "Lead-acid battery capacity in solar home systems - Field tests and experiences in Lundazi, Zambia". *Solar Energy,* **79**, pp. 551–558.